Ordering molecular organics into functionality

Diss. ETH No. 19794

Ordering Molecular Organics into Functionality

A dissertation submitted to

ETH ZURICH

for the degree of
Doctor of Sciences

presented by
PASCAL WOLFER

Dipl. Werkstoff-Ing. ETH
born January 8, 1981
citizen of Ossingen (ZH), Switzerland

accepted on the recommendation of

Prof. Dr. Paul Smith, examiner
Prof. Dr. Dirk J. Broer, co-examiner
Prof. Dr. Hans-Werner Schmidt, co-examiner
Dr. Assunta Marrocchi, co-examiner
Dr. Natalie Stingelin, co-examiner

Zürich, 2011

CONTENTS

SUMMARY

In recent years, organic materials have attracted much attention for potential use in a variety of optic, electronic and optoelectronic applications. Generally, target functionalities and the performance of devices created with such organic compounds strongly depend on the order of the active species over a range of length scales, from the sub-molecular and molecular to microscopic and macroscopic levels. Hence, in order to fine tune and optimize functionalities of organic species, it is crucial to obtain a comprehensive understanding of structure-property interrelations at these different levels. As the different structural scales often are interdependent, though, consideration of isolated regimes is not sufficient resulting in the necessity to take structural characteristics and phenomena at all length scales involved into account.

Due to their rich chemistry, organic compounds provide ideal model systems for investigating order-related effects – indeed over a wide range of length scales. Compared to macromolecular species, small molecules feature well-defined chemical structures and corresponding physicochemical properties. In addition, they provide the option of homogeneously incorporating them in polymeric matrices. For these reasons, studies described in this thesis are based principally on molecular organic species.

In a first part, a series of small-molecular trisazobenzene derivatives is explored. Azobenzene moieties attached to the side-groups of these species impart optical activity to the systems investigated, providing insight in the correlation of sub-molecular chemical modifications and the compounds' optical activity. Employing a large library of such trisazobenzene species, it is demonstrated that stable light-induced alignment in initially amorphous thin films is only observed for derivatives with a chemical structure that allows formation of both an amorphous and a liquid-crystalline (LC) phase, thus, indicating the interdependence of molecular architecture, phase behavior and optical characteristics. Interestingly, compounds exhibiting a latent liquid-crystalline phase are found to display a "post-development", *i.e.*, an increase of photo-induced alignment that is observed after arresting exposure to light. Most intriguingly, the order in photo-oriented domains can be significantly enhanced by selected annealing protocols, allowing manipulation of photo-induced alignment with light *and* temperature.

Subsequently, thin films of these trisazobenzenes are employed as alignment layers for commercial nematic liquid-crystalline compounds. Different surface characterization techniques and concomitant optical analysis indicate that organization of the LC species

into macroscopic domains by such films is induced via an inter-molecular attractive interaction between the azobenzene containing layer and the LC material – and not by a surface relief structure. Accordingly, these azobenzene based systems allow straightforward photo-induced patterning of manifold structures without requiring tedious relief structuring of the commanding surface.

In a second part, the interrelation of order and electronic characteristics of blends of small-molecular semiconductors and insulating polymers are studied. Besides improved film-forming characteristics, imparted by the polymeric component, these binaries provide the possibility for manipulating their phase behavior and, hence, the microstructure induced with both temperature and composition, significantly expanding the range of processing options compared to single-component systems. Structure-property investigations reveal that the extent of solid-solid phase separation that occurs during formation of films of the blends strongly affects the electronic performance of devices fabricated with them. One approach employed to create particular thin-film microstructures is based on solidification-rate-control – here by increasing the processing temperature applied, generally resulting in finer structured and more homogeneous active layers that exhibit clean field-effect transistor (FET) characteristics. However, as for many applications processing of active species at ambient conditions is desirable, alternatively, the phase behavior can be tailored by adjusting the molecular architecture of the semiconducting species. This procedure offers further processing routes for the binaries explored, allowing film fabrication at room temperature without sacrificing the blends' electronic characteristics. For instance, binaries of insulator contents as high as about 70 to 80 wt-% feature electronic properties in FETs comparable to those of the neat small-molecular organic semiconductor.

ZUSAMMENFASSUNG

Aufgrund ihrer vielfältigen Einsatzmöglichkeiten in optischen, elektronischen und optoelektronischen Anwendungsgebieten stiessen organische Materialien in den letzten Jahren auf ein breites Interesse. Die angestrebten Funktionalitäten sowie die Leistung von Bauelementen, welche auf solchen organischen Materialien basieren, hängen erheblich von der Ordnung der aktiven Verbindungen in den verschiedenen Längenskalen vom sub-molekularen und molekularen Regime bis hin zu mikroskopischen und makroskopischen Bereichen ab. Zur Optimierung der meisten Funktionalitäten von organischen Materialien ist deshalb ein umfassendes Verständnis des Zusammenhangs von Struktur und Eigenschaften auf den entsprechenden Längenskalen unerlässlich. Dabei gilt es stets zu beachten, dass Effekte auf den unterschiedlichen Skalen oft miteinander verflochten sind. Folglich reicht die Betrachtung von einem isolierten Längenbereich oft nicht aus, sondern nur die gleichzeitige Berücksichtigung von strukturellen Eigenschaften und Phänomenen aller Grössenskalen führt zum Ziel.

Um strukturbezogene Effekte über einen grossen Bereich von Längenskalen zu erforschen, stellen organische Verbindungen dank ihrer vielseitigen chemischen Natur ideale Modellsysteme dar. Verglichen mit Makromolekülen weisen kleine Moleküle sowohl wohldefinierte chemische Strukturen wie auch physikalisch-chemische Eigenschaften auf und können ohne grössere Schwierigkeiten homogen in eine Polymermatrix eingebettet werden. Aus diesen Gründen basieren die Studien, die in dieser Arbeit abgehandelt werden, auf kleinen organischen Molekülen.

In einem ersten Schritt werden sternförmige Trisazobenzolmoleküle untersucht. Azobenzoleinheiten, welche in den Seitengruppen von solchen Molekülen integriert sind, vermitteln dabei den untersuchten Systemen eine optische Aktivität. Diese Funktionalität ermöglicht es, einen Zusammenhang zwischen chemischen Eingriffen auf dem sub-molekularen Level und den optischen Eigenschaften von solchen Verbindungen herzustellen. Basierend auf einer breiten Palette von solchen Trisazobenzolen wird gezeigt, dass eine stabile lichtinduzierte Orientierung in anfänglich amorphen Dünnfilmen nur dann möglich ist, wenn die chemische Struktur der untersuchten Verbindungen die Ausbildung sowohl einer amorphen wie auch einer flüssigkristallinen Phase erlaubt. Damit verdeutlichen diese Ergebnisse den Zusammenhang von Moleküldesign, Phasenverhalten und optischen Eigenschaften. Interessanterweise tritt bei Verbindungen mit einer latenten flüssigkristallinen Phase auch eine Nachentwicklung auf, d. h. es wird ein Anstieg der

lichtinduzierten Orientierung beobachtet, welcher nach dem Ausschalten der Einschreiblichtquelle einsetzt. Bemerkenswert ist, dass die lichtinduzierte Ordnung in solchen Domänen deutlich erhöht werden kann, wenn die beschriebenen Filme spezifischen Wärmebehandlungen unterzogen werden. Eine solche Behandlung ermöglicht in der Folge eine Anpassung der lichtinduzierten Orientierung sowohl mittels Licht wie auch mittels Temperatur.

In aufbauenden Versuchen werden Dünnfilme von Trisazobenzolen zur Orientierung von kommerziell erhältlichen, nematischen Flüssigkristallen verwendet. Verschiedene Oberflächencharakterisierungstechniken und einhergehende optische Untersuchungen weisen darauf hin, dass die Orientierung der flüssigkristallinen Verbindungen durch eine intermolekulare anziehende Wechselwirkung zwischen der Orientierungsschicht und dem Flüsskigkristall hervorgerufen wird. Diese Ergebnisse schliessen folglich aus, dass die Orientierung durch eine Reliefstruktur in der Oberfläche verursacht wird. Aus diesen Gründen ermöglichen solche azobenzolbasierten Filme eine unkomplizierte Herstellung vielfältiger lichtinduzierter Strukturierungen, ohne dazu eine aufwändige Bearbeitung der Filmoberfläche zu benötigen.

In einem weiterführenden Abschnitt wird der Zusammenhang von Ordnung und elektronischen Eigenschaften anhand von Mischungen kleiner halbleitender Moleküle mit isolierenden Polymeren untersucht. Im Vergleich zu Einkomponentensystemen erlauben solche Mischungen eine Einflussnahme auf ihr Phasenverhalten und ihre Mikrostruktur sowohl mittels Temperatur als auch über die Zusammensetzung, was den Spielraum an möglichen Verarbeitungsverfahren erheblich erweitert. Ein weiterer positiver Effekt ist dabei, dass sich Dünnfilme dank der Zugabe eines Makromoleküls wesentlich leichter aus einer Lösung herstellen lassen. Eine Analyse des Zusammenhangs von Struktur und Eigenschaften von solchen Mischungen zeigt dabei deutlich, dass der Grad an fest-fest Phasenseparation, welcher während der Verarbeitung eingestellt wird, einen erheblichen Einfluss auf die Leistung der produzierten elektronischen Bauelemente hat. Eine Möglichkeit, um die gewünschten vorteilhaften Mikrostrukturen zu erzielen, basiert auf einer exakten Kontrolle der Eintrocknungsgeschwindigkeit von Filmen während ihrer Herstellung. Im vorliegenden Fall bedeutet dies, dass die Verarbeitungstemperatur erhöht wird, was zu feinstrukturierten und homogenen aktiven Schichten führt. Diese wiederum verfügen über gute charakteristische Kennwerte in sogenannten Feldeffekttransistoren. Für viele Anwendungen ist es jedoch von erheblichem Vorteil, wenn die halbleitenden Filme bei Raumtemperatur hergestellt werden können. Unter diesen Voraussetzungen kann das

Phasenverhalten alternativ auch über eine Anpassung der Molekülstruktur zweckdienlich verändert werden. Diese Methode eröffnet neue Verarbeitungsmöglichkeiten für die untersuchten halbleitenden Mischungen, welche die Herstellung von Filmen bei Raumtemperatur ermöglichen, ohne dabei Einbussen bezüglich ihrer elektronischen Eigenschaften in Kauf nehmen zu müssen. So können Filme mit 70 bis 80 Gew.-% Isolatorgehalt hergestellt werden, welche elektronische Kennwerte aufweisen, die mit jenen des reinen niedermolekularen organischen Halbleiters vergleichbar sind.

Chapter I

Introduction

BACKGROUND

Organic compounds offer versatile functionalities such as beneficial optic, electronic or optoelectronic characteristics that are relevant for a variety of applications, *e.g.* such as holographic devices,[1-7] field-effect transistors,[8-12] non-volatile data storage media,[13-15] photovoltaic cells,[16-23] light-emitting diodes,[24-29] sensors,[30-34] etc. Most often, there is a strong interdependence between the performance and the order of these organic species over a broad spectrum of length scales. Consequently, control of order over that range of length scales is required to tailor functionalities or impart new functionalities to such materials.

Length scales

In order to allow for a meaningful exploration and exploitation of structure-related order properties on different length scales, the essential structural domains and their size need to be defined first. The highest, macroscopic level defines the system, representing the arrangement of different macroscopic components that interact with each other. Macroscopic objects typically can be seen by the unaided eye and are in the range of >100 μm (*cf.* Table 1).[35] A descriptive example of such a system is a clockwork, in which carefully inter-coordinated cogwheels, springs and conn-rods drive the device. The design of a system, of course, is critical to ensure proper functioning of it. Accordingly, a clock can only fulfill its purpose, *i.e.* display the time, if each individual component performs reliably. In this example, the mode of operation is depending, among other things, on the components' macroscopic characteristics, *e.g.* their shape and mechanical properties. An off-sized cogwheel, for instance, cannot properly interact with its neighbors and, consequently, causes a system failure. Furthermore, a cogwheel should be able to transfer mechanical energy to its neighbors, demanding mechanical properties that allow an interaction without causing any malfunctioning, fracture, deformation or excessive wear to the involved cogs. In addition to shape and mechanical properties, other important macroscopic characteristics of an object are transparency, color, refractive index, (semi)conductivity, magnetism, etc.[35] However, many of these macroscopic aspects can only be understood, when considering the next smaller structural length scale, *i.e.* the microscopic level. As already implied by the Greek prefix "micro", this scale includes structural features in the micrometer (10^{-6} m) range and, thus, microscopic structures and processes typically cannot be observed with the unaided eye anymore. In the example of a

Table 1. Overview of approximate length scales discussed in this work with selective examples and dependent relationships.

	length scale	approx. dimensions	examples/description	factors of influence
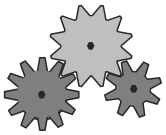	*system*	>100 μm	clockwork, engine, door lock, ball pen, fridge, car, plane, laser, transistor, etc.	system design, macroscopic properties of individual components
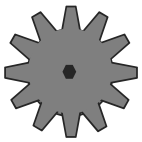	*macroscopic*	>100 μm	cogwheel, spring, handgrip, drinking glass, spoon, needle, key, coat hook, etc.	geometry, shape, type of material (metal, ceramic, polymer, composite), microstructure
	*microscopic*	10 nm - 100 μm	grain size, crystallinity, degree of phase separation, character of phase distribution	chemical nature of component(s), processing, composition (multi-component systems)
	*molecular*	1 Å - 100 μm[a]	molecular interaction, *i.e.* Coulomb, dipole-dipole, H-bridges, Van der Waals, π-stacking, entanglements	chemical structure (molecular design), ambient medium, polymers: molecular weight
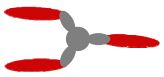	*sub-molecular*	small molecules 1 Å - 1 nm polymers 1 Å - 100 μm	chemical modifications (*cf.* Table 2)	synthetic procedures

a length that chains of uncured technical polymers reach. Biomacromolecules and polymer networks can excess the upper limit value considerably.

cogwheel in a clockwork that is, for instance, comprised of a semi-crystalline commodity polymer, it can be readily understood, how the microstructure strongly affects the macroscopic behavior. It is well-known that mechanical performance, *e.g.* Young's modulus, strength, wear resistance, etc., of such materials are related to length of constituent macromolecules or molecular weight.[36-43] If the molecular weight is low and, thus, the polymer chains short, the molecules are unable to physically entangle, resulting in the formation of extended-chain and unconnected crystallites (Figure 1). As a consequence of the absence of any molecular connections between the individual crystalline domains, components fabricated with such species feature poor mechanical characteristics. A cogwheel that is based on such oligomeric species is brittle and/or deforms very quickly under the influence of stress or shear and may feature mechanical properties comparable to paraffin wax. However, at increasing the molecular weight, an individual macromolecule can participate in more than one crystalline domain and more and more physical

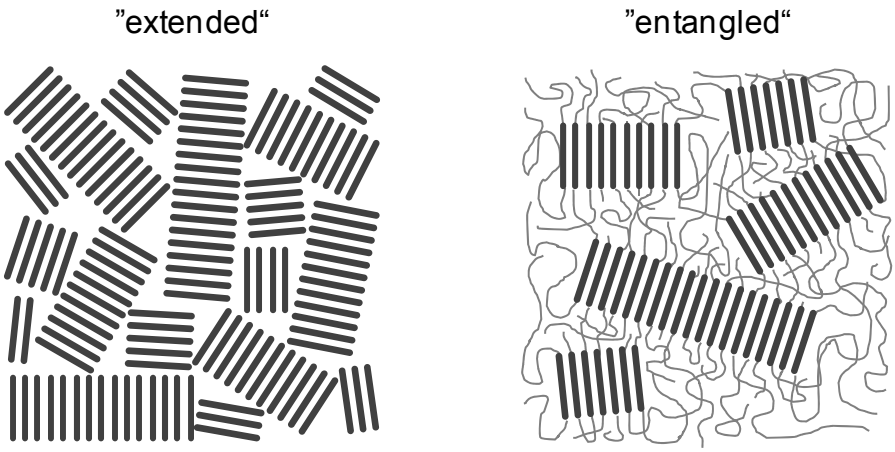

Figure 1. Schematic of the microstructures of (semi-crystalline) polymers of low-molecular weight (left) and high-molecular weight (right). Only in the latter case polymer chains are sufficiently long to participate in several molecularly ordered lamellae, significantly enhancing the mechanical performance of components fabricated with such materials.

entanglements are induced, resulting in the formation of amorphous regions that molecularly connect the ordered crystallites (Figure 1).[37,44] Hence, this (semi-crystalline) structure is significantly increasing the mechanical robustness of components fabricated with polymers of sufficient molecular weight and, consequently, is considerably enhancing the system reliability. Inevitably, also further structural length scales need to be considered, *i.e.* dimensions below the microscopic range. Whereas the molecular level involves physical interactions of a specific molecule with its neighbors, including Coulomb-interactions, dipole-dipole interactions, H-bridges, Van der Waals forces, π-stacking and entanglement of polymer chains, the sub-molecular level is addressing chemical modifications of a certain type of molecules, including molecular weight (change of chain-length), addition of substituents, modification of substituents, molecular rearrangements etc. (Tables 1 and 2).

As the above illustrates, the molecular weight dependence of mechanical properties of an object is a prime example demonstrating the direct correlation of macroscopic characteristics (robustness) and the molecular design (molecular weight, *i.e.* chain-length). Hence, considerations on one isolated length scale alone cannot provide a comprehensive understanding of materials characteristics and functionalities, emphasizing the importance of bridging all structural scales ranging from the sub-molecular to the macroscopic.

Bridging scales

Another example illustrating the interdependence of material properties and structural scales is related to the crystallization behavior of (semi-crystalline) polymers. Typically, nucleation and crystallization of macromolecular species such as isotactic polypropylene (i-PP), is hampered by their long-chain nature, often resulting in the formation of large spherulites of several tens of micrometers for this particular polymer, when crystallized from the melt.[45,46] Such a spherulitic microstructure is known to strongly scatter visible light, resulting in a milky, turbid appearance of macroscopic objects fabricated in this way. Hence, for producing objects of enhanced optical characteristics, for example, transparent containers, processing has to be tailored toward alter the structure of the solid polymer. This can either be realized, to a certain extent, by adjusting different processing parameters, such as, *e.g.,* cooling rate[47-50] and pressure,[51,52] or, alternatively, by employing specific additives that are able to nucleate the polymer and, therewith, modify the resulting microstructure. One class of such nucleating agents is based on small molecules that exhibit the characteristic of forming nanofibrillar networks during cooling of the additive:polymer binary melt.[53-68] The generated fibrils provide surfaces for heterogeneous nucleation of the macromolecules, drastically reducing the supercooling required for solidification and, simultaneously, the size and shape of crystallites formed considerably. Consequently, addition of a judiciously chosen additive allows fabrication of macroscopic components with significantly enhanced clarity and reduced opacity and haze. For this reason, this type of additives is also referred as clarifying agents. One group of such clarifiers that was intensely investigated in the past are substituted 1,3,5-benzene trisamides.[61,63-66] Screening of a large number of such compounds for their performance for increasing the transparency of i-PP impressively demonstrated the major effect of even minor modifications of the molecular design, *i.e.* change of the position of a specific functional group or replacement of a substituent by a slightly different group, on the microstructure induced and, therewith, on the optical appearance of a macroscopic sample produced (Table 2). Hence, clarifying agents are yet another example demonstrating the interdependence of structural order and properties over multiple length scales.

Material systems

As the above examples illustrate, organic compounds, small-molecular, oligomeric or macromolecular, offer a rich chemistry with an extraordinary broad spectrum of possibilities for developing new compounds or for modifying the chemical structure of

Table 2. Chemical structures and selected optical characteristics of 1,3,5-benzene trisamide based clarifying agents, as well as molecular concept of optical active compounds employed in this work.

compound	manipulated properties[a]		synthetic modification
core: 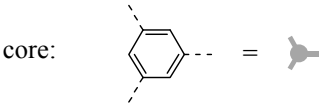	haze (%)[b]	clarity (%)[c]	
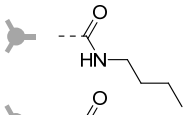	57.9	95.8	insertion of an additional methylene group
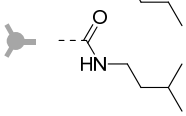	27.4	98.7	
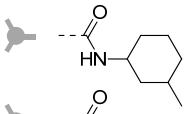	96.1	84.0	shifting of a methylene group by one position
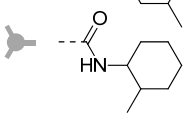	37.2	97.6	
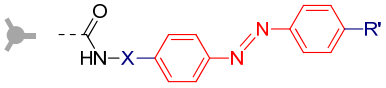	X: flexible spacer R': polar end-group		insertion of an *optical active azobenzene unit*

a data adopted from references 64, 65.
b fraction of visible light that is scattered at angles >2.5°, *i.e.* a measure for turbidity.
c fraction of visible light that is scattered at angles <2.5°, *i.e.* defining the sharpness of a viewed object.

specific molecules and, therewith, provide control of molecular interactions, microstructure and, ultimately, macroscopic characteristics. Compared to polymeric species, small molecules generally feature well-defined molecular structures and corresponding physicochemical properties. In addition, they can conveniently be homogeneously incorporated in polymeric matrices, allowing order-related studies of multi-component systems, similar to the clarifier:polypropylene blends described above. Therefore, small-molecular organic species were selected in this thesis to unravel the interdependence of order and materials properties over the range of length scales addressed above, *i.e.* from the sub-molecular to the macroscopic. Particular physical functionalities are imparted to the systems explored, allowing detailed characterization of the effect of molecular design and processing conditions at the microscopic and macroscopic levels. These functionalities provide a tool to measure the efficiency of order control and, besides, yield quantitative structure-related information of the systems explored.

Based on previous, successful experience with compounds based on the 1,3,5-benzene trisamide family for the development of clarifying agents, the chemical concept behind the synthesis of these species is further explored for certain structure-property investigations

described in this work. To this end, optical active azobenzene moieties are incorporated in the side-groups of these compounds, allowing to address these chromophore units with light and, hence, providing optical functionality to this class of molecules.[5,69-82] When exposing (initially amorphous) thin films of such trisazobenzene derivatives to linearly polarized light, photo-alignment is induced that results in a change in refractive index. Hence, the effect of sub-molecular modifications on macroscopic, photo-induced orientation can easily be monitored with various optical characterization techniques, permitting detailed investigation of the interrelation of chemical structure, phase behavior and optical performance.

Besides optical characteristics, another functionality that strongly depends on structural order on sub-macroscopic length scales is the (semi)conductivity of organic species.[83-94] Thus, in this study also small-molecular semiconductors are employed to investigate the influence of chemical tailoring and processing on microstructures induced and, consequently, on the electronic performance of devices fabricated with them. To facilitate processing of the small-molecular semiconductors, insulating semi-crystalline commodity polymers are added to the small-molecular species, providing improved film-forming characteristics of the resulting blend systems. Furthermore, this approach allows expansion of processing options, as in multi-component mixtures the phase behavior can be controlled *via* composition *and* temperature. In addition to chemical tailoring the molecular structure of the functional species, differing processing routes provide an effective tool for manipulating microstructures and, thus, for fine tuning the electronic characteristics of these systems.

SCOPE AND SURVEY OF THESIS

The focus of the research presented in this thesis is to develop comprehensive insight in structure-property interrelationships of small-molecular organic species over a wide range of length scales, ranging from the sub-molecular to the macroscopic level. To this end, model systems are employed that allow modification of structural order by tailoring the molecular design or, alternatively, by controlling processing parameters. The influence of structural manipulation is evaluated by monitoring different optical and electronic functionalities. The examples presented in the following chapters will demonstrate the importance of bridging different length scales to obtain a detailed understanding of

structure-property interrelations in functional organic materials needed to be able to fine tune the performance of device architectures fabricated with them.

In *Chapters II and III*, the effect of sub-molecular structure modifications on the phase behavior and optical characteristics of a series of trisazobenzene derivatives are presented. Optical properties are evaluated with different characterization techniques including, *e.g.*, ultraviolet/visible light (UV/Vis) spectroscopy, infrared (IR) spectroscopy, optical microscopy and holographic experiments.

In *Chapter IV*, the structure-property interrelations are expanded to trisazobenzene derivatives that are employed as alignment layers[73,95-101] for conventional (nematic) liquid-crystalline (LC) compounds. The interaction of trisazobenzene alignment layers and deposited LC species are investigated with scanning electron microscopy (SEM) and atomic force microscopy (AFM). Optical characterization techniques are used to provide deeper insight in the alignment of LC layers.

In *Chapters V and VI* blends of semiconducting small molecules and insulating polymers are presented that allow detailed investigation of microstructural implications on electronic characteristics. Whereas in Chapter V the solid-state structure is controlled *via* specific processing parameters such as solidification rate and blend composition, in Chapter VI the microstructure is tailored by adjusting the molecular design of the organic semiconductor species. A comprehensive study of the interrelated chemical structure, processing parameters, phase behavior and electronic performance in field-effect transistors (FETs) of blend systems is presented, and shown to be an efficient tool towards unraveling structure-property relations over a wide range of length scales in such systems.

Finally, in *Chapter VII* general conclusions and an outlook are presented.

The work described in this thesis is of interdisciplinary character, including the fields of organic chemistry, material science and experimental physics. Hence, several projects were carried out in collaborations with other research groups. This author's contributions included material science aspects, phase behavior studies, processing issues and structural- and optical characterization.

The synthesis of trisazobenzene compounds discussed in *Chapters II - IV* as well as the associated holographic characterization were performed in the framework of a tremendously fruitful collaboration with the University of Bayreuth, Germany. The synthetic part was conducted by Dr. Klaus Kreger in the group of Prof. Hans-Werner Schmidt. Holographic experiments were carried out in collaboration with Dr. Hubert Audorff and Prof. Lothar Kador. For completeness of this thesis, synthetic procedures and characterization of trisazobenzene derivatives explored are described in the *Appendix*. The preparation of liquid-crystal cells presented in *Chapter IV* was performed with advice of Ivelina Sishmanova, Prof. Cees W. M. Bastiaansen and Prof. Dick J. Broer, of the Technical University of Eindhoven, The Netherlands. Further substantial contributions were made by Drs. Maria-Laura Santarelli, University of Rome Sapienza, Italy, and Luigi Vaccaro and Assunta Marrocchi, University of Perugia, Italy, who synthesized the arylacetylene derivative investigated in *Chapter VI*. Electronic characterization of the binary blends explored in *Chapters V and VI* was carried out in very fruitful collaboration with Mohammed A. Baklar and Liyang Yu in the group of Dr. Natalie Stingelin, Imperial College London, United Kingdom. These measurements were performed in the laboratories of Merck Chemicals Ldt., Southampton, United Kingdom, (*Chapter V*) and of Dr. Thomas D. Anthopoulos, Imperial College London, United Kingdom (*Chapter VI*).

This dissertation is based on the following collection of manuscripts:

Chapter II. K. Kreger, P. Wolfer, H. Audorff, L. Kador, N. Stingelin-Stutzmann, P. Smith, H.-W. Schmidt, *J. Am. Chem. Soc.* **2010**, *132*, 509.
"Stable Holographic Gratings with Small-Molecular Trisazobenzene Derivatives"

Chapter III. P. Wolfer, H. Audorff, K. Kreger, L. Kador, H.-W. Schmidt, N. Stingelin, P. Smith, *J. Mater. Chem.* **2011**, *21*, 4339.
"Photo-Induced Molecular Alignment of Trisazobenzene Derivatives"

Chapter IV. P. Wolfer, K. Kreger, H.-W. Schmidt, N. Stingelin, P. Smith, in preparation
"Liquid Crystal Alignment with Photo-Oriented Trisazobenzene Layers"

Chapter V. P. Wolfer, C. Müller, P. Smith, M. A. Baklar, N. Stingelin-Stutzmann, *Synth. Met.* **2007**, *157*, 827.
"*α*-Quaterthiophene:Polyethylene Blends: Phase Behavior and Electronic Properties"

Chapter VI. P. Wolfer, M. L. Santarelli, L. Vaccaro, L. Yu, T. D. Anthopoulos, P. Smith, N. Stingelin, A. Marrocchi, *Org. Electron.* **2011**, submitted.
"Influence of Molecular Architecture and Processing on Properties of Semiconducting Arylacetylene:Insulating Poly(vinylidene fluoride) Blends"

In addition, following patent application is related to this project:

WO 2008/001123. S. Goffri, C. Müller, P. Wolfer, N. Stingelin-Stutzmann, C. P. Radano, R. A. J. Janssen, P. Smith, H. Sirringhaus.
"Blended Polymer FETs"

References

(1) M. Eich, J. H. Wendorff, B. Reck, H. Ringsdorf, *Macromol. Chem. Rapid Commun.* **1987**, *8*, 59.

(2) R. H. Berg, S. Hvilsted, P. S. Ramanujam, *Nature* **1996**, *383*, 505.

(3) L. Nikolova, T. Todorov, M. Ivanov, F. Andruzzi, S. Hvilsted, P. S. Ramanujam, *Appl. Opt.* **1996**, *35*, 3835.

(4) Y. Sabi, M. Yamamoto, H. Watanabe, T. Bieringer, D. Haarer, R. Hagen, S. G. Kostromine, H. Berneth, *Jpn. J. Appl. Phys.* **2001**, *40*, 1613.

(5) R. Hagen, T. Bieringer, *Adv. Mater.* **2001**, *13*, 1805.

(6) M. Häckel, L. Kador, D. Kropp, H.-W. Schmidt, *Adv. Mater.* **2007**, *19*, 227.

(7) H. Audorff, K. Kreger, R. Walker, D. Haarer, L. Kador, H.-W. Schmidt, *Adv. Polym. Sci.* **2010**, *228*, 59.

(8) G. Horowitz, D. Fichou, X. Z. Peng, Z. G. Xu, F. Garnier, *Solid State Commun.* **1989**, *72*, 381.

(9) F. Garnier, R. Hajlaoui, A. Yassar, P. Srivastava, *Science* **1994**, *265*, 1684.

(10) G. Horowitz, *Adv. Mater.* **1998**, *10*, 365.

(11) H. Sirringhaus, N. Tessler, R. H. Friend, *Science* **1998**, *280*, 1741.

(12) H. E. Katz, Z. N. Bao, S. L. Gilat, *Acc. Chem. Res.* **2001**, *24*, 359.

(13) J. C. Scott, L. D. Bozano, *Adv. Mater.* **2007**, *19*, 1451.

(14) K. Asadi, D. M. de Leeuw, B. de Boer, P. W. M. Blom, *Nature Mater.* **2008**, *7*, 547.

(15) K. Asadi, T. G. de Boer, P. W. M. Blom, D. M. de Leeuw, *Adv. Funct. Mater.* **2009**, *19*, 3173.

(16) C. W. Tang, *Appl. Phys. Lett.* **1986**, *48*, 183.

(17) J. J. M. Halls, C. A. Walsh, N. C. Greenham, E. A. Marseglia, R. H. Friend, S. C. Moratti, A. B. Holmes, *Nature* **1995**, *376*, 498.

(18) G. Yu, J. Gao, J. C. Hummelen, F. Wudl, A. J. Heeger, *Science* **1995**, *270*, 1789.

(19) M. Granström, K. Petrisch, A. C. Arias, A. Lux, M. R. Andersson, R. H. Friend, *Nature* **1998**, *395*, 257.

(20) A. Hagfeldt, M. Grätzel, *Acc. Chem. Res.* **2000**, *33*, 269.

(21) C. J. Brabec, *Sol. Energy Mater. Sol. Cells* **2004**, *83*, 273.

(22) G. Li, V. Shrotriya, J. Huang, Y. Yao, T. Moriarty, K. Emery, Y. Yang, *Nature Mater.* **2005**, *4*, 864.

(23) S.-C. Lo, P. L. Burn, *Chem. Rev.* **2007**, *107*, 1097.

(24) C. W. Tang, S. A. VanSlyke, *Appl. Phys. Lett.* **1987**, *51*, 913.

(25) J. H. Borroughes, D. D. C. Bradley, A. R. Brown, R. N. Marks, K. Mackay, R. H. Friend, P. L. Burns, A. B. Holmes, *Nature* **1990**, *347*, 539.

(26) P. L. Burn, A. B. Holmes, A. Kraft, D. D. C. Bradley, A. R. Brown, R. H. Friend, R. W. Gymer, *Nature* **1992**, *356*, 47.

(27) P. Furuta, J. Brooks, M. E. Thompson, J. M. J. Fréchet, *J. Am. Chem. Soc.* **2003**, *125*, 13165.

(28) A. P. Kulkarni, C. J. Tonzola, A. Babel, S. A. Jenekhe, *Chem. Mater.* **2004**, *16*, 4556.

(29) P. L. Burn, S. C. Lo, I. D. W. Samuel, *Adv. Mater.* **2007**, *19*, 1675.

(30) P. N. Bartlett, S. K. Ling-Chung, *Sensors and Actuators* **1989**, *20*, 287.

(31) B. Crone, A. Dodabalapur, A. Gelperin, L. Torsi, H. E. Katz, A. J. Lovinger, Z. Bao, *Appl. Phys. Lett.* **2001**, *78*, 2229.

(32) T. Someya, H. E. Katz, A. Gelperin, A. J. Lovinger, A. Dodabalapur, *Appl. Phys. Lett.* **2002**, *81*, 3079.

(33) H. Cavaye, A. R. G. Smith, M. James, A. Nelson, P. L. Burn, I. R. Gentle, S.-C. Lo, P. Meredith, *Langmuir* **2009**, *25*, 12800.

(34) Y. Han, K. Pacheco, C. W. M. Bastiaansen, D. J. Broer, R. P. Sijbesma, *J. Am. Chem. Soc.* **2010**, *132*, 2961.

(35) J. N. Lalena, D. A. Cleary, *Principles of Inorganic Materials Design, Second Edition*; John Wiley & Sons, Inc.: Hoboken, NJ, USA, **2010**.

(36) P. J. Flory, *J. Am. Chem. Soc.* **1945**, *67*, 2048; A. M. Snooke, M. Harris, *Ind. Eng. Chem.* **1945**, *37*, 478.

(37) P. I. Vincent, *Polymer*, **1960**, *1*, 425.

(38) D. C. Prevorsek, *J. Polym. Sci. C* **1971**, *32*, 343.

(39) J. R. Martin, J. F. Johnson, A. R. Cooper, *J. Macromol. Sci. Revs. Macromol. Chem.* **1972**, *C8*, 57.

(40) P. Smith, P. J. Lemstra, J. P. L. Pijpers, *J. Polym. Sci., Polym. Phys. Ed.* **1982**, *20*, 2229.

(41) T.-Y. Hu, N. S. Eiss Jr., *Wear* **1983**, *84*, 203.

(42) R. Popli, L. Mandelkern, *J. Polym. Sci. B: Polym. Phys.* **1987**, *25*, 441.

(43) T. A. Tervoort, J. Visjager, P. Smith, *Macromolecules* **2002**, *35*, 8467.

(44) H. D. Keith, F. J. Padden Jr., R. G. Vadimsky, *J. Polym. Sci. A* **1966**, *4*, 267.

(45) F. J. Padden Jr., H. D. Keith, *J. Appl. Phys.* **1959**, *30*, 1479.

(46) J. Varga, *J. Mater. Sci.* **1992**, *27*, 2557.

(47) S. Piccarolo, *J. Macromol. Sci. Phys. B* **1992**, *31*, 501.

(48) B. E. Tiganis, R. A. Shanks, Y. Long, *J. Appl. Polym. Sci.* **1996**, *59*, 663.

(49) K. Sondergaard, P. Mina, S. Piccarolo, *J. Macromol. Sci. Phys. B* **1997**, *36*, 733.

(50) A. Wasiak, P. Sajkiewicz, A. Wozniak, *J. Polym. Sci. Polym. Phys.* **1999**, *37*, 2821.

(51) F. Asmussen, W. Schiwon, K. Ueberreiter, *Colloid & Polymer Sci.* **1976**, *254*, 290.

(52) V. la Carrubba, V. Brucato, S. Piccarolo, *Polym. Eng. Sci.* **2000**, *40*, 2430.

(53) K. Hamada, H. Uchiyama, US Patent 4,016,118 **1977**.

(54) R. L. Mahaffey, US Patent 4,371,645 **1983**.

(55) R. L. Mahaffey, US Patent 4,419,473 **1983**.

(56) G. Marschell, US Patent 4,562,265 **1985**.

(57) A. Thierry, C. Straupe, B. Lotz, J.-C. Wittmann, *Polym. Commun.* **1990**, *31*, 299.

(58) J. W. Rekers, US Patent 5,049,605 **1991**.

(59) M. J. Mannion, US Patent 5,198,484 **1993**.

(60) T. A. Shepard, C. R. Delsorbo, R. M. Louth, J. L. Walborn, D. A. Norman, N. G. Harvey, R. J. Spontak, *J. Polym. Sci. Polym. Phys.* **1997**, *35*, 2617.

(61) H.-W. Schmidt, P. Smith, M. Blomenhofer, PCT WO 02/46300 A2 **2002**.

(62) M. Kristiansen, M. Werner, T. Tervoort, P. Smith, M. Blomenhofer, H.-W. Schmidt, *Macromolecules* **2003**, *36*, 5150.

(63) H.-W. Schmidt, M. Blomenhofer, K. Stoll, H.-R. Meier, PCT WO 2004, 072168 A2 **2004**.

(64) P. M. Kristiansen, Ph.D. thesis, ETH Zurich, **2004**.

(65) M. Blomenhofer, S. Ganzleben, D. Hanft, H.-W. Schmidt, M. Kristiansen, P. Smith, K. Stoll, D. Mäder, K. Hoffmann, *Macromolecules* **2005**, *38*, 3688.

(66) P. M. Kristiansen, A. Gress, P. Smith, D. Hanft, H.-W. Schmidt, *Polymer* **2006**, *47*, 249.

(67) C. Xie, J. Li, J. Xia, PCT WO 2006/044187 A1 **2006**.

(68) C. Xie, L. R. Rieth, T. D. Danielson, PCT WO 2007/127067 A1 **2007**.

(69) G. Zimmerman, L.-Y. Chow, U.-J. Paik, *J. Am. Chem. Soc.* **1958**, *80*, 3528.

(70) G. S. Kumar, D. C. Neckers, *Chem. Rev.* **1989**, *89*, 1915.

(71) H. Rau, Photoisomerization of Azobenzenes. In *Photochemistry and Photophysics*; J. F. Rabek, Ed., CRC Press: Boca Raton, FL, USA, **1990**; Vol. 2, p 119.

(72) M. Eich, J. Wendorff, *J. Opt. Soc. Am. B* **1990**, *7*, 1428.

(73) W. M. Gibbons, P. J. Shannon, S.-T. Sun, B. J. Swetlin, *Nature* **1991**, *351*, 49.

(74) T. Ikeda, O. Tsutsumi, *Science* **1995**, *268*, 1873.

(75) M. Dumont, *Mol. Cryst. Liq. Cryst.* **1996**, *282*, 437.

(76) K. Ichimura, *Chem. Rev.* **2000**, *100*, 1847.

(77) K. Ichimura, S.-K. Oh, M. Nakagawa, *Science* **2000**, *288*, 1624.

(78) A. Natansohn, P. Rochon, *Chem. Rev.* **2002**, *102*, 4139.

(79) Y. Yu, M. Nakano, T. Ikeda, *Nature* **2003**, *425*, 145.

(80) K. D. Harris, R. Cuypers, P. Scheibe, C. L. van Oosten, C. W. M. Bastiaansen, J. Lub, D. J. Broer, *J. Mater. Chem.* **2005**, *15*, 5043.

(81) K. G. Yager, C. J. Barrett, *J. Photochem. Photobiol. A* **2006**, *182*, 250.

(82) Y. Zhao, T. Ikeda, *Smart Light-Responsive Materials: Azobenzene-Containing Polymers and Liquid Crystals*; John Wiley & Sons, Inc.: Hoboken, NJ, USA **2009**.

(83) Y. Cao, P. Smith, *Synth. Met.* **1995**, *69*, 191.

(84) A. Facchetti, M. Mushrush, M.-H. Yoon, G. R. Hutchison, M. A. Ratner, T. J. Marks, *J. Am. Chem. Soc.* **2004**, *126*, 13859.

(85) N. Stingelin-Stutzmann, E. Smits, H. Wondergem, C. Tanase, P. Blom, P. Smith, D. de Leeuw, *Nature Mater.* **2005**, *4*, 601.

(86) R. J. Kline, M. D. McGehee, E. N. Kadnikova, J. Liu, J. M. J. Fréchet, M. F. Toney, *Macromolecules* **2005**, *38*, 3312.

(87) M. Surin, P. Leclère, R. Lazzaroni, J. D. Yuen, G. Wang, D. Moses, A. J. Heeger, S. Cho, K. Lee, *J. Appl. Phys.* **2006**, *100*, 033712-1.

(88) I. McCulloch, M. Heeney, C. Bailey, K. Genevicius, I. MacDonald, M. Shkunov, D. Sparrowe, S. Tierney, R. Wagner, W. Zhang, M. L. Chabinyc, R. J. Kline, M. D. McGehee, M. F. Toney, *Nature Mater.* **2006**, *5*, 328.

(89) A. Salleo, *Mater. Today* **2007**, *10*, 38.

(90) C. Müller, S. Goffri, D. W. Breiby, J. W. Andreasen, H. D. Chanzy, R. A. J. Janssen, M. M. Nielsen, C. P. Radano, H. Sirringhaus, P. Smith, N. Stingelin-Stutzmann, *Adv. Funct. Mater.* **2007**, *17*, 2674.

(91) C. Müller, T. A. M. Ferenczi, M. Campoy-Quiles, J. M. Frost, D. D. C. Bradley, P. Smith, N. Stingelin-Stutzmann, J. Nelson, *Adv. Mater.* **2008**, *20*, 3510.

(92) M. L. Chabinyc, L. H. Jimison, J. Rivnay, A. Salleo, *MRS Bull.* **2008**. *33*, 683.

(93) D. J. Gundlach, J. E. Royer, S. K. Park, S. Subramanian, O. D. Jurchescu, B. H. Hamadani, A. J. Moad, R. J. Kline, L. C. Teague, O. Kirillov, C. A. Richter, J. G. Kushmerick, L. J. Richter, S. R. Parkin, T. N. Jackson, J. E. Anthony, *Nature Mater.* **2008**, *7*, 216.

(94) J. Clark, J.-F. Chang, F. C. Spano, R. H. Friend, C. Silva, *Appl. Phys. Lett.* **2009**, *94*, 163306-1.

(95) D. W. Berreman, *Phys. Rev. Lett.* **1972**, *28*, 1683.

(96) J. Cognard, *Mol. Cryst. Liq. Cryst.* **1982**, *51*, 1.

(97) J. M. Geary, J. W. Goodby, A. R. Kmetz, J. S. Patel, *J. Appl. Phys.* **1987**, *62*, 4100.

(98) K. Ichimura, Y. Suzuki, T. Seki, A. Hosoki, K. Aoki, *Langmuir* **1988**, *4*, 1214.

(99) J. C. Wittmann, P. Smith, *Nature* **1991**, *352*, 414.

(100) S. Varghese, G. P. Crawford, C. W. M. Bastiaansen, D. K. G. de Boer, D. J. Broer, *Appl. Phys. Lett.* **2004**, *85*, 230.

(101) H.-S. Kwok, V. G. Chigrinov, H. Takada, H. Takatsu, *J. Disp. Technol.* **2005**, *1*, 41.

Chapter II

Stable Holographic Gratings with Small-Molecular Trisazobenzene Derivatives

---

INTRODUCTION

Owing to the rich photochemistry of azobenzene chromophores, a large variety of both small-molecular and polymeric compounds has been synthesized for use as smart light-responsive materials in various potential applications.[1] One feature of azobenzene-containing species is their well-known *trans*-to-*cis* isomerization.[2,3] In addition, exposure to linearly polarized light of thin films of these compounds leads to in-plane orientation of chromophores by repeated *trans*-*cis*-*trans* isomerization cycles.[4-6] In holographic experiments, photo-induced alignment in such thin-film architectures obtained with two superimposed lasers was extensively explored for use in high-density data storage.[7-10] On the basis of this technique, optical gratings have been successfully inscribed and highly useful optical characteristics and long-term stability of light-induced orientation have been demonstrated for selected *macro*-molecular species – especially those that feature liquid-crystalline (LC) phases.[11,12] By contrast, related *small*-molecular compounds have been less explored. The latter have the advantage, among other things, of relatively simple synthesis, being of higher purity, resulting in well-defined structures and corresponding physicochemical properties and providing the option of homogeneously incorporating them in polymeric matrices. Hence, in this chapter we set out to focus on those azobenzene chromophores of low-molecular weight and in particular those that are prone to form molecular glasses.

Molecular glasses represent an emerging class of materials which is particularly investigated for potential application in optoelectronic devices, photoconductor drums and photo lithography.[13-17] These compounds combine high glass transition temperatures (T_g) with pronounced – critically important – stable amorphous phases.[18-20] According to Naito *et al*., these features are met by small molecules exhibiting low entropic contributions, resulting in a high T_g, and low enthalpic contributions, minimizing the tendency for crystallization of a vitrified supercooled liquid.[21,22] Furthermore, it was demonstrated that hydrogen bonding between the molecular species may enhance the stability of an amorphous phase in thin films of small molecules.[23]

In recent years, *photochromic* molecular glasses have been investigated by several research groups with particular interest in the formation of surface relief gratings (SRGs).[24-27] In those studies, the light-induced mass transport over micrometer distances driven by the photoisomerization of the above-mentioned azobenzene moieties was demonstrated and characterized for the purposes of optical information storage and surface

structuring. Recently, this feature was investigated for a series of azobenzene-containing molecular glasses, and structure-property relationships between the height of the SRGs and the optical susceptibility of the azobenzene moieties were unveiled.[28] Whereas those compounds were designed to efficiently form *surface relief gratings* with modulation heights up to 600 nm, practical use of azobenzene-containing molecular glasses for fabrication of *volume gratings* has been limited, since photo-induced molecular alignment in thin films typically was lost over a period of days or less. Owing to the promising optical performance, designing photochromic small molecules that can be applied for long-term stable volume gratings remains a challenge of fundamental interest.

On the basis of the design of molecular glasses featuring latent mesogenic character, azobenzene derivatives are presented that are suitable for volume holographic data storage with remarkably stable gratings.

In the approach discussed, compounds that comprise three photoactive side-groups that are linked, but decoupled with spacers of different lengths, to a central core in a C_3-symmetric pattern are employed.[29] Moreover, two trisazobenzene derivatives in which the chromophores are linked directly to the core are utilized as reference compounds. To compensate the reduction of the glass transition temperatures due to the decoupling spacers, the molecules exhibit polar moieties, *i.e.*, amides or esters, between the side-groups and the core. Especially, the first – exhibiting the potential to form hydrogen bonds – will lead to higher glass transition temperatures as well as melting points. In addition to spacers, introduction of terminal dipolar substituents, *e.g.*, methoxy- or cyano-groups, was employed as another effective tool to enhance the mesogenic character of the molecules.

On the basis of a systematic study of a range of the above-described trisazobenzene derivatives it is demonstrated that for optimal holographic performance, design of structures that feature a liquid-crystalline phase at elevated temperatures is critical.

RESULTS AND DISCUSSION

Thermal properties

An overview of the chemical structures of the compounds discussed in this chapter is given in Table 1. The design of the functional side-groups was chosen in such a way that they could either be directly linked to the core or exhibit aliphatic spacers with three and five methylene units, effectuating a decoupling of the chromophores from the central core.

Table 1. Chemical structures, thermal properties and selected holographic characteristics of the trisazobenzene trisamides and trisazobenzene trisesters explored.

compound	T_g (°C)[a]	transition temperatures (°C)[b]	n_1 in 10^{-3} (-)[c]	t (s)[d]
core: 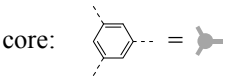				
1 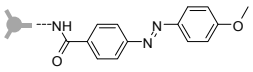	134	G $\xrightarrow{187/233}$ Cr $\xrightarrow{305}$ Iso; Iso $\xrightarrow{134}$ G	14	6
2 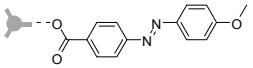	65	Cr $\xrightarrow{163}$ Iso; Iso $\xrightarrow{109}$ Cr	8	2
3 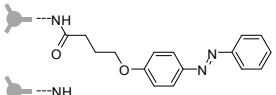	68	G $\xrightarrow{114/156}$ Cr $\xrightarrow{192}$ Iso; Iso $\xrightarrow{68}$ G	3	~0.5
4 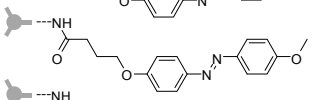	64	Cr $\xrightarrow{232}$ LC $\xrightarrow{167}$ Iso; Iso $\xrightarrow{155}$ LC $\xrightarrow{}$ Cr	5	8
5 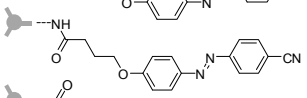	68	Cr $\xrightarrow{251}$ LC $\xrightarrow{193}$ Iso; Iso $\xrightarrow{132}$ LC $\xrightarrow{}$ Cr	29	5
6 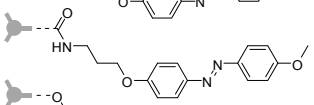	78	Cr $\xrightarrow{228}$ LC $\xrightarrow{189}$ Iso; Iso $\xrightarrow{159}$ LC $\xrightarrow{}$ Cr	23	20
7 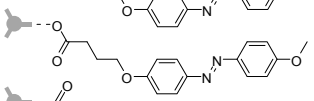	58	Cr $\xrightarrow{162}$ LC $\xrightarrow{146}$ Iso; Iso $\xrightarrow{112}$ LC $\xrightarrow{}$ Cr	43	~350
8 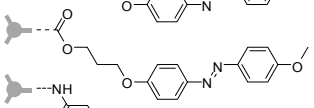	38	Cr $\xrightarrow{169}$ LC $\xrightarrow{177}$ Iso; Iso $\xrightarrow{126}$ LC $\xrightarrow{175}$ Cr	41	10
9 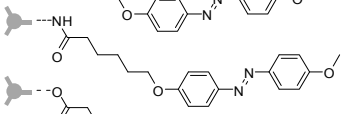	44	Cr $\xrightarrow{199}$ LC $\xrightarrow{150}$ Iso; Iso $\xrightarrow{114}$ LC $\xrightarrow{}$ Cr	27	12
10 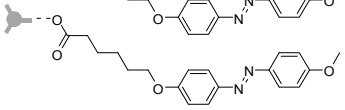	40	Cr $\xrightarrow{150}$ LC $\xrightarrow{138}$ Iso; Iso $\xrightarrow{111}$ LC $\xrightarrow{}$ Cr	23	~200

a T_g: glass transition temperature (determined with differential scanning calorimetry (DSC) first-heating thermograms employing samples that were previously quenched from the melt in liquid nitrogen).
b *Key:* G, glass; Cr, crystalline; LC, liquid-crystalline; Iso, isotropic melt (transitions correspond to peak temperatures of DSC second-heating/cooling thermograms).
c Maximum amplitude of refractive-index modulation at inscription of holographic gratings.
d Writing time to maximum of refractive-index modulation (argon ion laser, 488 nm, 1 W/cm^2).

In addition, different azobenzene chromophores were employed, *i.e.*, azobenzene, (cyanoazo)benzene and (methoxyazo)benzene derivatives. This set, comprising several star-shaped compounds following a construction-kit principle, allowed convenient evaluation of the required properties, *e.g.*, the glass transition temperature, film-forming behavior, and photoactive characteristics.

The thermal properties of the trisazobenzene derivatives were explored with differential scanning calorimetry (DSC) and supported by variable-temperature polarizing optical microscopy. The results of these studies are presented in Table 1 and Figure 1. In general, higher glass transition (T_g), melting (T_m), and crystallization (T_c) temperatures were found for the amide homologues when compared to their ester counterparts. This difference illustrates the influence of a potential hydrogen bond formation in the former species. With

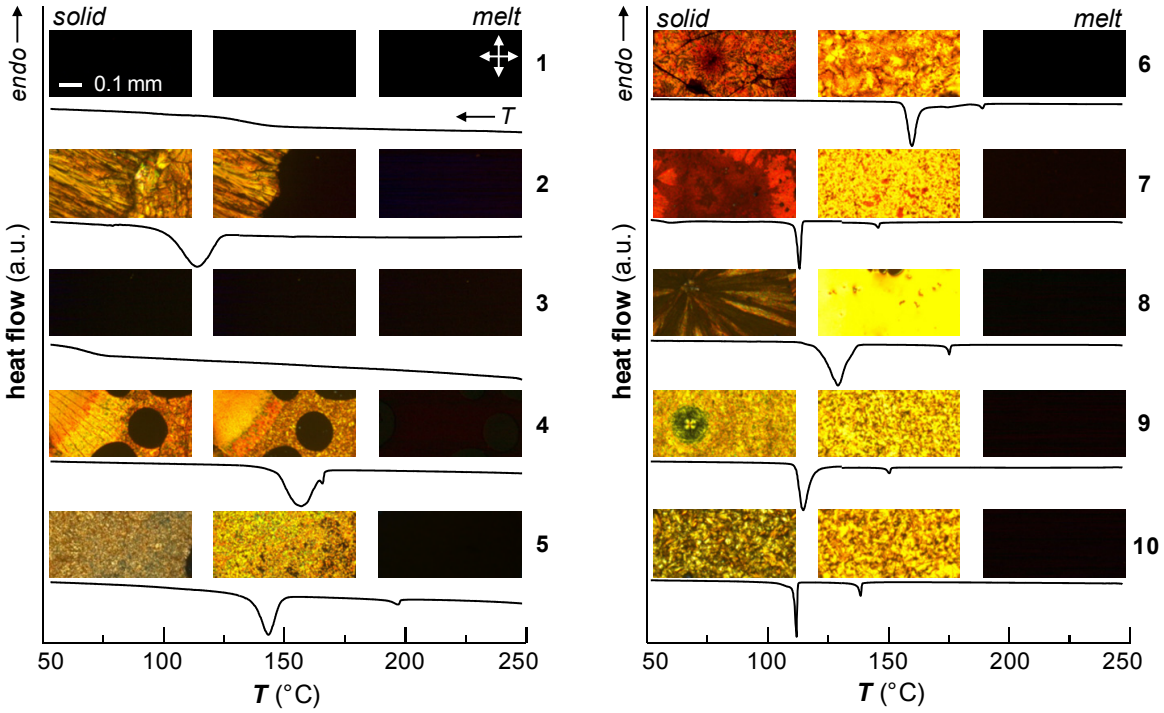

Figure 1. Differential scanning calorimetry (second-cooling thermograms, recorded under N_2 atmosphere at a rate of 10 °C/min) and corresponding variable-temperature polarizing optical microscopy of the trisazobenzene derivatives indicate a liquid-crystalline phase for compounds **4**-**10** (polarizer/analyzer position illustrated with white arrows). Representative images taken, respectively, above, between, and below the relevant transition temperatures.

increasing spacer length, however, this feature is reduced and, owing to strongly increased conformational arrangement possibilities, the influence of the spacers becomes more dominant, leading to a reduction in glass transition temperature with increasing length, as observed for compound series **1**, **4**, **9** and **2**, **7**, **10**. All trisazobenzene derivatives discussed featured a T_g above ambient, and hence, quenching to room temperature resulted in the formation of thermodynamic non-equilibrium amorphous glasses that were found to be stable at ambient conditions.

All compounds that were designed with decoupling spacers between the central core and the side-groups and with terminal substituents, *i.e.*, **4**-**10**, had liquid-crystalline mesophases featured when they were cooled from the isotropic phase at a relatively moderate rate of 10 °C/min (*cf.* Table 1 and Figure 1). The values of the isotropic to liquid-crystalline transition enthalpies were found to be relatively small and ranged from -1.2 to -4.0 kJ/mol. In combination with typical defects in the Schlieren textures as observed in the polarizing microscope, this suggests the presence of nematic phases for trisazobenzenes **4**-**10**. When the compounds were heated from the solidified state at the same rate, on the

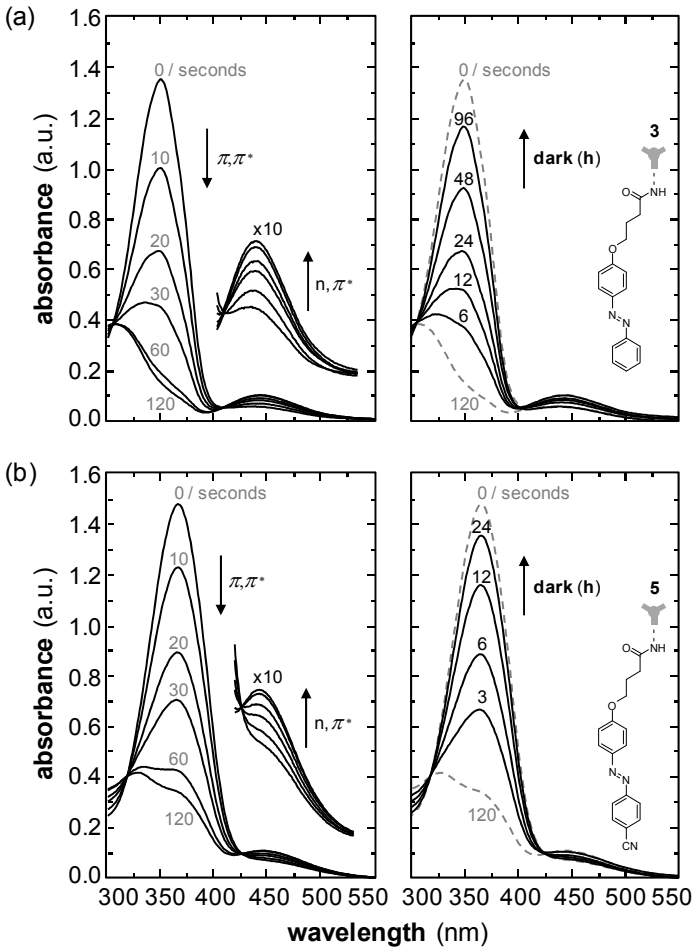

Figure 2. (a) *Cis*-to-*trans* isomerization of compounds **3** and (b) **5** in THF solutions monitored with UV/Vis spectroscopy: left, spectra taken after irradiation with UV light (365 nm) for different exposure times; right, thermal back-relaxation in the dark indicated in hours (solid lines), as well as spectra before and after 120 s of irradiation with UV light (dashed lines). The reversible character of the isomerization is emphasized by isosbestic points at 304 and 407 nm for derivative **3** and at 317 and 425 nm for compound **5**.

other hand, only compound **8** featured an LC phase prior to melting. In contrast to species **4**-**10**, compounds **1** and **3** displayed vitrification and the trisester **2** was found to crystallize upon cooling. The above findings indicate that our design approach towards molecular glasses with liquid-crystalline character was successful with respect to thermal properties.

Photochemical behavior

Determination of the photochemical behavior of the different compounds in tetrahydrofuran (THF) solutions, allowing analysis of the *trans*-to-*cis* as well as the *cis*-to-*trans* isomerization, was employed as a first tool toward the optical characterization of thin films. Reassuringly, a strong photo-response in solutions was found for all species in a series of ultraviolet/visible (UV/Vis) light absorption spectra (Figure 2). This

observation has its origin in the well-known *trans*-to-*cis* isomerization of the azobenzene moieties when exposed to unpolarized, monochromatic UV light. The photochemical reaction continued until a photo-stationary *cis*-rich state was reached. Subsequently, the corresponding back-relaxation to the thermodynamically more stable *trans* state was recorded when the samples were stored in the dark (Figure 2). Whereas during exposure to UV light the π,π^* absorbance decreased drastically, the n,π^* absorbance increased, while the reverse process occurred when keeping the solutions in the dark. Characteristically for reversible photochemical reactions, distinct isosbestic points were present in the sequences of UV/Vis spectra.

Holography

For analyzing the suitability of the trisazobenzene derivatives for photo-induced volume gratings, their response in the solid state was investigated in a set of holographic experiments. To this end, thin, amorphous films were produced by spin-coating THF solutions of the azobenzene compounds. Based on this technique, films of good quality and homogeneous optical properties were fabricated. To increase the film thickness to a level required in holographic experiments, the viscosity of the solutions was enhanced by adding ~5 wt-% (with respect to the solute) atactic, ultra-high molecular weight polystyrene (UHMW-PS), resulting in active layers of ~400 nm average thickness. In contrast to the UV light used for irradiating the solutions in the UV/Vis examinations discussed above, here an argon ion laser at 488 nm was employed. Exposure to this source led to repeated *trans-cis-trans* isomerization cycles of the chromophores in the film. Hence, in-plane orientation of the azobenzene moieties perpendicular to the polarization of the interfering laser beams was induced in irradiated areas.

All compounds showed photo-orientation – here expressed as the amplitude of the refractive-index modulation (n_1) between oriented and non-oriented domains of the optical intensity gratings inscribed in holographic experiments. That optical characteristic was analyzed by the diffraction efficiency of the grating employing a laser diode of 685 nm wavelength, which is outside the absorption band of the azobenzene moieties, thus avoiding affecting the inscribed pattern. A schematic of the experimental setup is presented in the *"Experimental"* and more details describing the generation of holographic gratings have been published elsewhere.[30]

Typical for molecular glasses, n_1 was found to decrease for **1**-**3** after the writing beams were shut off. However, most intriguingly, highly stable photo-orientation was observed

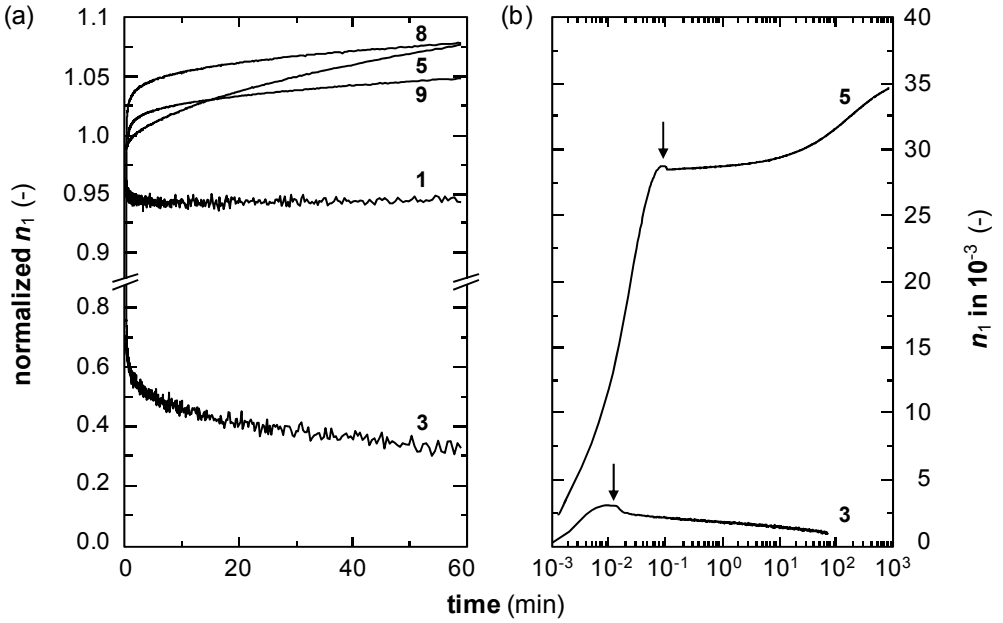

Figure 3. Refractive-index modulation of ~400 nm thin films of small-molecular trisazobenzene compounds, prepared from THF solutions by spin-coating onto glass substrates, as a function of time: (a) amplitude of refractive-index modulation n_1, normalized to 1 when the writing laser was stopped, of **1**, **3**, **5**, **8** and **9**; (b) absolute values for **3** and **5** demonstrating the "post-development" of the latter species on a logarithmic time scale (writing laser off indicated by arrows).

for **4**-**10**. These compounds, which feature spacers *and* additional terminal groups, also displayed a remarkable "post-development" – *i.e.*, an increase of n_1 after writing of the holographic gratings was arrested – exceeding, for instance, 20% for derivative **5**. As a consequence of overexposure and the resulting decrease of contrast between irradiated and unexposed areas, the refractive-index modulation features a maximum during inscription. Thus, this amplification of n_1 is a very useful tool for fabricating holographic intensity gratings with better contrast than achievable with optical writing methods only. To the author's knowledge, this highly beneficial phenomenon so far only has been reported for macromolecular systems[31,32] and for trisazobenzene compounds featuring liquid-crystalline phases at elevated temperatures.[33]

The present library of trisazobenzene compounds permitted realization of a cursory examination of the influence of certain key elements of the molecular architectures of these materials on their performance. Comparison of the characteristics of **1** and **2** with those of species **3**-**10**, for instance, demonstrates that the introduction of a spacer promotes, in most cases, the long-term stability of the photo-induced molecular alignment (*cf.* Table 1 and Figure 3).

An exception is compound **3**, which does not possess a polar end-group and shows a rapid decay of the molecular orientation. This is in contrast to the behavior of all other spacer-decoupled azobenzene derivatives, indicating that these substituents have a positive effect on the stability of photo-aligned patterns. Increasing spacer length, inversion of the amide or ester sequence in the side-groups, and substitution of an amide by an ester or *vice versa*, did, however, not affect the presence of the stability but did have an effect on the absolute values of the refractive-index modulation n_1, writing time t to the maximum of refractive-index modulation, and degree of "post-development". Accordingly, the formation of hydrogen bonds in the amide homologues cannot be the origin of the observed stability found for selected species.

Whereas n_1 typically was found to be higher for compounds featuring a liquid-crystalline phase at elevated temperatures, a clear correlation among n_1, t, and the detailed molecular structure appears to be absent (*cf.* Table 1). Hence, the above observations suggest that two components, *i.e.*, spacers *and* end-groups, are crucial for stable photo-induced alignment of the trisazobenzene derivatives explored. Interestingly, it is found that species featuring these specific architectural elements form molecular glasses with a latent liquid-crystalline phase (*cf.* Table 1 and Figure 3).

CONCLUSIONS

In summary, azobenzene-containing low-molecular-weight compounds have been presented; those that feature liquid-crystalline behavior appear to be attractive non-polymeric candidates for fabrication of stable holographic volume gratings. Different structural elements in the design of these star-shaped molecules allowed tailoring the phase behavior of the compounds explored. Liquid-crystalline character was induced by integrating decoupling spacers between the benzene core and the three azobenzene moieties, as well as additional polar end-groups. The glassy nature of the trisazobenzene derivatives was controlled with polar linkages, *i.e.*, amide or ester bonds, between the core and the spacers. In solutions, reversible *trans*-to-*cis* isomerization was observed for all compounds. In a set of holographic experiments with amorphous films, however, stable intensity gratings only were obtained with species exhibiting decoupling spacers and additional end-groups, *i.e.*, liquid-crystalline molecular glasses **4**-**10**. For the same compounds an unusual "post-development" of the refractive-index modulation was

demonstrated. By contrast, typical for molecular glasses, no stable volume gratings were obtained with reference compounds **1**-**3**, featuring either decoupling spacers *or* polar end-groups only. These results indicate that it is critical for fabricating stable holographic gratings to design structures that feature liquid-crystalline behavior at elevated temperatures but still allow formation of stable amorphous films at ambient. Nevertheless, several characteristics observed in present investigations of the trisazobenzene derivatives, as well as the alignment mechanism on a molecular level, remain unclear and, thus, will be addressed more detailed in *Chapter III*.

EXPERIMENTAL

Materials. Synthesis and characterization of trisazobenzene derivatives **1-10** is described in the *Appendix*. Atactic, ultra-high molecular weight polystyrene (UHMW-PS) (M_w ~30'000 kg/mol) was purchased from Polysciences, Inc., Warrington, PA, USA. Tetrahydrofuran (THF) was supplied by Acros, Geel, Belgium, and dried over a molecular sieve.

Thermal analysis. Differential scanning calorimetry (DSC) was conducted under N_2 atmosphere at a scan rate of 10 °C/min with a Mettler Toledo DSC 822^e instrument. For the determination of the glass transition temperatures T_g of the trisazobenzene derivatives explored, amounts of about 3 mg (±0.2 mg) each compound were sealed in Al standard 40 μl crucibles, heated to 260 °C (except **1**; 310 °C), and subsequently quenched from the melt in liquid nitrogen. For all other phase transition temperatures, similar amounts were analyzed employing identical sample holders.

Glass transition temperatures T_g of all compounds were determined from DSC first-heating thermograms of the melt-quenched samples. All other phase transitions were taken to be the peak temperatures in the DSC second-heating and -cooling thermograms.

Thin-film preparation. Thin films of all compounds were spin-cast at ambient with a Laurell WS-400B-6NPP/LITE spin-coater at 800 rpm from ~2 wt-% THF solutions (total content) onto glass slides. To increase the film thickness to a level required in holographic experiments, ~5 wt-% (with respect to the solute) ultra-high molecular weight polystyrene (UHMW-PS) was added to the solutions.

Ultraviolet/visible (UV/Vis) light analysis. Absorption spectra of about 0.01 mg/ml THF solutions of all compounds were recorded after different exposure times to UV light (365 nm) with a Perkin Elmer Lambda 900 spectrophotometer. Subsequently, the thermal back-relaxation in the dark was analyzed in a second series of measurements.

Optical microscopy. Polarized optical microscopy was carried out with a Leica DMRX polarizing microscope equipped with a Mettler Toledo FP82HT hot stage. The thermal behavior of the compounds was examined applying a continuous N_2 flow and a scan rate of 10 °C/min.

Holography. Holographic experiments were performed using the blue-green line (488 nm) of an argon ion laser. A beam splitter generated two coherent parts of the laser beam, which were brought to interference in the sample plane as schematically depicted in Figure 4.

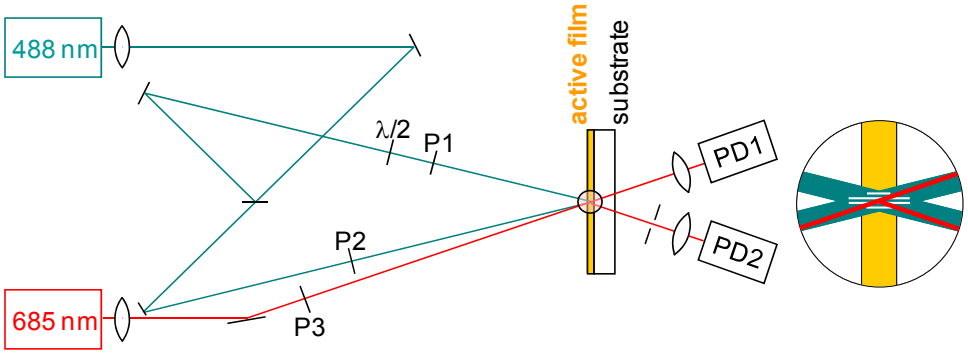

Figure 4. Schematic of the setup used for inscribing holographic volume gratings with an argon ion laser (488 nm) and for monitoring the temporal evolution of the diffraction efficiency with a laser diode (685 nm). P1, P2, P3 denote polarizers, $\lambda/2$ a half-wave plate and PD1, PD2 photodiodes.[34]

The diameter of the s-polarized laser beams was about 1 mm; the intensity of each beam was adjusted to 0.5 W/cm^2. The angle of incidence relative to the surface normal was ±14°, resulting in a grating period of about 1 μm. A laser diode at 685 nm, a wavelength range outside the absorption band of the azobenzene moiety, was used for in-situ monitoring of the diffraction efficiency without affecting the writing process. To determine the diffraction efficiency of the grating, the power of the transmitted and the diffracted beams were measured with two photodiodes. For improving the signal-to-noise ratio, the laser diode was modulated and lock-in detection was used.

References

(1) Y. Zhao, T. Ikeda, *Smart Light-Responsive Materials: Azobenzene-Containing Polymers and Liquid Crystals*; John Wiley & Sons, Inc.: Hoboken, NJ, USA, **2009**.

(2) H. Rau, Photoisomerization of Azobenzenes. In *Photochemistry and Photophysics*; J. F. Rabek, Ed., CRC Press: Boca Raton, FL, USA, **1990**; Vol. 2, p 119.

(3) G. Zimmerman, L.-Y. Chow, U.-J. Paik, *J. Am. Chem. Soc.* **1958**, *80*, 3528.

(4) M. Dumont, *Mol. Cryst. Liq. Cryst.* **1996**, *282*, 437.

(5) R. Hagen, T. Bieringer, *Adv. Mater*. **2001**, *13*, 1805.

(6) K. G. Yager, C. J. Barrett, *J. Photochem. Photobiol. A* **2006**, *182*, 250.

(7) M. Eich, J. H. Wendorff, B. Reck, H. Ringsdorf, *Macromol. Chem. Rapid Commun.* **1987**, *8*, 59.

(8) R. H. Berg, S. Hvilsted, P. S. Ramanujam, *Nature* **1996**, *383*, 505.

(9) L. Nikolova, T. Todorov, M. Ivanov, F. Andruzzi, S. Hvilsted, P. S. Ramanujam, *Appl. Opt*. **1996**, *35*, 3835.

(10) Y. Sabi, M. Yamamoto, H. Watanabe, T. Bieringer, D. Haarer, R. Hagen, S. G. Kostromine, H. Berneth, *Jpn. J. Appl. Phys.* **2001**, *40*, 1613.

(11) A. Natansohn, P. Rochon, *Chem. Rev.* **2002**, *102*, 4139.

(12) S. Hvilsted, F. Andruzzi, C. Kulinna, H. W. Siesler, P. S. Ramanujam, *Macromolecules* **1995**, *28*, 2172.

(13) C. W. Tang, S. A. VanSlyke, *Appl. Phys. Lett.* **1987**, *51*, 913.

(14) U. Bach, D. Lupo, P. Comte, J. E. Moser, F. Weissortel, J. Salbeck, H. Spreitzer, M. Gratzel, *Nature* **1998**, *395*, 583.

(15) J. Dai, S. W. Chang, A. Hamad, D. Yang, N. Felix, C. K. Ober, *Chem. Mater.* **2006**, *18*, 3404.

(16) A. de Silva, N. M. Felix, C. K. Ober, *Adv. Mater.* **2008**, *20*, 3355.

(17) M. Van der Auweraer, F. C. De Schryver, P. M. Borsenberger, H. Bassler, *Adv. Mater.* **1994**, *6*, 199.

(18) Y. Shirota, *J. Mater. Chem.* **2000**, *10*, 1.

(19) P. Strohriegl, J. V. Grazulevicius, *Adv. Mater.* **2002**, *14*, 1439.

(20) Y. Shirota, *J. Mater. Chem.* **2005**, *15*, 75.

(21) K. Naito, A. Miura, *J. Phys. Chem.* **1993**, *97*, 6240.

(22) K. Naito, *Chem. Mater.* **1994**, *6*, 2343.

(23) O. Lebel, T. Maris, M.-E. Perron, E. Demers, J. D. Wuest, *J. Am. Chem. Soc.* **2006**, *128*, 10372.

(24) H. Nakano, T. Takahashi, T. Kadota, Y. Shirota, *Adv. Mater.* **2002**, *14*, 1157.

(25) C. Chun, M.-J. Kim, D. Vak, D. Y. Kim, *J. Mater. Chem.* **2003**, *13*, 2904.

(26) E. Ishow, B. Lebon, Y. He, X. Wang, L. Bouteiller, L. Galmiche, K. Nakatani, *Chem. Mater.* **2006**, *18*, 1261.

(27) M.-J. Kim, E.-M. Seo, D. Vak, D.-Y. Kim, *Chem. Mater.* **2003**, *15*, 4021.

(28) H. Audorff, R. Walker, L. Kador, H.-W. Schmidt, *J. Phys. Chem. B* **2009**, *113*, 3379.

(29) D. M. Junge, D. V. McGrath, *J. Am. Chem. Soc.* **1999**, *121*, 4912.

(30) M. Häckel, L. Kador, D. Kropp, H.-W. Schmidt, *Adv. Mater.* **2007**, *19*, 227.

(31) J. Stumpe, L. Läsker, T. Fischer, M. Rutloh, S. Kostromin, R. Ruhmann, *Thin Solid Films* **1996**, *284-285*, 252.

(32) S. J. Zilker, M. R. Huber, T. Bieringer, D. Haarer, *Appl. Phys. B* **1999**, *68*, 893.

(33) A. Stracke, J. H. Wendorff, D. Goldmann, D. Janietz, *Liq. Cryst.* **2000**, *27*. 1049.

(34) M. Häckel, Ph.D. thesis, University of Bayreuth, **2006**.

Chapter III

Photo-Induced Molecular Alignment of Trisazobenzene Derivatives

INTRODUCTION

Azobenzene-based small organic compounds, that usually are designed to efficiently form surface relief gratings, are an emerging class of materials in the field of holographic applications[1] and as such could also be exploited for the purpose of optical data storage,[2-18] if it were not for the relatively poor stability in time of structures created with them. This phenomenon manifests itself in a decrease of the amplitude of refractive-index modulation n_1 – *i.e.*, the difference in refractive index between irradiated ("inscribed") and unexposed ("non-inscribed") areas – in such volume gratings. This is unfortunate, since small molecules can provide various advantages over macromolecular structures, amongst other things, ease of synthesis and purification and more flexibility in molecular design. In addition, systems based on small molecules generally feature shorter writing times compared to their polymeric counterparts – clearly a technologically much sought-after advantage.[9] As a consequence, there remains a persistent need for small-molecular organic holographic materials that permit manufacture of volume gratings that are stable over time.

Promisingly, selected members of the small-molecular trisazobenzene derivatives introduced in *Chapter II* were found not to suffer from the above mentioned poor holographic stability. As a matter of fact, refractive-index modulations created in films of some of those species did not only not decay with time, but, surprisingly, featured a rather remarkable "post-development", originating in an increase of n_1 after the writing laser was switched off that resulted in an *enhancement* of the contrast of the grating inscribed. This effect is known for certain macromolecular systems;[19-25] yet, for small organic molecules, this desirable phenomenon so far has been observed only for trisazobenzene compounds that featured mesophase(s) at elevated temperatures.[26] A detailed molecular structure-property relation that may explain this useful feature has, however, not yet been advanced.

In this chapter, therefore, the focus is on gaining a better insight into the origin of this attractive "post-development" of members of this trisazo family. For this purpose three compounds were selected which all contain photoactive side-groups that are linked with amide moieties to a central benzene core in C_3-symmetry, with a spacer between the core and the azobenzene chromophore comprising methoxy substituents (Figure 1a). The principal difference between the three species is the length of the decoupling spacer. As a consequence of the different molecular design, the phase behavior of the three derivatives varied: whilst compound **1** formed a molecular glass when cooled from the isotropic melt, **4** and **9** featured liquid-crystalline (LC) phases at elevated temperatures, and were previously shown to display the favorable "post-development" of n_1 (*cf. Chapter II*).

RESULTS AND DISCUSSION

Photo-induced alignment

In a first set of experiments, the molecular origin of the photo-alignment of compounds **1**, **4** and **9** was analyzed, using polarized ultraviolet/visible (UV/Vis) light and infrared (IR) spectroscopy, as well as polarized optical microscopy. For this purpose, the three materials were spin-cast from solution into largely amorphous, thin-film structures, and subsequently illuminated at room temperature with polarized visible light for, respectively, 2 h for UV/Vis spectroscopy and optical microscopy and 20 h for IR-spectroscopy studies.

After irradiation with polarized light ("writing"), films of the two derivatives **4** and **9**, featuring a latent LC phase, displayed a UV/Vis absorbance that was strongly dependent on the direction of polarization of the incident "reading" light beam (Figure 1b), resulting in dichroic ratios, *D*, of, respectively, 1.9 and 2.6. Consistently, when illuminating thin-film architectures of, for instance, **4**, a pronounced, light-induced birefringence was observed in the irradiated areas (*cf.* Figure. 2a). By strong contrast, only a faint optical anisotropy (dichroic ratio of maximum 1.3, Figure 1c) and significantly reduced birefringence was detected in the irradiated films of **1**. For all three compounds, the strongest absorption, which is along the azobenzene chromophores (denoted here as 0°-orientation), was observed perpendicular to the polarization direction of the writing irradiation. In addition, in IR spectroscopy, in which the focus was on the carbonyl-groups (located at the core of the trisazobenzene derivatives) and the methoxy end-groups (Figure 3, respectively, top and bottom), a strong anisotropy was found for the vibrations resulting from the latter moieties (ν_{MeO}(**1**) = 1255 cm^{-1}, ν_{MeO}(**4**) = 1248 cm^{-1}, ν_{MeO}(**9**) = 1249 cm^{-1});[27-31] this was most pronounced for compound **9**. Vibrations associated with the carbonyl moieties ($\nu_{C=O}$(**1**) = 1655 cm^{-1}, $\nu_{C=O}$(**4**) = 1669 cm^{-1}, $\nu_{C=O}$(**9**) = 1664 cm^{-1}),[27-31] in strong contrast, were virtually not affected by exposure to linearly polarized visible light of thin films of all three trisazobenzenes.

Hence, it appears that the short flexible spacers in species **4** and **9** allow the side-groups linking the optically active azobenzene moieties to move relatively independently of the central core. As a consequence, upon irradiation with polarized light, the molecules seem to arrange into a "fork-like" conformation of the side-groups, as schematically depicted in Figure 2b, in agreement with both UV/Vis and IR spectroscopy data. This would explain why these trisazobenzene compounds of latent LC nature display significantly enhanced photo-alignment effects in comparison with those that do not form this mesophase

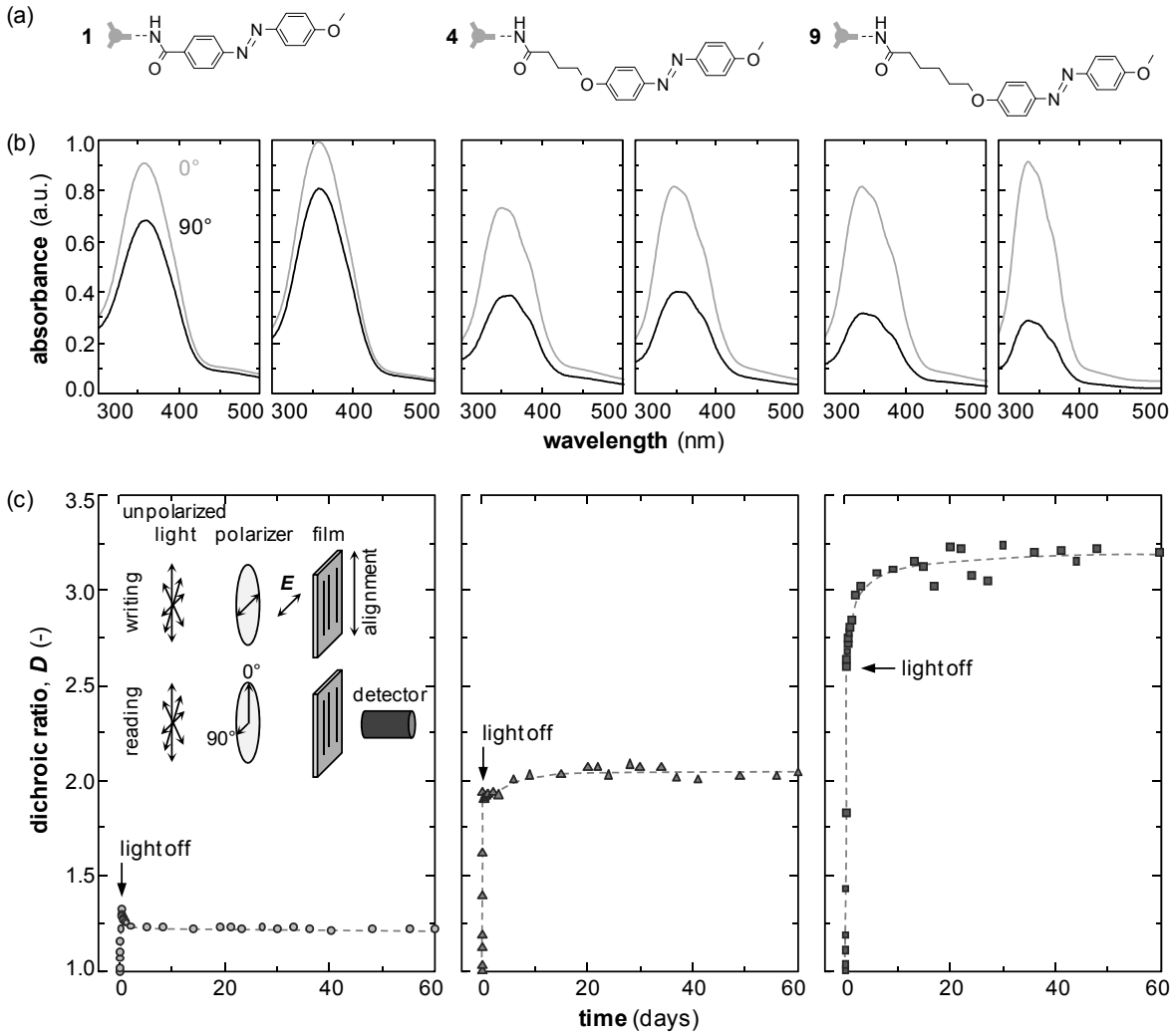

Figure 1. Photo-alignment at room temperature. (a) Chemical structures of compounds **1**, **4** and **9** (represents central benzene core) and (b) corresponding polarized UV/Vis spectra of thin films recorded with polarizers positioned at 0° and 90° angles (0°: parallel to absorbing azobenzene chromophore / perpendicular to polarization of writing light) directly after 2 h exposure to linearly polarized light (left) and after 60 days storage in the dark (right). (c) Corresponding temporal evolution of the dichroic ratio *D* (ratio between absorbance at 90° and 0°) at λ_{max} of the unexposed films: λ_{max}(**1**) = 356 nm; λ_{max}(**4**) = 347 nm; λ_{max}(**9**) = 345 nm. Dashed lines are drawn as a guide to the eye only and the end of the writing process is indicated with arrows. Whereas a stable photo-induced alignment and an additional "post-development" are observed for LC derivatives **4** and **9**, a decrease of *D* is found for the molecular glass **1**. Configurations used for writing and reading are schematically depicted in the insert.

(*i.e.* compound **1**) – since such phase can be expected to facilitate the formation of ordered domains. In compound **1**, on the other hand, in which the side-groups are directly linked to the amide bond at the central core, reorganization of the azobenzene moieties is restricted.

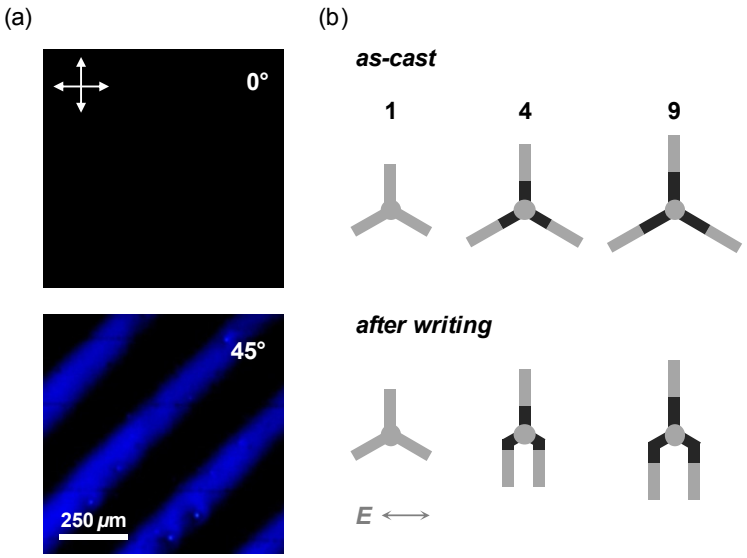

Figure 2. (a) Polarized optical micrographs of a photo-induced pattern inscribed in a spin-coated thin film of compound **4**, taken at 0° and 45° with respect to the polarizer/analyzer system (indicated with white arrows). (b) Simplified illustration of the alignment of the chromophores of the selected trisazobenzene derivatives upon exposure to linearly polarized light. Only in compounds **4** and **9** with decoupling spacers between the central core and the azobenzene units, the side-groups were found to align perpendicular to the polarization direction of the writing light and allow formation of ordered domains. By contrast, in molecular non-LC glass **1**, in which the chromophores are directly connected to the core, independent movement of the side-groups was hampered.

Stability of photo-induced alignment

In order to scrutinize the long-term stability of the photo-alignment of the three trisazobenzene derivatives, the temporal evolution of the dichroic ratio of irradiated films of the compounds was recorded over a period of 60 days. The results are summarized in Figure 1c. For both derivatives **4** and **9**, the photo-induced dichroic ratio was not only highly stable in the time frame investigated, but, indeed, *increased* in the first 10 days after irradiation before reaching saturation. For instance, a change of *D* from 2.6 to 3.2 was observed for photo-aligned films produced with compound **9**. This phenomenon was less pronounced for **4**, for which *D* increased from 1.9 to 2.0. For compound **1**, which does not feature a liquid-crystalline phase, by contrast, the dichroic ratio *D* actually *decreased* from 1.3 to 1.2, already during the first 24 h.

Annealing

Annealing is often used to increase the molecular order in liquid-crystalline systems. Therefore, the effect of heat treatment on the photo-alignment in the above trisazobenzene architectures was explored in experiments, in which the dichroic ratio *D* and the amplitude

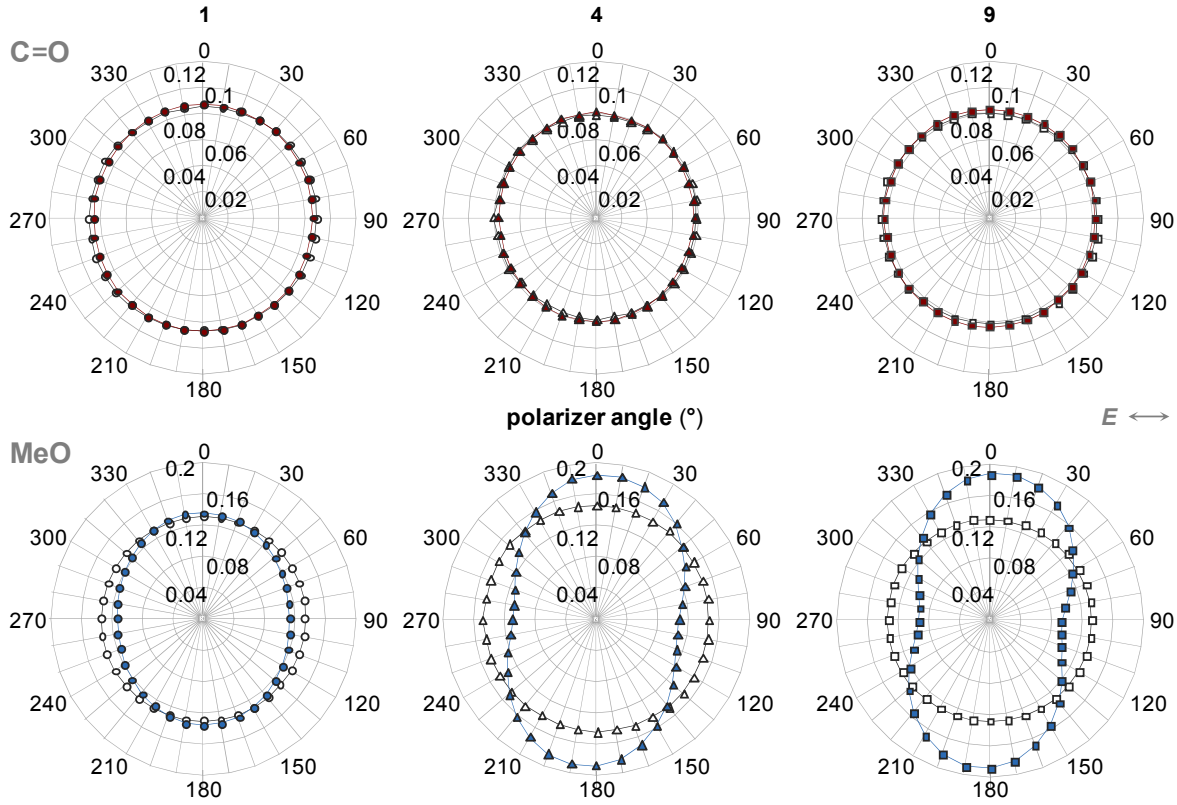

Figure 3. Polarized IR absorbance of the carbonyl (C=O; top) and the methoxy-group (MeO; bottom) of compounds **1**, **4** and **9** (0°: parallel to azobenzene moiety / perpendicular to polarization of the light used for the writing procedure): $\nu_{C=O}$(**1**) = 1655 cm^{-1}, $\nu_{C=O}$(**4**) = 1669 cm^{-1}, $\nu_{C=O}$(**9**) = 1664 cm^{-1}; ν_{MeO}(**1**) = 1255 cm^{-1}, ν_{MeO}(**4**) = 1248 cm^{-1}, ν_{MeO}(**9**) = 1249 cm^{-1}. Spectra were recorded before (open symbols) and after (filled symbols) exposure to linearly polarized light. Whereas the carbonyl-groups, located at the core of the molecule, remain virtually unaffected, the methoxy end-groups display a pronounced optical anisotropy in exposed films, *i.e.*, an alignment perpendicular to the polarization of the inscribing light beam that increases with spacer length. A derivation from perfect alignment, with a theoretical maximum of the absorbance at 0° polarizer angle, originates from experimental errors when calibrating and setting the polarizer manually.

of the refractive-index modulation n_1 created at room temperature were probed *in-situ* at different temperatures using variable-temperature UV/Vis spectroscopy and holographic experiments, respectively (for details see *"Experimental"*).

Pronounced amplification of both D and n_1 was observed for compounds **4** and **9**, when reading was carried out at elevated temperatures (Figure 4, respectively, a and b). Reassuringly, a similar development of D and n_1 with temperature was found in UV/Vis spectroscopy and holographic experiments, with maximum amplification observed for both LC compounds analyzed above their glass transition temperature, T_g (*cf.* Figure 4), where the dichroic ratio nearly doubled and n_1 increased by more than 40% for **9**. Only when heating the thin-film structures to even higher temperatures, closer to their LC-to-isotropic

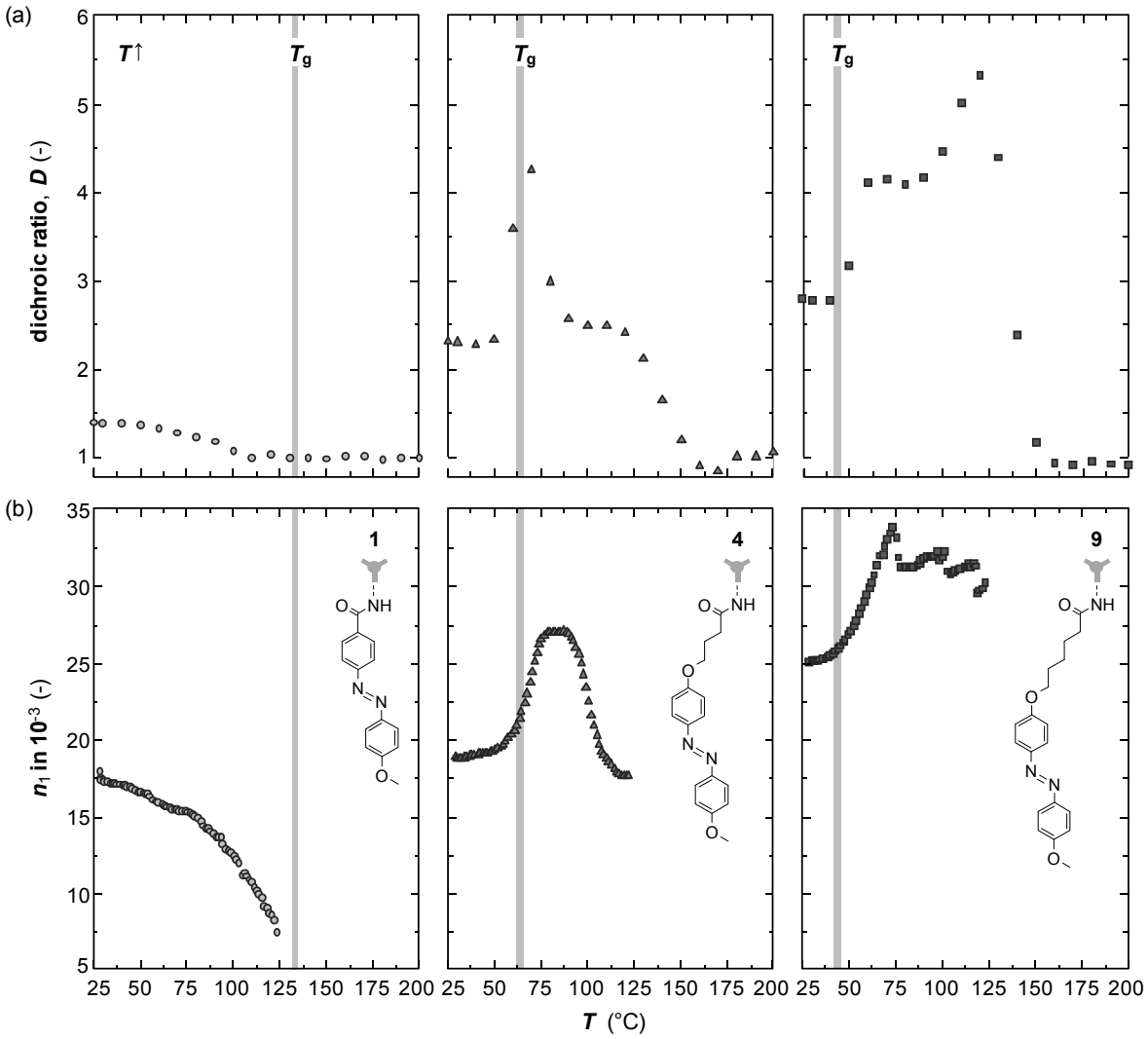

Figure 4. (a) Development of dichroic ratio D and (b) refractive-index modulation n_1 during heating of thin films of **1**, **4** and **9**, as deduced from variable-temperature polarized UV/Vis spectroscopy and holographic experiments, respectively. Both data sets indicate a thermally induced amplification of the photo-induced alignment for LC structures **4** and **9** above T_g (indicated with grey lines). Molecular order disappeared at temperatures close to the clearing point. In strong contrast, no amplification but a continuous decrease of the photo-orientation was found for compound **1** already at temperatures considerably below T_g.

transition, the optical anisotropy was lost, as indicated by a continuous decrease of D to 1; and a concomitant reduction of the birefringence was observed in polarized optical microscopy. (NB: Due to limits of the experimental setup the holographic experiments were confined to temperatures <125 °C). By contrast, the optical patterns created in the molecular glass **1** were already severely affected at $T << T_g$, as manifested by a rapid, continuous decrease of both D and n_1.

Clearly, this thermally enhanced amplification of D and n_1 may provide the interesting tool to increase the photo-induced optical anisotropy of holographic structures – without

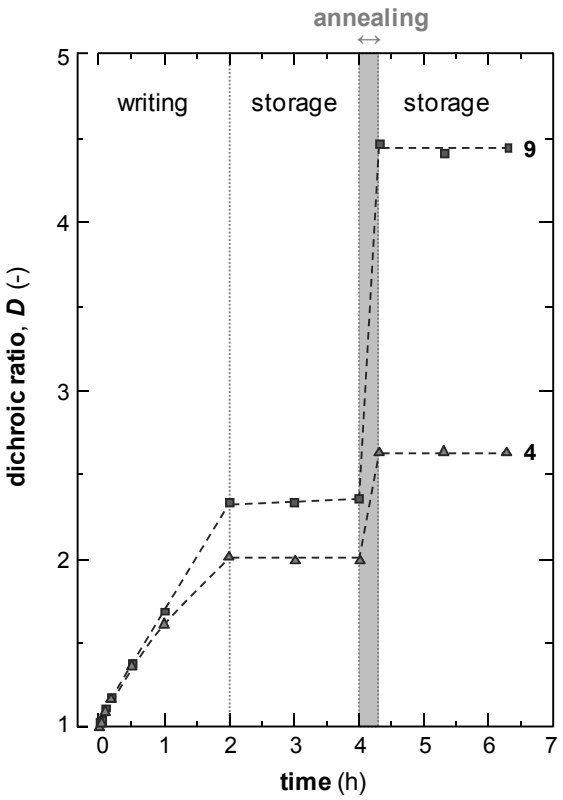

Figure 5. Temporal evolution of the dichroic ratio *D* for compounds **4** and **9** during writing at ambient and annealing at elevated temperatures of 10 to 20 °C above T_g for 20 min. Before and after the annealing step the films were stored for 2 h at room temperature in the dark. The thermal treatment resulted in a remarkable increase of *D* from 2.0 to 2.6 and from 2.3 to 4.4 for trisazobenzene derivatives **4** and **9**, respectively. Dashed lines are drawn as a guide to the eye only.

compromising their temporal stability – by applying suitable annealing procedures. To explore this further, thin films of **4** and **9** were irradiated for 2 h with polarized light at ambient conditions, followed by a 20 min annealing step at temperatures of 10 to 20 °C above T_g, *i.e.*, at temperatures at which reading resulted in a maximum optical contrast (*cf.* Figure 4). This protocol resulted in a significant increase in *D*, measured at room temperature, compared to thin-film architectures that were illuminated for the same period of time, but without being subjected to such a heat treatment procedure (Figure 5). As a matter of fact, for compound **9** an enhancement of the value of *D* from 2.3 to 4.4 was found, which is an amplification that is more than three times the increase of the dichroic ratio over time (*i.e.* "post-development") observed for untreated films of this specific compound at room temperature (*cf.* Figure 1c).

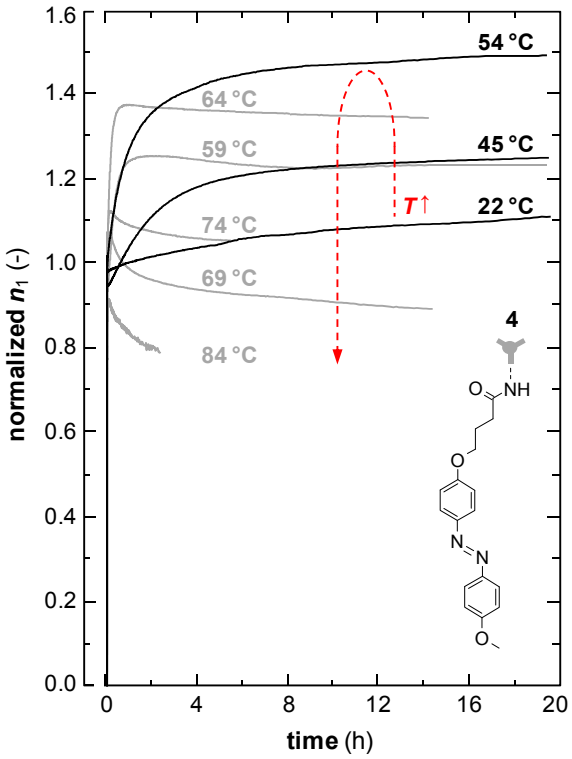

Figure 6. Amplitude of the refractive-index modulation n_1 as a function of time of thin films of compound **4**, normalized to unity after the writing laser was turned off. Inscription and reading of the holographic intensity gratings were conducted at isothermal conditions at different temperatures. Below T_g (*i.e.* <64 °C), "post-development" was found to increase without sacrificing stability. At higher temperatures, the stability decreased with increasing temperature, indicating that the formation of ordered domains is hampered.

Photo-alignment at elevated temperatures

Finally, it was also explored if exposure to elevated temperatures during the writing process provides additional means to manipulate the photo-alignment in trisazobenzene structures. For these investigations, compound **4** was employed. Inscription and – for efficient data collection also subsequent reading – was conducted at isothermal conditions as a function of time (Figure 6). Interestingly, writing times required to reach the maximum refractive-index modulations n_1 were found to decrease from ~10 s at ambient temperature down to ~1.5 s at ~85 °C; *i.e.*, at $T > T_g$. However, this benefit was found to come at the expense of stability of the gratings at this temperature. From Figure 6, for instance, it is clear that stable gratings only can be written at temperatures below the glass transition of this compound (~64 °C). Nonetheless, inscription of holographic gratings at elevated temperatures may still be exploited to reduce the writing times – provided writing is followed by subsequent rapid cooling of the active layers to room temperature.

CONCLUSIONS

Small-molecular trisazobenzene derivatives with a latent liquid-crystalline phase were found to undergo a pronounced molecular realignment when exposed to linearly polarized visible light, while their non-LC counterpart was significantly less affected by the optical writing procedures. Polarized UV/Vis and IR spectroscopy suggest that during writing, ordered domains form, in which the three side-groups of these trisazobenzene compounds orient perpendicular to the polarization of the inscribing light beam, provided that a sufficiently long spacer is introduced between the molecule's core and the active chromophore moieties – as is the case in compounds **4** and **9**. Molecular order in these domains improved relatively slowly at ambient conditions over a period of days (*cf*. Figure 1c); however, similar to more standard LC materials, this effect can be increased when following annealing protocols between T_g and the clearing point (*cf*. Figures 4 and 5). Apparently, during this amplification process, photo-induced ordered regions nucleate the less ordered surrounding, resulting in an enhanced overall alignment. But, if writing is conducted at too high temperatures, the high molecular mobility will not permit formation of such stable, oriented domains.

Clearly, the observed "post-development" of n_1 in the trisazobenzene derivatives **4** and **9** is interesting from a technological point-of-view, as it permits relatively short writing times, as well as fabrication of stable holographic intensity gratings. The contrast of these gratings can be adjusted not only with optical writing methods but also by exploiting suitable annealing procedures, offering an additional tool for designing them.

EXPERIMENTAL

Materials. Synthesis and characterization of the trisazobenzene compounds explored is described in the *Appendix*. Atactic, ultra-high molecular weight polystyrene (UHMW-PS) (M_w ~30'000 kg/mol) was purchased from Polysciences, Inc., Warrington, PA, USA. Tetrahydrofuran (THF) was supplied by Acros, Geel, Belgium, and dried over a molecular sieve.

Thin-film preparation. Thin films of ~400 nm thickness for optical microscopy, spectroscopy and holographic characterization were prepared from ~2 wt-% tetrahydrofuran (THF) solutions (total content) that were heated to 55 °C for 60 min and subsequently cooled to room temperature. Resulting homogeneous solutions were spin-cast at ambient with a Laurell WS-400B-6NPP/LITE spin-coater at 800 rpm onto glass slides or onto polished sodium chloride discs for infrared spectroscopy. To increase the film thickness to a level required in holographic experiments, ~5 wt-% (respective to the solute) of atactic, ultra-high molecular weight polystyrene (UHMW-PS) was added to the solutions prior to heating.

Photo-alignment. Photo-induced alignment of the azobenzene chromophores was performed at ambient by exposure of thin films to linearly polarized light in a box of the dimensions 25 x 85 x 40 cm, fitted with an Osram® S Luminux® 9 W/860 (Daylight) source. The distance between sample and lamp was 10 cm in all experiments and a Polaroid HN-32 sheet polarizer was placed on top of the films. To inscribe patterns for optical microscopy studies, a shadow mask of 100 μm thickness was positioned between the sheet polarizer and the trisazobenzene films.

Optical microscopy. Optical microscopy was carried out with a Leica DM4000M polarizing microscope.

Ultraviolet/visible (UV/Vis) light analysis. UV/Vis spectra of thin films were recorded with a Perkin Elmer Lambda 900 spectrophotometer equipped with rotating Glan-Thompson polarizers. To characterize the development of dichroic ratios during the 2 h exposure phase and after certain storage periods in the dark, scans were taken from 280 to 700 nm at polarizer angles of 0°, 45° and 90° with respect to the alignment direction of the

azobenzene chromophores. At the end of each measurement, a second spectrum was recorded at 0° to ensure that no further undesired orientation effects were induced during the experiment.

Variable-temperature UV/Vis spectroscopy was performed under N_2 atmosphere employing a Harrick Scientific Products ATC-024-2 temperature controller equipped with a temperature-controlled demountable TFC-S25 flow cell. UV/Vis spectra of each thin film were recorded at ambient before and after 2 h exposure to linearly polarized light, as well as in steps of 10 °C over a temperature range from 30 to 200 °C.

Infrared (IR) spectroscopy. IR spectra were recorded with a Bruker Vertex 70 spectrometer equipped with a Spectra-Tech IR polarizer. Scans were taken from 4000 to 600 cm^{-1} before and after 20 h illumination with linearly polarized light, rotating the polarizer in 10° steps between 0° and 360°.

Holography. The blue-green line (488 nm) of an argon ion laser was used to perform holographic experiments. A beam splitter generated two coherent parts of the laser beam, which were brought to interference in the sample plane (*cf.* schematic in *Chapter II*). The diameter of the s-polarized laser beams was about 1 mm; the intensity of each beam was adjusted to 0.5 W/cm^2. The angle of incidence relative to the surface normal was ±14°, resulting in a grating period of about 1 μm. A laser diode at 685 nm, a wavelength range outside the absorption band of the azobenzene moiety, was used for in-situ monitoring of the diffraction efficiency without affecting the writing process. To determine the diffraction efficiency, the power of the transmitted and the diffracted beam were measured with two photodiodes. For improving the signal-to-noise ratio, the laser diode was modulated and lock-in detection was used. Variable-temperature holographic experiments were performed with a similar holographic setup, but in this case the sample was placed in a temperature-controlled box. The equipment allowed adjusting the temperature in a range between 20 to 125 °C with an accuracy of 1 °C. To avoid a possible influence of effects related to the thermal history of the samples, a new film was employed for each experiment. The heating rate for reading at elevated temperatures was 0.4 °C/min.

References

(1) Y. Shirota, *J. Mater. Chem*. **2005**, *15*, 75.

(2) D. Y. Kim, S. K. Tripathy, L. Li, J. Kumar, *Appl. Phys. Lett.* **1995**, *66*, 1166.

(3) P. Rochon, E. Batalla, A. Natansohn, *Appl. Phys. Lett.* **1995**, *66*, 136.

(4) T. Fuhrmann, T. Tsutsui, *Chem. Mater.* **1999**, *11*, 2226.

(5) Y. Shirota, *J. Mater. Chem.* **2000**, *10*, 1.

(6) E.-M. Seo, M. J. Kim, Y.-D. Shin, J.-S. Lee, D.-Y. Kim, *Mol. Cryst. Liq. Cryst.* **2001**, *370*, 143.

(7) H. Nakano, T. Takahashi, T. Kadota, Y. Shirota, *Adv. Mater.* **2002**, *14*, 1157.

(8) P. Strohriegl, J. V. Grazulevicius, *Adv. Mater.* **2002**, *14*, 1439.

(9) M.-J. Kim, E.-M. Seo, D. Vak, D.-Y. Kim, *Chem. Mater.* **2003**, *15*, 4021.

(10) C. Chun, M.-J. Kim, D. Vak, D. Y. Kim, *J. Mater. Chem.* **2003**, *13*, 2904.

(11) H. Ando, T. Takahashi, H. Nakano, Y. Shirota, *Chem. Lett.* **2003**, *32*, 710.

(12) C. Chun, J. Ghim, M.-J. Kim, D. Y. Kim, *J. Polym. Sci., Part A: Polym. Chem.* **2005**, *43*, 3525.

(13) E. Ishow, B. Lebon, Y. He, X. Wang, L. Bouteiller, L. Galmiche, K. Nakatani, *Chem. Mater.* **2006**, *18*, 1261.

(14) H. Nakano, T. Takahashi, T. Tanino, Y. Shirota, *J. Photopolym. Sci. Technol.* **2007**, *20*, 87.

(15) H. Nakano, T. Tanino, T. Takahashi, H. Ando, Y. Shirota, *J. Mater. Chem.* **2008**, *18*, 242.

(16) H. Audorff, R. Walker, L. Kador, H.-W. Schmidt, *J. Phys. Chem. B* **2009**, *113*, 3379.

(17) R. Walker, H. Audorff, L. Kador, H.-W. Schmidt, *Adv. Funct. Mater.* **2009**, *19*, 2630.

(18) H. Audorff, K. Kreger, R. Walker, D. Haarer, L. Kador, H.-W. Schmidt, *Adv. Polym. Sci.* **2010**, *228*, 59.

(19) J. Stumpe, L. Läsker, T. Fischer, M. Rutloh, S. Kostromin, R. Ruhmann, *Thin Solid Films* **1996**, *284*, 252.

(20) T. Fischer, L. Läsker, S. Czapla, J. Rübner, J. Stumpe, *Mol. Cryst. Liq. Cryst.* **1997**, *298*, 213.

(21) S. J. Zilker, T. Bieringer, D. Haarer, R. S. Stein, J. W. van Egmond, S. G. Kostromine, *Adv. Mater.* **1998**, *10*, 855.

(22) S. J. Zilker, M. R. Huber, T. Bieringer, D. Haarer, *Appl. Phys. B* **1999**, *68*, 893.

(23) R. Rosenhauer, T. Fischer, S. Czapla, J. Stumpe, A. Vinuales, M. Pinol, J. L. Serrano, *Mol. Cryst. Liq. Cryst.* **2001**, *364*, 295.

(24) M. Kidowaki, T. Fujiwara, S. Morino, K. Ichimura, J. Stumpe, *Appl. Phys. Lett.* **2000**, *76*, 1377.

(25) M. Han, K. Ichimura, *Macromolecules* **2001**, *34*, 90.

(26) A. Stracke, J. H. Wendorff, D. Goldmann, D. Janietz, *Liq. Cryst.* **2000**, *27*, 1049.

(27) Y. Watanabe, Y. Tsuji, T. Kondo, R. Takeuchi, *J. Org. Chem.* **1984**, *49*, 4451.

(28) K. K. Prasad, R. V. Venkataratnam, *Aust. J. Chem.* **1973**, *26*, 1263.

(29) N. B. Abbott, A. Elliott, *Proc. Roy. Soc. A* **1956**, *234*, 247.

(30) L. Skulski, S. Smialek-Kazmierowska, *Polish J. Chem.* **1985**, *59*, 17.

(31) R. J. W. Lefevre, R. L. Werner, *Aust. J. Chem.* **1957**, *10*, 26.

Chapter IV

Liquid Crystal Alignment with Photo-Oriented Trisazobenzene Layers

---

INTRODUCTION

Driven by recent developments of liquid-crystal display (LCD) technologies, there exists a major need for tools that allow ever more precise control of the spatial order of liquid-crystalline species.[1-4] A widely used approach is utilizing the characteristic of some surfaces – so-called orientation layers – that induce homogeneous order of liquid-crystalline (LC) compounds that are in contact with those substrates. Already in 1913, Mauguin observed that azoxyanisole can be oriented in its liquid-crystalline phase when placed between two sheets of mica.[5] Since that time, many other alignment systems and techniques were identified and developed. These approaches are based, for instance, on rubbed or buffed surfaces of certain polymers – most frequently, polyimide (PI),[6-13] micro-grooved surfaces[14-16] or highly oriented thin films of poly(tetrafluoroethylene) (PTFE).[17,18] Indeed, these techniques and materials allow efficient fabrication of homogeneously oriented LC layers. However, the creation of patterned structures with these methods remains cumbersome if not unfeasible. In addition, surface relief structures used in most of the above techniques – when incorporated in useful devices – by virtue suffer from inhomogeneous electrical fields, once electrodes are applied and activated across the ultimate LC cells. Hence, the need for alternative orientation methods that allow combining the advantageous alignment properties of above mentioned systems with the feasibility for straightforward patterning into versatile structures remains.

One promising class of materials to create such layers is based on azobenzene containing species, *i.e.* azobenzene dyes, azobenzene-dye doped polymers or azobenzene containing polymers.[19-24] Here, we explored the use of films of trisazobenzene derivatives as orientation layers for liquid crystals. Such films feature the advantage that they can readily be patterned into oriented domains by exposure to linearly polarized light, as shown in *Chapters II and III*.

Due to the excellent experience with compound **9** (*cf.* Figure 1) in holographic experiments and in optical spectroscopy presented in the previous chapters, this species was selected for use as the orientation layer material. The common 4-cyano-4'-heptylbiphenyl[4,25-26] (7CB; *cf.* Figure 1) was employed as the liquid-crystalline compound, as this material exhibits a nematic LC phase at ambient conditions, allowing straightforward deposition on the trisazobenzene based layers at room temperature.

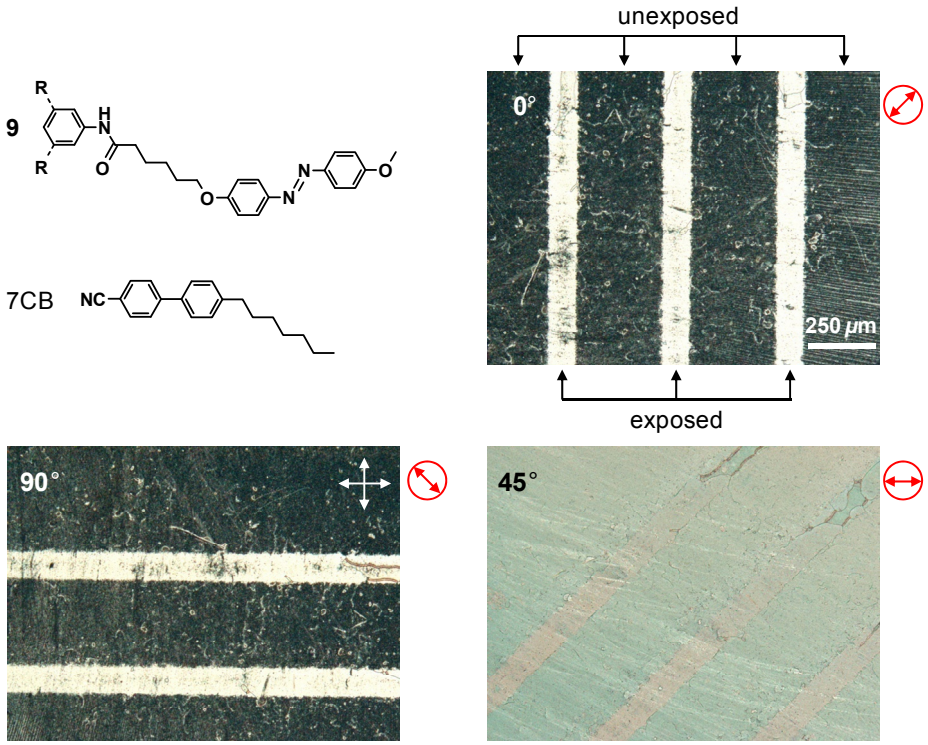

Figure 1. Chemical structures of compounds employed and polarized optical micrographs of an LC cell with trisazobenzene (**9**)-based orientation layers that were patterned with linearly polarized light and subsequently filled with the nematic liquid crystal 7CB, revealing alignment of the LC in exposed areas. The alignment of trisazobenzene orientation layers in irradiated areas, *i.e.* the direction perpendicular to the polarization of the writing light, is indicated with red arrows and the polarizer/analyzer position in microscopy studies is denoted with white arrows.

RESULTS AND DISCUSSION

Glass substrates were coated with the trisazobenzene **9** and appropriate cells were assembled with them (see *"Experimental"*). Subsequently, these cells were exposed for 2 h to linearly polarized visible light through a shadow mask and thereafter filled with 7CB at ambient conditions. Intriguingly, as indicated by a series of polarized optical micrographs, the liquid crystal oriented only on those trisazobenzene regions that were irradiated with polarized light, *i.e.* on areas where the trisazobenzene derivative was subjected to photo-induced alignment (Figure 1). It should be noted that weak alignment of 7CB along the filling direction was observed in an identical, but unexposed reference cell, resulting in a birefringent appearance when examined with polarized light. This birefringence was also observed at an angle of 45° with respect to the polarizer/analyzer system for both the areas that were and were not exposed to photo-alignment of the trisazobenzene orientation layers.

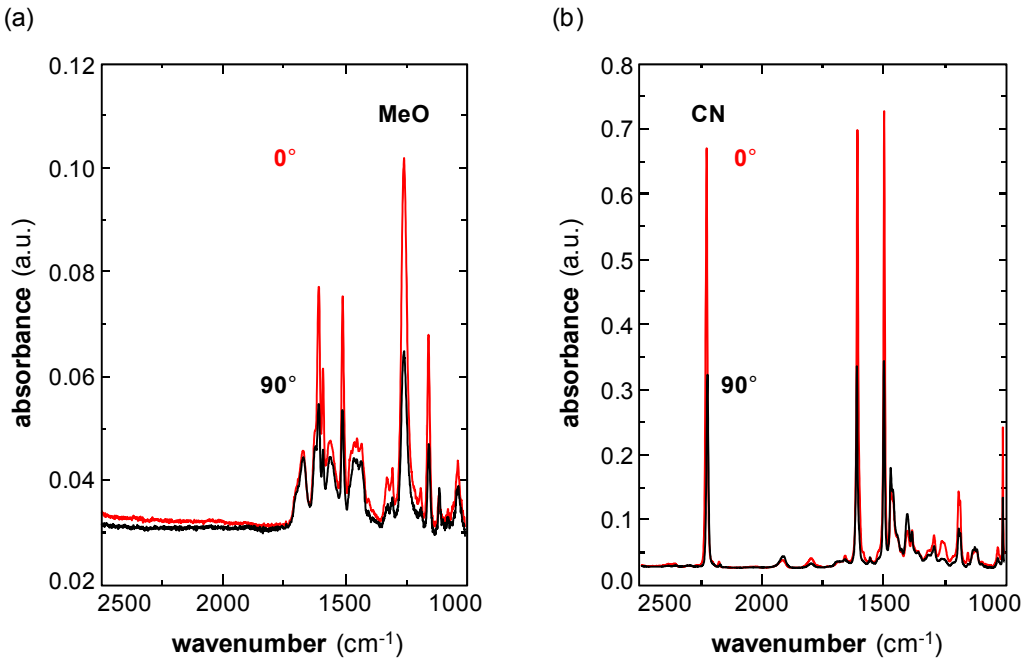

Figure 2. (a) Polarized infrared spectra of an empty cell constructed with trisazobenzene **9**-coated sodium chloride substrates that was irradiated for 2 h with linearly polarized light. The alignment of the orientation layers is evident from the dichroic absorbance of the methoxy-groups (ν_{MeO} = 1249 cm^{-1}).[27] (b) Identical spectra of the same cell but filled with 7CB. The absorbance recorded for the cyano-groups (ν_{CN} = 2227 cm^{-1}),[28] which are only present in the LC species (*cf.* Figure 1), features the same dichroic characteristic as determined for the methoxy-groups in the orientation layer, indicating alignment of the LC molecules along the azobenzene chromophores. 0° denotes the direction parallel to the azobenzene chromophores/perpendicular to the polarization of the writing light.

In order to gain more detailed insight into the trisazobenzene-mediated alignment of 7CB, the above microscopic analysis was complemented with polarized infrared (IR) spectroscopy. This technique allows comparing photo-induced alignment of the orientation layer with order in the LC component by analyzing dichroism of vibration bands of specific chemical moieties. In accord with results presented in *Chapter III*, the methoxy substituents in the trisazobenzene orientation layer of an empty, 2 h irradiated cell featured alignment perpendicular to the polarization direction of the inscribing light beam (Figure 2a). Polarized IR spectra of cells filled with 7CB revealed dichroism of the cyano-groups of the liquid-crystalline species identical to the absorbance characteristics observed for the methoxy-groups in the trisazobenzene layers (Figure 2b). In agreement with the polarized optical micrographs presented in Figure 1, these findings indicate a preferred orientation of the LC component in irradiated domains along the photo-oriented azobenzene chromophores.

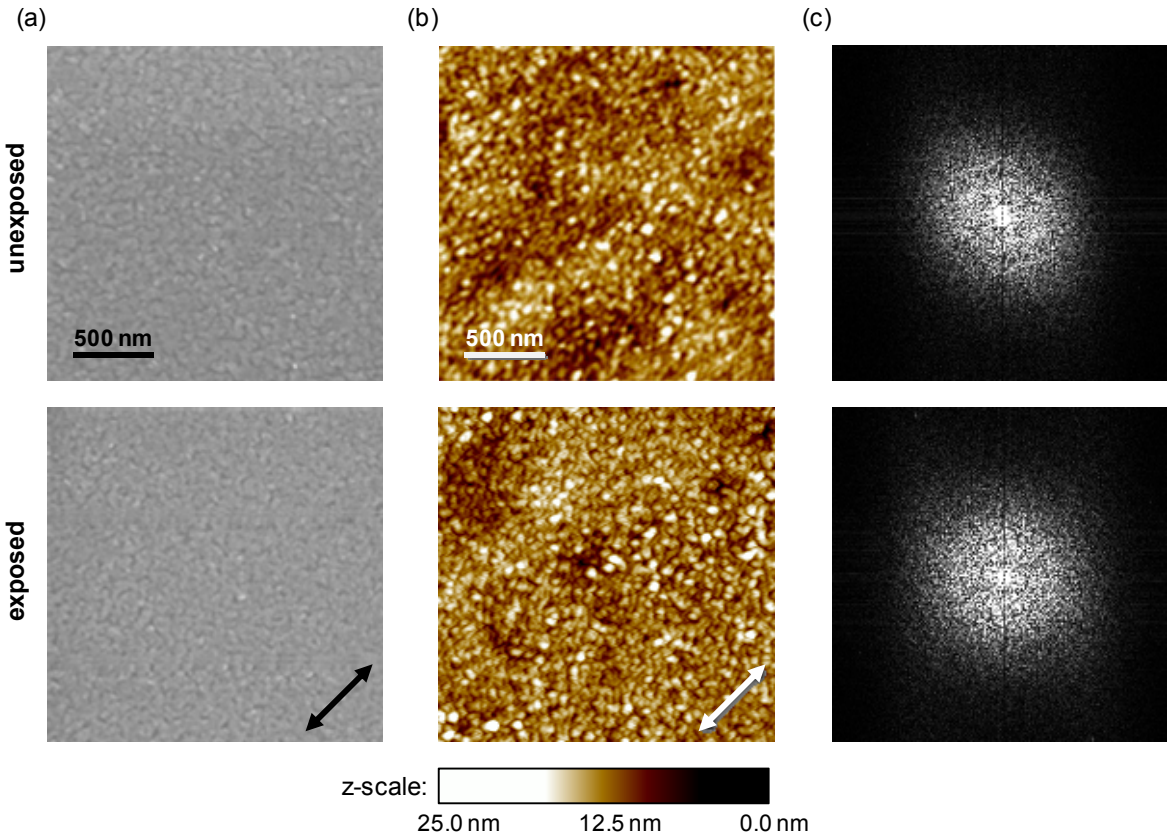

Figure 3. (a) SEM images and (b) AFM patterns of an unexposed (top) and a photo-oriented (bottom) trisazobenzene alignment layer (alignment direction of azobenzene chromophores indicated with arrows). Both techniques reveal an absence of any surface relief structures, indicating that the alignment of the liquid-crystalline component is induced by an inter-molecular attraction between orientation layer and LC species. (c) Fourier transformed AFM patterns, demonstrating that no preferred structural features along the trisazobenzene alignment are present in the surface of the irradiated thin film.

Subsequently, the focus was on elucidating the mechanism of alignment of the LC species by the trisazobenzene orientation layers, *i.e.* on the nature of their physicochemical interaction. In order to scrutinize if molecular orientation in the trisazobenzene films or photo-induced surface topography was responsible for the alignment of the LC compound, these layers were examined with scanning electron microscopy (SEM) and atomic force microscopy (AFM). Both characterization techniques revealed that both the unexposed and exposed films featured relatively smooth surfaces, with an average roughness, R_a, less than ~2 nm (Figure 3a, b). Importantly, no preferred order along the azobenzene chromophores (perpendicular to the polarization direction of the inscribing light beam) is discernable in SEM and AFM analysis of the irradiated trisazobenzene-based orientation layers. This finding is supported by the Fourier transforms of the AFM images, revealing no features that indicate any preferential orientation of the trisazobenzene surface structure in any

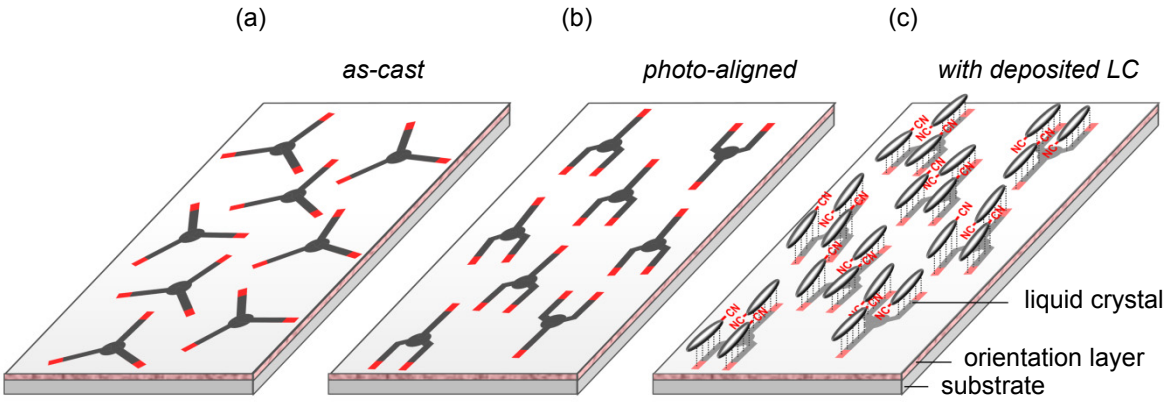

Figure 4. Schematic illustration of the liquid crystal alignment with trisazobenzene based orientation layers. (a) Isotropic and (b) photo-aligned trisazobenzene layers on glass substrates. (c) Inter-molecular attraction between orientation layer and deposited liquid-crystalline species, resulting in an uniform planar alignment of the LC compound.

direction (Figure 3c). Accordingly, our data strongly indicate that the observed alignment of the LC material should be attributed to inter-molecular attraction ordering effects between trisazobenzene based orientation layers and the LC species and not to a surface relief structure (Figure 4).

CONCLUSIONS

In summary, orientation layers were presented that are based on trisazobenzene derivatives that were photo-aligned. Therewith, a promising alternative to, *e.g.* rubbed surfaces, was advanced, as the trisazobenzene system explored allows combining straightforward LC alignment with readily accessible photo-induced patterning options that do not require tedious relief structuring of the commanding surface. In addition, as a consequence of their small-molecular architecture, trisazobenzene films, in principle, offer the potential to be employed as sacrificial alignment layers that – after orienting and cross-linking the LC material – can be removed with common solvents.

EXPERIMENTAL

Materials. Synthesis and characterization of trisazobenzene derivative **9** is described in the *Appendix*. 4-Cyano-4'-heptylbiphenyl (7CB) was purchased from Frinton Laboratories, Inc., Vineland, NJ, USA, and used as received. Tetrahydrofuran (THF) was supplied by Acros, Geel, Belgium, and dried over a molecular sieve.

Preparation of liquid-crystal cells. Thin films of compound **9** were spin-cast at ambient with a Laurell WS-400B-6NPP/LITE spin-coater at 800 rpm from ~1 wt-% THF solutions (total solid content) onto glass slides for optical microscopy and surface analysis or onto polished sodium chloride discs for infrared spectroscopy. 18 μm-sized glass spacer beads were added to a UV-curable glue to define the cell thickness, which was used to assemble the cell. For complete curing of the glue, the assembly was exposed for 4 min to the UV-light of a UVP, Blak-Ray Long Wave Ultraviolet Lamp, Model B 100 AP. To avoid undesired UV-exposure of the trisazobenzene layers, glue-free areas of the LC cells were protected with a black sheet during irradiation.

Photo-alignment. Photo-induced alignment of the trisazobenzene orientation layers in the LC cells was performed at ambient conditions by 2 h exposure of the cells to linearly polarized light in a box of the dimensions 25 x 85 x 40 cm, fitted with an Osram® S Luminux® 9 W/860 (Daylight) source. The distance between sample and lamp was 10 cm in all experiments and a Polaroid HN-32 sheet polarizer was placed on top of the films. To inscribe patterns for optical microscopy studies, a shadow mask of 100 μm thickness was positioned between the sheet polarizer and the LC cells.

Optical microscopy. Optical microscopy was carried out with a Leica DM4000M polarizing light microscope.

Infrared (IR) spectroscopy. IR spectra were recorded with a Bruker Vertex 70 spectrometer equipped with a Spectra-Tech IR polarizer. Scans were taken from 3000 to 600 cm^{-1} before and after 2 h illumination of the empty LC cell with linearly polarized light, as well as of a filled cell comprising previously photo-aligned trisazobenzene layers.

Scanning electron microscopy (SEM). Thin films of compound **9** were coated with a thin conductive layer of platinum and images of irradiated and unexposed layers were recorded with a LEO 1530 Gemini microscope.

Atomic force microscopy (AFM). Atomic force microscopy was performed with a Digital Instrument, Nano Scope IIIa, operating the device in the tapping mode. Fourier-transformed 2D patterns were calculated using MATLAB R2010a.

References

(1) M. Schadt, W. Helfrich, *Appl. Phys. Lett.* **1971**, *18*, 127.

(2) M. Schadt, *Annu. Rev. Mater. Sci.* **1997**, *27*, 305.

(3) D. J. Broer, J. A. M. M. van Haaren, P. van de Witte, C. Bastiaansen, *Macromol. Symp.* **2000**, *154*, 1.

(4) H. Kawamoto, *Proc. IEEE* **2002**, *90*, 460.

(5) C. Mauguin, *C. R. Hebd. Séances Acad. Sci.* **1913**, *156*, 1246.

(6) J. Cognard, *Mol. Cryst. Liq. Cryst.* **1982**, *51*, 1.

(7) M. E. Becker, R. A. Kilian, B. B. Kosmowski, D. A. Mlynski, *Mol. Cryst. Liq. Cryst.* **1986**, *132*, 167.

(8) J. M. Geary, J. W. Goodby, A. R. Kmetz, J. S. Patel, *J. Appl. Phys.* **1987**, *62*, 4100.

(9) S. Ishihara, H. Wakemoto, K. Nakazima, Y. Matsuo, *Liq. Cryst.* **1989**, *4*, 669.

(10) N. A. J. M. van Aerle, M. Barmentlo, R. W. J. Hollering, *J. Appl. Phys.* **1993**, *74*, 3111.

(11) M. F. Toney, T. P. Russell, J. A. Logan, H. Kikuchi, J. M. Sands, S. K. Kumar, *Nature* **1995**, *374*, 709.

(12) J. Stöhr, M. G. Samant, A. Cossy-Favre, J. Diaz, Y. Momoi, S. Odahara, T. Nagata, *Macromolecules* **1998**, *31*, 1942.

(13) S. Varghese, G. P. Crawford, C. W. M. Bastiaansen, D. K. G. de Boer, D. J. Broer, *Appl. Phys. Lett.* **2004**, *85*, 230.

(14) D. W. Berreman, *Phys. Rev. Lett.* **1972**, *28*, 1683.

(15) U. Wolff, W. Greubel, H. Krüger, *Mol. Cryst. Liq. Cryst.* **1973**, *23*, 187.

(16) Y. Kawata, K. Takatoh, M. Hasegawa, M. Sakamoto, *Liq. Cryst.* **1994**, *16*, 1027.

(17) J. C. Wittmann, P. Smith, US Patent 5,180,470 **1989**.

(18) J. C. Wittmann, P. Smith, *Nature* **1991**, *352*, 414.

(19) K. Ichimura, Y. Suzuki, T. Seki, A. Hosoki, K. Aoki, *Langmuir* **1988**, *4*, 1214.

(20) W. M. Gibbons, P. J. Shannon, S.-T. Sun, B. J. Swetlin, *Nature* **1991**, *351*, 49.

(21) T. Kosa, P. Palffy-Muhoray, *Pure Appl. Opt.* **1996**, *5*, 595.

(22) M. Schadt, *Mol. Cryst. Liq. Cryst.* **2001**, *364*, 151.

(23) D. D. Huang, E. P. Pozhidaev, V. G. Chigrinov, H. L. Cheung, Y. L. Ho, H. S. Kwok, *Displays* **2004**, *25*, 21.

(24) H.-S. Kwok, V. G. Chigrinov, H. Takada, H. Takatsu, *J. Display Technol.* **2005**, *1*, 41.

(25) G. W. Gray, D. G. McDonnell, *Mol. Cryst. Liq. Cryst.* **1979**, *53*, 147.

(26) D. W. Berreman, W. R. Heffner, *Appl. Phys. Lett.* **1980**, *37*, 109.

(27) R. J. W. Lefevre, R. L. Werner, *Aust. J. Chem.* **1957**, *10*, 26.

(28) A. Tsujimoto, H. Goto, *Mol. Cryst. Liq. Cryst.* **2008**, *493*, 82.

Chapter V

Phase Behavior and Electronic Properties of α-Quaterthiophene:Polyethylene Blends

---

INTRODUCTION

In recent years, there has been increasing interest in organic semiconductors, as these materials promise low-cost fabrication of, *e.g.*, discrete thin-film field-effect transistors,[1-3] light-emitting diodes,[4,5] photovoltaic cells,[6] sensors,[7,8] as well as more integrated structures such as radio-frequency identification tags.[9-11] Both, small molecules and polymers have been investigated for this purpose, with the former usually exhibiting superior electronic properties and the latter generally allowing use of more straightforward processing methods.

In this chapter, the focus is on small-molecular species as they display well-defined conjugation lengths and provide simple model systems for elucidating relevant structure-property correlations, especially with respect to their electronic behavior.

One promising class of semiconducting small molecules are the thiophene homologues,[12] in part due to the rich chemistry of the aromatic thiophene ring, which allows a wide variety of systems to be synthesized. This permits design and tuning of the semiconducting properties of these materials.[13,14] For instance, charge-carrier mobilities determined in field-effect transistor (FET) configuration, μ_{FET}, of the simple, unsubstituted oligomers increase with conjugation length, apparently saturating around 10^{-1} cm^2/Vs for molecules that comprise six thiophene groups or more (see Table 1).

Generally, oligothiophenes are processed via relatively cumbersome vapour deposition techniques.[15-20] Melt- and solution-based pathways are less common due to their comparatively high melting temperatures, limited solubility at ambient as well as low viscosities of these species, which restricts growth of continuous thin films over large areas.[21,22]

Some issues in melt- and solution-processing, here exemplary of α-quaterthiophene (4T), are addressed below; and in particular, the use of 4T in blends with the insulating linear (high-density) polyethylene (HDPE). Addition of a high polymer to the small-molecular oligothiophene is expected, among other things, to increase solution- and melt-viscosity, which provides, for example, improved film-forming characteristics. Furthermore, highly desirable mechanical (solid-state) properties will be imparted to these two-component systems if tough polymers (such as polyethylene, PE) are utilized for this purpose. This has recently been demonstrated with poly(*3*-hexylthiophene) (P3HT):PE blends and diblock co-polymers.[26,29] Importantly, in these studies, it was reported that μ_{FET} was not significantly affected by the presence of the insulator at a PE weight fraction as high as 97 wt-% in blends and 90 wt-% in block co-polymers. Compared to these systems

Table 1. Melting temperatures, T_m, and charge-carrier mobilities, μ_{FET}, of oligothiophenes and one of its polymeric derivatives, as well as appearance of selected solids and solutions.

Species	Abbreviation	T_m (°C)	μ_{FET} (cm^2/Vs)	Solid	Solution[a]	References
α-Bithiophene	2T	34[b]	--			
α-Terthiophene	3T	95[b]	--			23
α-Quaterthiophene	4T	213[b]	0.1 - 6 x 10^{-3}		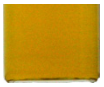	15, 16
α-Quinquethiophene	5T	253	0.6 - 5 x 10^{-2}			17, 18, 24
α-Sexithiophene	6T	298[b]	2.5 - 8 x 10^{-2}		--	18, 19
α-Septithiophene	7T	328	1 x 10^{-1}		--	18, 24
α-Octithiophene	8T	370	0.7 - 3 x 10^{-1}		--	15, 20, 25
Poly(*3*-hexylthiophene)	P3HT[c]	220[b]	0.6 - 1.2 x 10^{-1}			26, 27, 28

a Solvent: decalin at $T = 140$ °C.
b Deduced from DSC second-heating thermograms.
c $M_w = 22$ kg/mol.

that are comprised of two macromolecular species, oligothiophene:polyethylene (*i.e.* small-molecular:polymeric) binaries provide additional insight into such crystalline:crystalline semiconducting:insulating organic blends, for instance, as shown here, the influence of the rate of solidification on microstructures induced and the dependence of the resulting electronic characteristics of these materials systems on the latter.

RESULTS AND DISCUSSION

Phase behavior of α-quaterthiophene

Among existing (non-substituted) oligothiophenes, α-quaterthiophene offers a good trade-off between electronic properties and processability in terms of the material's melting temperature and solubility. Bi- and terthiophene, for instance, would provide good solubility and low melting temperatures, T_m, but their short conjugation length results in relatively poor semiconducting properties/device performance. Oligothiophenes

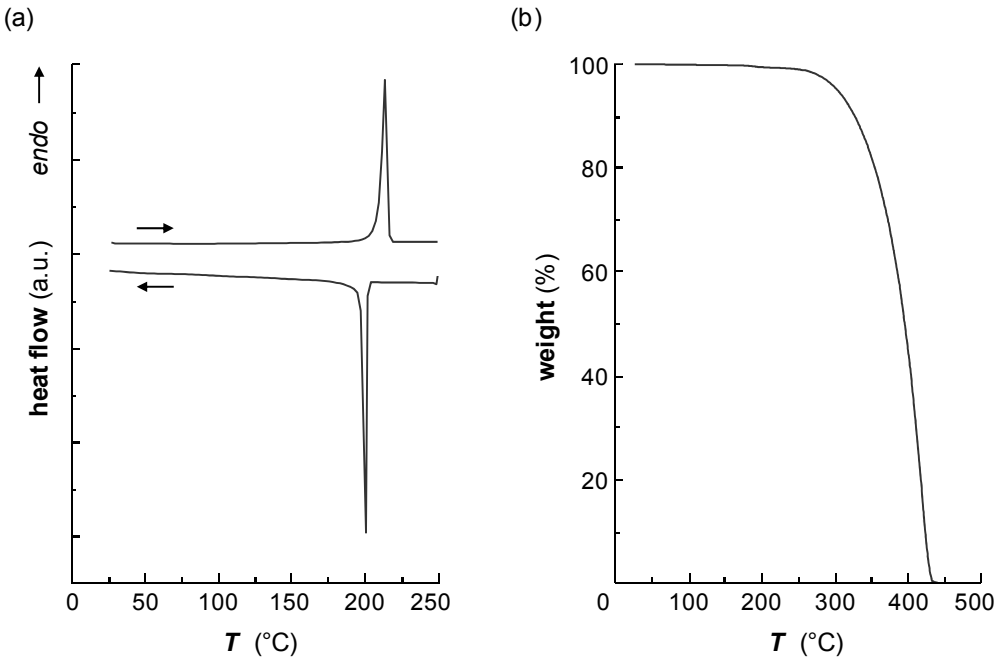

Figure 1. (a) Differential scanning calorimetry (DSC) and (b) thermo-gravimetric analysis (TGA) of 4T (heating/cooling rate 10 °C/min). DSC peak melting temperature T_m = 213 °C, enthalpy of fusion ΔH_m = 119 J/g, crystallization temperature T_c = 201 °C and enthalpy of crystallization ΔH_c = 118 J/g.

comprising five thiophene units and more, on the other hand – although interesting for their superior electronic characteristics – feature inconveniently high melting temperatures in excess of 250 °C (*cf.* Table 1).

Differential scanning calorimetry (DSC) of α-quaterthiophene indicates that melt processing of this compound requires also relatively elevated temperatures >215 °C, with sublimation commencing at similar temperatures (see Figure 1). This allows, accordingly, only a relatively small processing window. However, in contrast to its higher homologues, 4T permits relatively straightforward processing from solution. For instance, dissolution temperatures <~140 °C for concentrations up to ~10 wt-% of this species are found in common non-chlorinated benign solvents such as decalin, with crystallization temperatures of T_c < 110 °C (*cf.* crystallization/composition diagram of 4T and decalin in Figure 2a). Such solutions were found to be thermally rather stable (as confirmed by nuclear magnetic resonance (NMR)-data – not shown), contrary to those of other conjugated oligomers, such as the polycyclic tetracene and pentacene.[30]

Phase behavior of 4T:HDPE blends

Blends of 4T and HDPE formed homogenous dilute solutions in decalin at elevated temperatures (see *"Experimental"*). In contrast to the P3HT:PE binaries described in

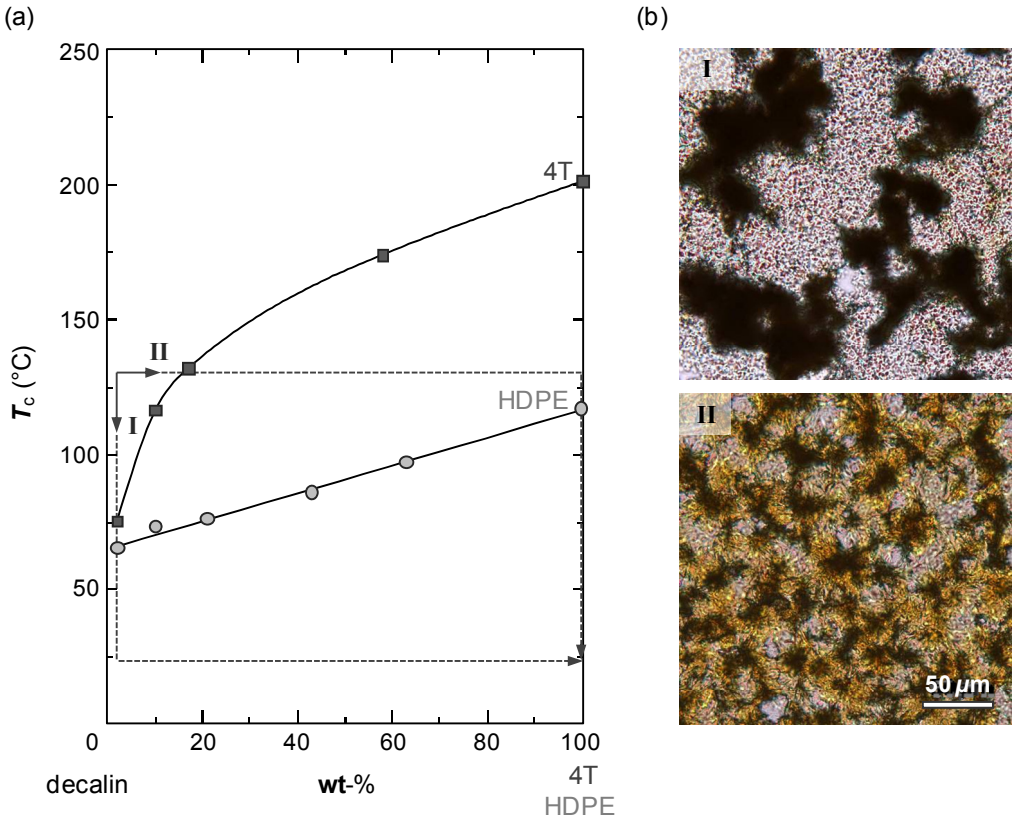

Figure 2. (a) Crystallization temperature/composition diagrams of 4T:decalin and HDPE:decalin binaries (superimposed) constructed from DSC second-cooling thermograms. In path I, a dilute solution was cooled to room temperature, followed by slow solvent removal at ambient, whereas in path II the solvent was rapidly evaporated at ~130 °C, followed by cooling to room temperature. (b) Optical micrographs (unpolarized transmitted light) of 50:50 4T:HDPE blends processed via pathway I (top) and II (bottom), respectively. Darker regions correspond to *α*-quaterthiophene.

references 26 and 29, for which two different solidification sequences can be induced (*i.e.* P3HT crystallizing prior to PE and *vice versa*), it was found that 4T exhibits a higher crystallization temperature than PE at all concentrations explored and, accordingly, invariably crystallized prior to the polymer. Conveniently, this was reported to be the crystallization sequence most favourable to yield high-mobility, low-percolation threshold systems.[26,29]

Hence, the 4T:HDPE blends allowed exploring the influence of different rates of solidification on the microstructures induced and, in turn, their influence on the electronic properties of the blends. For this purpose the two processing pathways indicated in Figure 2a were followed. In path I, hot solutions of the two components were cast at ambient, followed by solvent evaporation at that same temperature, causing the materials to slowly crystallize from dilute solutions. “Flash”-removal of the solvent was conducted

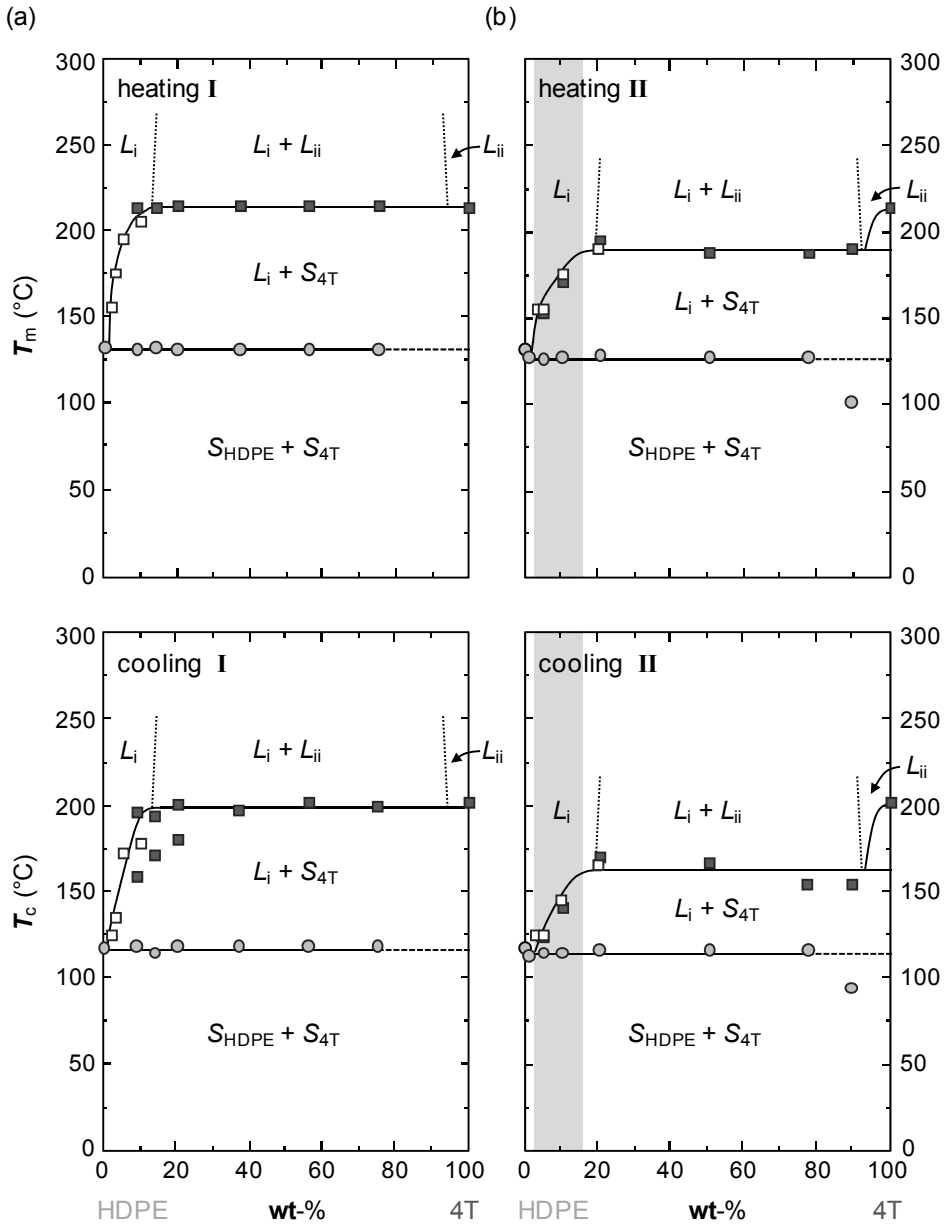

Figure 3. (a, b) Binary non-equilibrium temperature/composition diagrams of 4T:HDPE blends (top: heating; bottom: cooling) processed under conditions allowing respectively slow (pathway I) (a) and fast (pathway II) (b) solidification. The diagrams were constructed from DSC peak temperatures observed in first-heating and -cooling thermograms (filled symbols) and optical microscopy (open symbols). L_i, L_{ii} denote liquid phases and S_{4T}, S_{HDPE} solid 4T and polyethylene.

at elevated temperature of ~130 °C (path II), which resulted in faster crystallization of 4T from more concentrated viscous liquids, followed by solidification of the polymer.

Casting and solvent removal at ambient resulted in coarse microstructures, while 4T:HDPE films produced at elevated temperatures (*i.e.* fast solvent removal) featured a distinctly finer and more homogenous distribution of the semiconductor (Figure 2b).

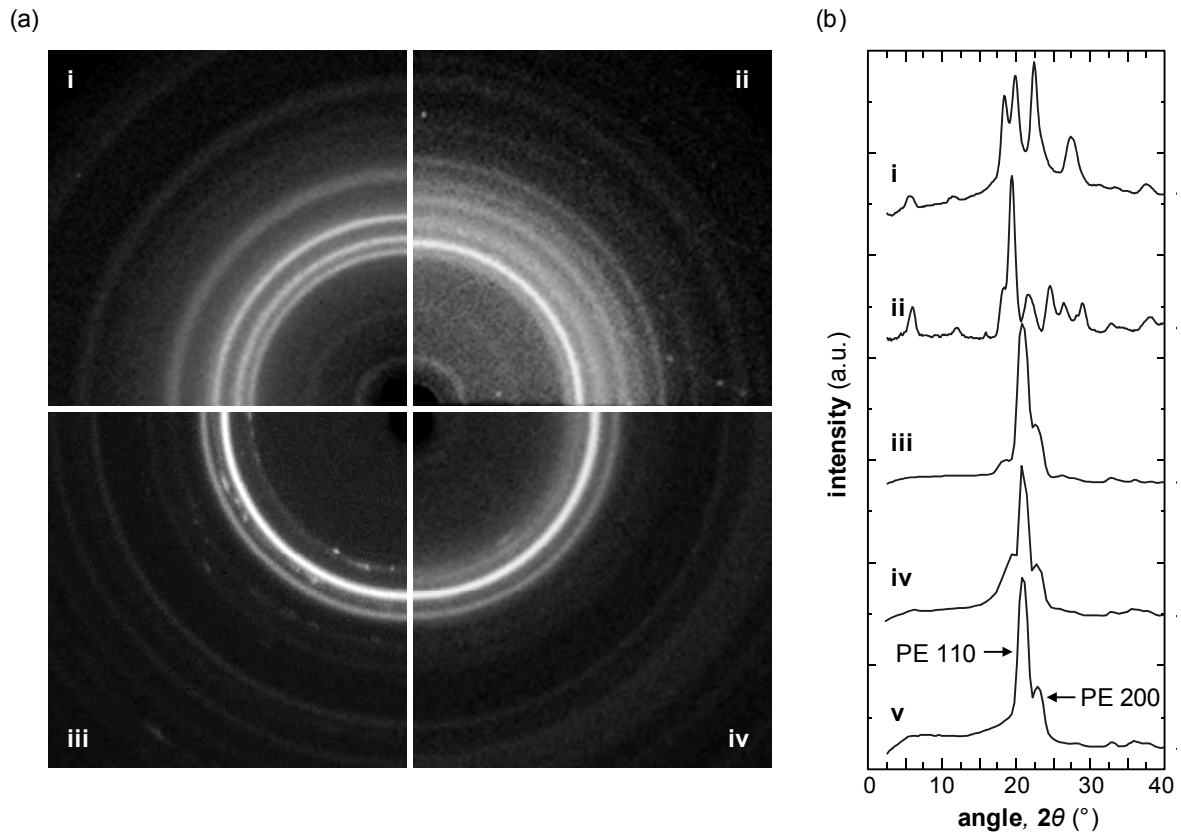

Figure 4. (a) Wide-angle X-ray scattering patterns and (b) radially integrated diffractograms of neat 4T (i: path I, ii: path II), 10:90 4T:HDPE binaries (iii: path I, iv: path II) and HDPE (v).

A significant influence of the rate of solidification was also found on the phase behavior of binary 4T:HDPE mixtures (see Figure 3). All temperature/composition diagrams indicate simple monotectic phase behavior with a miscibility gap of the two components over a wide range of temperatures and compositions (NB: Partial miscibility of the two blend components has previously been reported).[31] However, the melting, dissolution and crystallization temperatures of the semiconducting species were significantly affected by the manner in which the 4T:HDPE blends were produced. Considerably lower values of both T_m and T_c of 4T were recorded in blends obtained by casting at elevated temperatures, consistent with a smaller crystal and domain size of this species (*cf.* Figure 2b).

As the processing pathway selected is likely to affect also molecular order – known to potentially influence semiconducting properties of conjugated species[18,19] – wide-angle X-ray scattering (WAXS) was performed on the differently processed 4T:HDPE blends, as well as neat 4T and HDPE references (Figure 4). For the binary mixtures, diffraction patterns resulting from both individual components were observed. Neat 4T crystallized in the low temperature polymorph when processed according to path I and in the high

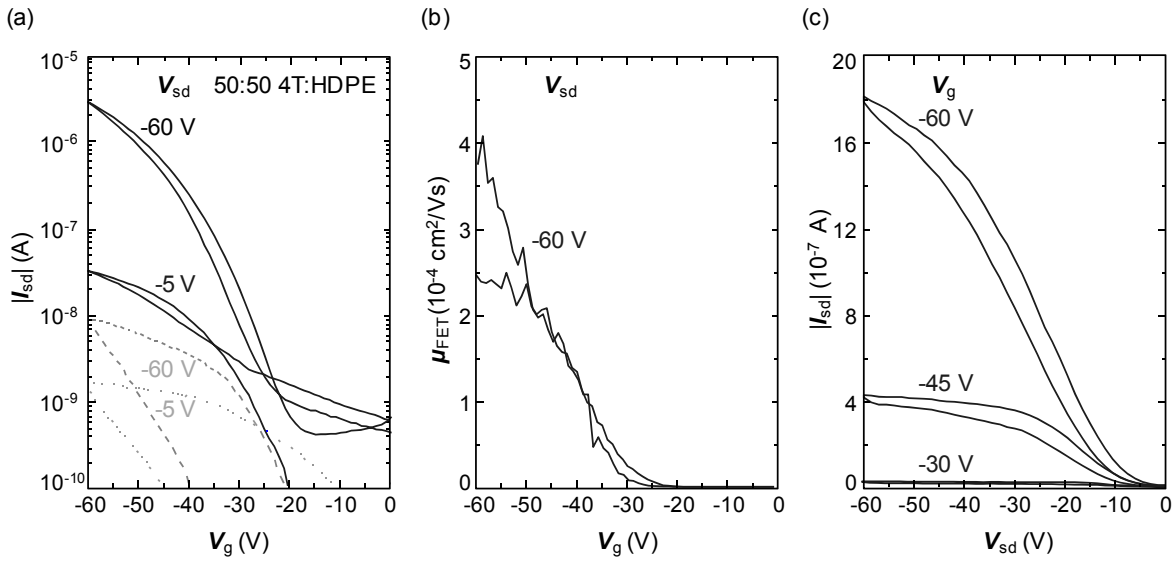

Figure 5. (a) Transfer characteristics of bottom-gate bottom-contact FET comprising a 50:50 4T:HDPE blend (channel length, L = 5 μm; channel width, W = 10 mm) fabricated by rapid solvent evaporation at ~130 °C (solid lines) and slow, at ambient (dashed lines). (b) Corresponding charge-carrier mobilities. (c) Output characteristics of an FET comprising an active layer cast at ~130 °C. Both forward and backward scans are shown.

temperature version via route II,[32] as was also found for 4T in the blends with HDPE (*cf.* Figure 4). For α-oligothiophenes of even number of thiophene units, however, charge transport characteristics were reported to be little affected by the polymorph,[18] and, hence, here of lesser concern.

Electronic properties of 4T:HDPE blends

In a first set of experiments, electronic properties of thin films of 4T:HDPE blends were examined in bottom-gate bottom-contact FET-configurations. Small source-drain currents were recorded in transistors based on 4T:HDPE produced by slow solvent removal at ambient. Mobilities in such films were estimated to be less than 10^{-6} cm^2/Vs.

In sharp contrast, clean FET characteristics were observed for devices comprising 4T:HDPE layers produced at elevated temperatures. In fact, current modulations of 10^3 and charge-carrier mobilities of ~1 x 10^{-4} cm^2/Vs were measured for blends comprising 10 wt-% 4T or more, exemplarily shown in Figure 5 for 50:50 4T:HDPE solidified in this manner. This is comparable with μ_{FET} values reported for vapour-deposited neat α-quaterthiophene.[15,16] Note, however, the sub-linear dependence of source-drain current, I_{sd}, on source-drain bias, V_{sd}, observed in the output characteristics at small V_{sd}, and the relatively small I_{sd} at V_{sd}=-5 V in the transfer characteristic, both suggesting limited charge

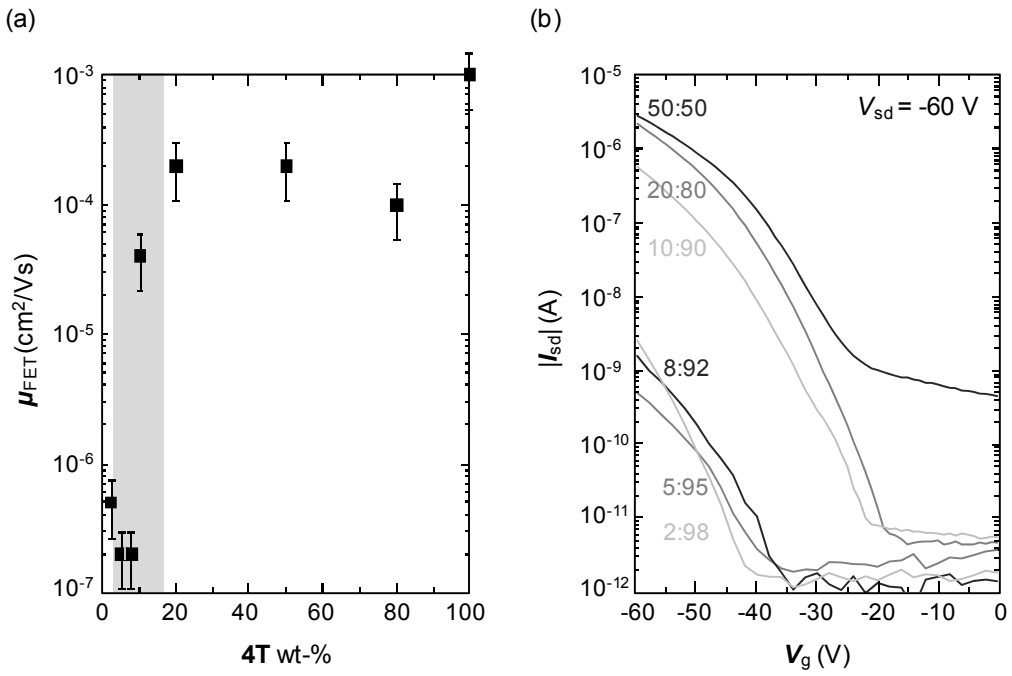

Figure 6. (a) Field-effect mobility and (b) transfer characteristics of 4T:HDPE blends cast at ~130 °C as function of composition.

injection (Figure 5). No significant dependence on channel length was observed for devices of $L = 5$ μm and 20 μm.

Electronic characteristics deteriorated rapidly when the semiconductor content in 4T:HDPE binaries was reduced to <~10 wt-%. Charge-carrier mobilities of $<10^{-6}$ cm^2/Vs were obtained for these devices, and a distinct shift of the threshold voltage, V_{th}, of ~15 V was observed (see Figure 6). This indicates that a barrier may have formed preventing efficient injection of charge carriers from the source-drain electrodes into the active layers that comprised larger concentrations of insulator.

Importantly, FET performance comparable to that of neat 4T was recorded with devices based on 4T:HDPE binaries that were processed via path II (at elevated temperatures) *and* featured liquid-liquid phase separation. In contrast, blends in which the two components were miscible in the liquid state (grey-shaded concentration regimes in Figures 3 and 6) showed rapidly deteriorating charge transport with decreasing semiconductor content, with device performance similar to that found for FETs based on active layers displaying large-scale phase separation, as induced by solidification path I.

CONCLUSIONS

In conclusion, blending α-quaterthiophene with insulating high-density polyethylene yields architectures of semiconducting characteristics comparable to those found for the neat semiconducting compound, provided that (i) the α-quaterthiophene content exceeds ~10 wt-% and (ii) the solidification rate is adjusted to prevent large-scale phase separation.

EXPERIMENTAL

Materials. α-Quaterthiophene (M_w = 330.5 g/mol, T_m = 213 °C, T_c = 201 °C) was purchased from Sigma-Aldrich, Buchs, Switzerland, and linear high-density polyethylene (Stamylan 7048, M_w = 10^5 g/mol, T_m = 132 °C, T_c = 117 °C) was supplied by DSM, Urmond, The Netherlands.

Thermal analysis. Thermo-gravimetric analysis (TGA) and differential scanning calorimetry (DSC) were conducted under N_2 atmosphere at a scan rate of 10 °C/min with a Mettler Toledo TGA/SDTA851^e and a Mettler Toledo DSC 822^e instrument, respectively. For DSC analysis of α-quaterthiophene and polyethylene in decalin (Fluka, Buchs, Switzerland; used as received), medium pressure 120 μl Mettler stainless steel crucibles sealed with Viton O-rings were utilized. The sample weight, including solvent, was ~50 mg. For characterization of the dried 4T:HDPE blends, amounts of about 5 mg were sealed in Al standard 40 μl crucibles.

Blend preparation. For thermal analysis and X-ray scattering studies, α-quaterthiophene: polyethylene blends were mixed by co-dissolving the materials in decalin (~1 wt-% total material content) at a temperature of ~140 °C, followed by solvent evaporation at ambient (path I) or at ~130 °C (path II). The latter temperature was selected to be above the crystallization temperature T_c of polyethylene, but below that of 4T (*cf.* Figure 2a).

Thin-film preparation. Thin films of blends of different compositions were cast from ~1 wt-% solutions (total solids content) at ambient or ~130 °C, onto glass slides for optical microscopy and onto doped silicon-silicon oxide (Si-SiO_2) substrates treated with octadecyltrichlorsilane (OTS) for FET studies. The thickness of these films after solvent evaporation was 5 - 10 μm.

Optical microscopy. Optical microscopy was carried out with a Leica DMRX polarizing microscope equipped with a Mettler Toledo FP82HT hot stage. For construction of the sections of the binary phase diagrams at low concentrations of one component, blend films were heated and cooled at 10 °C/min in the hot stage and the transition temperatures were deduced from appearance/disappearance of birefringence of the respective crystalline phases.

Wide-angle X-ray scattering (WAXS). Wide-angle X-ray scattering patterns of different 4T:HDPE blends were recorded with an Xcalibur PX instrument (Oxford Diffraction).

Field-effect transistors (FETs). Bottom-gate bottom-contact FETs were fabricated in a N_2 atmosphere on highly doped Si-wafers with a thermally grown ~250 nm SiO_2 layer; the two layers served as the gate electrode and gate insulator, respectively. Prior to application of the semiconductor, the Si-wafers were surface-treated with octadecyltrichlorsilane according to the following procedure. Si-SiO_2 substrates were cleaned in an ultrasonic bath with acetone, water and isopropyl alcohol (in this sequence) and exposed to UV-light for 20 min. Subsequently, the substrates were heated to 60 °C for 15 to 20 min in a mixture of toluene and OTS (3:7 ratio). Finally, the OTS-treated Si-SiO_2 was cleaned in hexane, acetone and isopropyl alcohol, followed by drying with nitrogen. Au source and drain electrodes (~30 nm thick) were defined by standard photolithography (channel lengths, $L = 5$ μm and 20 μm; channel width, $W = 10$ mm). Electronic characterization of the FETs was conducted in a N_2 atmosphere with a HP4155B semiconductor parameter analyzer. Field-effect mobilities were calculated from transfer characteristics (saturation regime) employing the relation:

$$\frac{\delta I_{sd}(V_g)}{d V_g} = \frac{C_i \cdot W}{L} \mu_{FET}(V_g, V_{sd}) \cdot (V_g - V_0) \qquad (1)$$

where I_{sd} is the source-drain current (saturation regime), V_g and V_{sd} gate and source-drain voltage, respectively, C_i the insulator capacitance, W and L the channel width and length, and V_0 the turn-on voltage.[33]

References

(1) G. Horowitz, *Adv. Mater.* **1998**, *10*, 365.

(2) H. E. Katz, Z. N. Bao, S. L. Gilat, *Acc. Chem. Res.* **2001**, *24*, 359.

(3) H. Sirringhaus, N. Tessler, R. H. Friend, *Science* **1998**, *280*, 1741.

(4) J. H. Borroughes, D. D. C. Bradley, A. R. Brown, R. N. Marks, K. Mackay, R. H. Friend, P. L. Burns, A. B. Holmes, *Nature* **1990**, *347*, 539.

(5) P. Furuta, J. Brooks, M. E. Thompson, J. M. J. Fréchet, *J. Am. Chem. Soc.* **2003**, *125*, 13165.

(6) W. U. Huynh, J. J. Dittmer, J. Janke, W. C. Libby, G. L. Whiting, A. P. Alivisatos, *Adv. Funct. Mater.* **2003**, *13*, 73.

(7) B. Crone, A. Dodabalapur, A. Gelperin, L. Torsi, H. E. Katz, A. J. Lovinger, Z. Bao, *Appl. Phys. Lett.* **2001**, *78*, 2229.

(8) T. Someya, H. E. Katz, A. Gelperin, A. J. Lovinger, A. Dodabalapur, *Appl. Phys. Lett.* **2002**, *81*, 3079.

(9) A. R. Brown, A. Pomp, C. M. Hart, D. M. de Leeuw, *Science* **1995**, *270*, 972.

(10) B. Crone, A. Dodabalapur, Y. Y. Lin, R. W. Filas, Z. Bao, A. la Duca, R. Sarpeshkar, H. E. Katz, W. Li, *Nature* **2000**, *403*, 521.

(11) C. J. Drury, C. M. Mutsaers, C. M. Hart, M. Matters, D. M. de Leeuw, *Appl. Phys. Lett.* **1998**, *73*, 108.

(12) C. D. Dimitrakopoulos, P. R. L. Malenfant, *Adv. Mater.* **2002**, *14*, 99.

(13) J. Nakayama, T. Konishi, M. Hoshino, *Heterocycles* **1988**, *27*, 1731.

(14) P. Bäuerle, *Handbook of Oligo- and Polythiophenes: The Synthesis of Oligothiophenes*; D. Fichou, Ed., Wiley-VCH: Weinheim, Germany, **1999**.

(15) G. Horowitz, R. Hajlaoui, D. Fichou, A. E. Kassmi, *J. Appl. Phys.* **1999**, *85*, 3202.

(16) H. E. Katz, L. Torsi, A. Dodabalapur, *Chem. Mater.* **1995**, *7*, 2235.

(17) X. M. Hong, H. E. Katz, A. J. Lovinger, B.-C. Wang, K. Raghavachari, *Chem. Mater.* **2001**, *13*, 4686.

(18) S. Nagamatsu, K. Kaneto, R. Azumi, M. Matsumoto, Y. Yoshida, K. Yase, *J. Phys. Chem. B* **2005**, *109*, 9374.

(19) B. Servet, G. Horowitz, S. Ries, O. Langorsse, P. Alnot, A. Yassar, F. Deloffre, P. Srivastave, R. Hajlaoui, P. Lang, F. Garnier, *Chem. Mater.* **1994**, *6*, 1809.

(20) M. E. Hajlaoui, F. Garnier, L. Hassine, F. Kouki, H. Bouchriha, *Synth. Met.* **2002**, *129*, 215.

(21) M. Melucci, M. Gazzano, G. Barbarella, M. Cavallini, F. Biscarini, P. Maccagnani, P. Ostoja, *J. Am. Chem. Soc.* **2003**, *125*, 10266.

(22) H. Akimichi, K. Waragai, S. Hotta, H. Kano, H. Sakaki, *Appl. Phys. Lett.* **1991**, *58*, 1500.

(23) F. Garnier, G. Horowitz, X. Z. Peng, D. Fichou, *Synth. Met.* **1991**, *45*, 163.

(24) J. Nakayama, Y. Nakamura, S. Murabayashi, M. Hoshino, *Heterocycles* **1987**, *26*, 939.

(25) D. Fichou, M.-P. Teulade-Fichou, G. Horowitz, F. Demanze, *Adv. Mater.* **1997**, *9*, 75.

(26) S. Goffri, C. Müller, N. Stingelin-Stutzmann, D. W. Breiby, C. P. Radano, J. W. Andreasen, R. Thompson, R. A. J. Janssen, M. M. Nielsen, P. Smith, H. Sirringhaus, *Nature Mater.* **2006**, *5*, 950.

(27) J.-F. Chang, J. Clark, N. Zhao, H. Sirringhaus, D. W. Breiby, J. W. Andreasen, M. M. Nielsen, M. Giles, M. Heeney, I. McCulloch, *Phys. Rev. B* **2006**, *74*, 115318.

(28) J.-F. Chang, B. Sun, D. W. Breiby, M. M. Nielsen, T. I. Sölling, M. Giles, I. McCulloch, H. Sirringhaus, *Chem. Mater.* **2004**, *16*, 4772.

(29) C. Müller, S. Goffri, J. W. Andreasen, D. W. Breiby, H. D. Chanzy, R. A. J. Janssen, M. M. Nielsen, C. P. Radano, H. Sirringhaus, P. Smith, N. Stingelin-Stutzmann, *Adv. Funct. Mater.* **2007**, *17*, 2674.

(30) A. Maliakal, K. Raghavachari, H. E. Katz, E. Chandross, T. Siegrist, *Chem. Mater.* **2004**, *16*, 4980.

(31) H. Kuhn, R. Eckert, Deutsches Patentamt, Auslegeschrift 1119546, B 57691 IXa/42h, **1961**.

(32) D. Fichou, *J. Mater. Chem.* **2000**, *10*, 571.

(33) A. R. Brown, C. P. Jarret, D. M. de Leeuw, M. Matters, *Synth. Met.* **1997**, *88*, 37.

Chapter VI

Influence of Molecular Architecture and Processing on Properties of Semiconducting Arylacetylene:Insulating Poly(vinylidene fluoride) Blends

INTRODUCTION

Over the past three decades, the field of organic electronics has advanced rapidly, driven by the synthesis of new semiconducting small molecules, oligomers and polymers that enabled better devices, and new functionalities. The strong interest in organics stems from the fact that this class of semiconductors holds the promise of cost-efficient processing characteristics, light weight, (semi-)transparency and mechanical flexibility. Most importantly, they have the potential to be readily chemically tailored to fine tune properties such as charge transport, light absorption, emission, etc., to address various application needs.[1-13]

Major challenges, however, still exist. Main drawbacks of many of the commonly used materials are, for instance, their often modest electrical performance, which in general remains well below that of the widely deployed inorganic materials (*e.g.* amorphous hydrogenated silicon), and their vulnerability to ambient oxidants, as many of the materials tend to degrade upon contact with air and/or light.[14-17] This environmental sensitivity of organic semiconducting compounds requires vacuum- or inert atmosphere-based device fabrication steps[18-21] and encapsulation in barrier (sandwich) structures.[22,23] Unfortunately, such stringent processing protocols significantly contribute to the cost of organic-based electronics, which has not declined as quickly as originally envisioned, while competitive technologies have enjoyed more rapid than anticipated economic advantage.[24] All these constraints render organic-based devices less obvious as a viable alternative to more conventional electronics.

This development may, however, be halted – if not reversed – provided that new organic semiconductor systems are developed that exhibit high charge-carrier mobilities, environmental stability *and* a beneficial economy of scale both through straightforward synthesis and processing. While a limited number of high mobility, environmental stable materials have been advanced,[7,25-30] one of the key challenges, which remains and limits further progress, is the provision of straightforward and meaningful comparisons between the electronic properties of different compounds. Such comparisons would allow for efficient materials design and screening but necessitates high reproducibility in synthesis, processing and reliable device fabrication and characterization.

Blending of organic semiconductors with insulating (semi-)crystalline polymers has been shown to be a useful strategy to address, among other things, the latter two issues (*cf. Chapter V* and references 31-33). In addition, blending properly selected commodity

polymers with the semiconducting material(s) should enable control over melt- and solution-viscosity. In the case of small-molecular semiconductors, a suitable polymer matrix may furthermore be mandatory to meet the ink rheology requirements for specific printing steps in solution-processed devices. From a device point of view, blending is an interesting approach, as it may also lead to multi-component structures with a property matrix that is often not accessible with the individual components. The latter is possibly best exemplified by organic semiconductor:insulator blends, which – under appropriate processing conditions – feature excellent performance in field-effect transistors (FETs) and organic photovoltaics (OPVs) at remarkably low semiconductor contents combined with highly desirable mechanical properties when a tough insulating component is utilized.[31] Besides improved and reliable film formation, blending promises the prospect for major cost reduction, truly "flexible" electronics and, often, significantly enhanced environmental stability of devices produced with them.

In this chapter we explored bi-component blends comprising arylacetylenes and the insulating poly(vinylidene fluoride) (PVDF). PVDF was selected as the insulating component as this polymer has been shown to allow film processing at room temperature of, for instance, poly(*3*-hexylthiophene) (P3HT):PVDF binaries;[32] this in contrast to, *e.g.*, blends based on high-density polyethylene which require deposition temperatures above ~70 °C, as demonstrated in *Chapter V*. For the semiconducting species, the focus was on *small-molecular* arylacetylenes.[34-45] From a synthetic point of view these compounds exhibit a number of advantages, including availability of efficient synthetic protocols[46-54] that offer the possibility to access in large quantities a broad variety of molecules with specific geometries and flexibility in new conceptions of steric and conformational structures. In addition, their shape-persistent rod-like structures may be of beneficial use for the construction of a broad spectrum of nano- and microstructures. A further major advantage of arylacetylenes is that they can be readily synthesized from easily accessible precursors, do not require exotic, rare materials, reducing risks regarding materials supply or costs; their production can easily be scaled up; and, finally, the compounds can readily be isolated in high purity.

Here, the concentration is on arylacetylenes with an anthracene[55,56] backbone, since this core may enable enhanced solubility and stability when compared to, for instance, pentacene, which has become a benchmark in the organic electronics field. Moreover, the anthracene core is a beneficial chromophore unit. Importantly, their chemical structure allows for derivatization with flexible chains at the terminal phenyl-ring systems to

modulate the phase behavior and solubility of the resulting arylacetylenes. Those latter attributes permit to manipulate their solid-state structure over a large range of length scales, the influence of which on simple electronic characteristics being the subject of this chapter.

RESULTS AND DISCUSSION

9,10-Bis(phenylethynyl)anthracene:PVDF

In a first set of experiments, the phase behavior of blends of the commercially available 9,10-bis(phenylethynyl)anthracene **1** (T_m = 256 °C) and PVDF was explored. For this purpose, the non-equilibrium temperature/composition diagram of the **1**:PVDF binary was determined by differential scanning calorimetry (DSC) and variable-temperature polarized optical microscopy – see Figure 1a. As is evident from this diagram, the small-molecular semiconductor and polymer insulator are largely incompatible, resulting in a classical monotectic behavior featuring an extremely large miscibility gap. The significant difference between the melting temperatures between the two components resulted in a $L_i + S_1$ two-phase region that extended over more than 100 °C.

The phase behavior of blends of **1**:PVDF naturally has a significant influence also when processing them from solution. This is illustrated with a 40:60 wt-% **1**:PVDF blend, the composition of which was selected to provide a good compromise between electronic characteristics and film forming properties. When cast at 25 °C from cyclohexanone (~2 wt-% total material content), the semiconducting:insulating binary formed a microstructure comprised of crystalline arylacetylene needles of hundreds of microns length coarsely distributed throughout a PVDF matrix (Figure 1c). The formation of this solid-state structure is readily understood on the basis of the superimposed crystallization temperature/composition diagrams of the two respective components and the solvent cyclohexanone, presented in Figure 1b. These diagrams indicate that during evaporation of the solvent from this blend, **1** solidified prior to PVDF essentially at all compositions. Due to the relatively large gap between the solidus of the two components, *i.e.* the significant difference in supercooling that is required for the semiconductor and insulator to solidify from cyclohexanone, a coarse, highly phase separated structure resulted.

Not unexpectedly, increasing the rate of solidification of the two components by applying higher deposition temperatures, causing an enhanced rate of solvent evaporation,

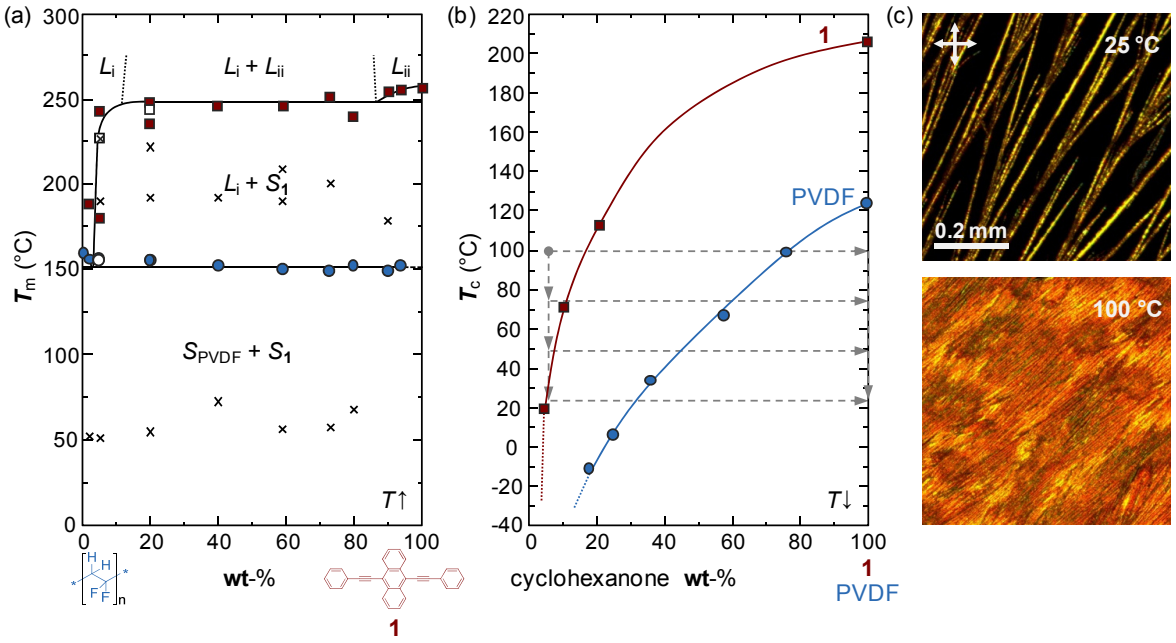

Figure 1. (a) Binary non-equilibrium temperature/composition diagram of **1**:PVDF blends produced by co-dissolution in cyclohexanone, followed by solvent evaporation at ambient. The diagrams were constructed with peak temperatures recorded during first heating in differential scanning calorimetry (DSC, filled symbols) and polarized optical microscopy (open symbols). L_i, L_{ii} denote liquid phases and S_1, S_{PVDF} solid phases of compound **1** and PVDF, resp.; x indicates exceedingly minor endothermic transitions. (b) Superimposed crystallization temperature/composition diagrams of **1**:cyclohexanone and PVDF:cyclohexanone constructed with DSC peak crystallization temperatures in second-cooling thermograms. The gray dashed lines indicate different processing routes applied for **1**:PVDF binaries with solvent removal at 25, 50, 75 or 100 °C, followed by cooling to room temperature. (c) Polarized optical micrographs of **1**:PVDF 40:60 blends solidified at 25 °C (top) and 100 °C (bottom), respectively (polarizer/analyzer indicated with white arrows).

yielded a much finer and more homogeneous microstructure (*cf.* Figure 1c), similar to those observed for *α*-quaterthiophene:polyethylene blends reported in *Chapter V*. However, from a processing point of view – particularly with respect to printing – high-temperature operations are not particularly desirable, and, therefore it was explored to influence the microstructure formation not by thermal means but by chemical modification of the semiconducting species.

9,10-Bis[3,4-bis(hexyloxy)phenylethynyl]anthracene:PVDF

In order to beneficially alter the phase- and solidification behavior of the semiconducting:insulating arylacetylene:PVDF blends through adjustment of the physico-chemical properties of the small-molecular compound by chemical modification, we elected to introduce four flexible hexyloxy side-chains at the terminal phenyl-ring systems.

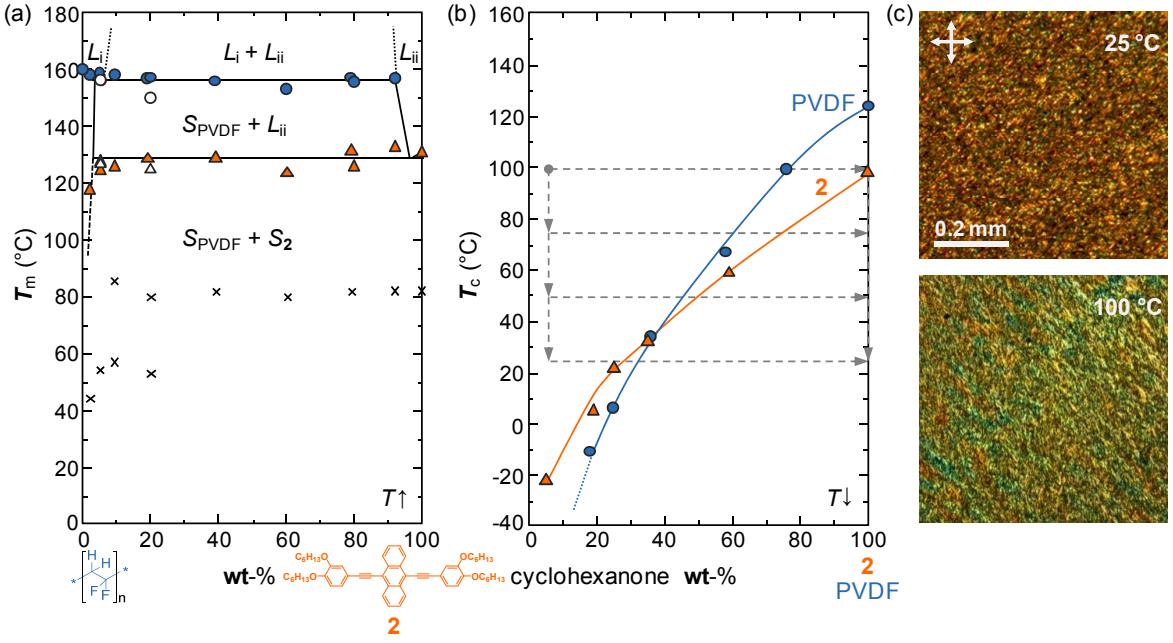

Figure 2. (a) Binary non-equilibrium temperature/composition diagram of **2**:PVDF blends. L_i, L_{ii} denote liquid phases and S_2, S_{PVDF} solid phases of compound **2** and PVDF, resp.; x indicates exceedingly minor endothermic transitions. (b) Superimposed crystallization temperature/composition diagrams of **2**:cyclohexanone and PVDF:cyclohexanone constructed with DSC peak crystallization temperatures in second-cooling thermograms. (c) Polarized optical micrographs of **2**:PVDF 40:60 blends solidified at 25 °C (top) and 100 °C (bottom), respectively (polarizer/analyzer indicated with white arrows).

This compound **2**, consequently, featured a considerably lower melting temperature (T_m = 131 °C), and associated enhanced solubility in common solvents, compared to its unsubstituted counterpart **1**. The **2**:PVDF temperature/composition diagram is shown in Figure 2a. From this diagram, it is clear that also this compound, like **1**, is largely incompatible with PVDF. However, due to its lower melting temperature, the temperature range between liquidus and solidus lines in the two systems is significantly reduced, *i.e.* from ΔT ~100 °C for **1**:PVDF blends to ~30 °C for the **2**:PVDF binaries.

The significantly increased solubility of **2** in cyclohexanone also resulted in a distinct shift of its solidus not only to lower temperatures but also higher concentrations (Figure 2b). As a consequence, the (superimposed) crystallization temperature/composition diagrams of **2**:cyclohexanone and PVDF:cyclohexanone feature a crossover of the two solidus lines; and, hence, there exist two distinct regimes in which, in principle, the semiconductor can either crystallize prior to, or after the polymer. In either case, however, at any given concentration or temperature, below their liquidus the difference in supercooling experienced by both components is relatively small when compared to the above described binary. As a consequence, invariably the organic semiconductor **2** and

PVDF solidified virtually simultaneously, yielding fine grained structures both at room temperature and 100 °C (*cf.* Figure 2c). Note, however, that above and below 40 - 50 °C the sequence of solidification reversed.

Electronic properties

Having the chemical means and corresponding processing protocols to readily adjust arylacetylenes:PVDF blend microstructure by either controlling composition or deposition temperature, we sought to elucidate the influence of solid-state morphology on the performance of devices fabricated with them, and also probed if their electronic characteristics were affected by the solubilizing side-chain substitutions. For this purpose, bottom-gate, bottom-contact field-effect transistors were fabricated with binaries of PVDF comprising 40 wt-% of, respectively, **1** and **2**, casting them at 25, 50, 75 or 100 °C. Electronic characteristics of these devices are presented in Figures 3 and 4.

What is immediately evident from the FET data presented is that the performance of devices with **1**:PVDF binaries increased steadily with the deposition temperature. By contrast, processing conditions had only a minor influence on FET performance of **2**:PVDF blends; however an optimum casting temperature was observed around 50 °C. These observations can be directly correlated with the superimposed temperature/composition diagrams presented in Figures 1 and 2. As shown above for **1**:PVDF blends, a rapid solidification sequence of the two components, realized through thermal control of the rate of solvent evaporation, resulted in a finely phase-separated blend microstructure, apparently, enhancing device performance. In the case of compound **2**, the reduced melting temperature and increased solubility resulting from the introduction of side-chains, caused the two components under most conditions to solidify rapidly after each other, if not simultaneously, even when casting the active layer at room temperature. The resulting finely phase-separated bi-component layers invariably lead to good device characteristics. Deposition at more elevated temperatures (>50°C), however (slightly) affected FET performance of **2**:PVDF blends in a negative manner, despite the observation that the degree of phase segregation in the binary film was not significantly different. This incident is attributed to the fact that in these cases the sequence of crystallization of the components is reversed at elevated temperatures, with the insulating polymer crystallizing *prior* to the active species. The latter observation is in agreement with previous work in which it was shown that this solidification mode not only does not promote the necessary percolation of the semiconducting species, but might even prevent that.[31,57]

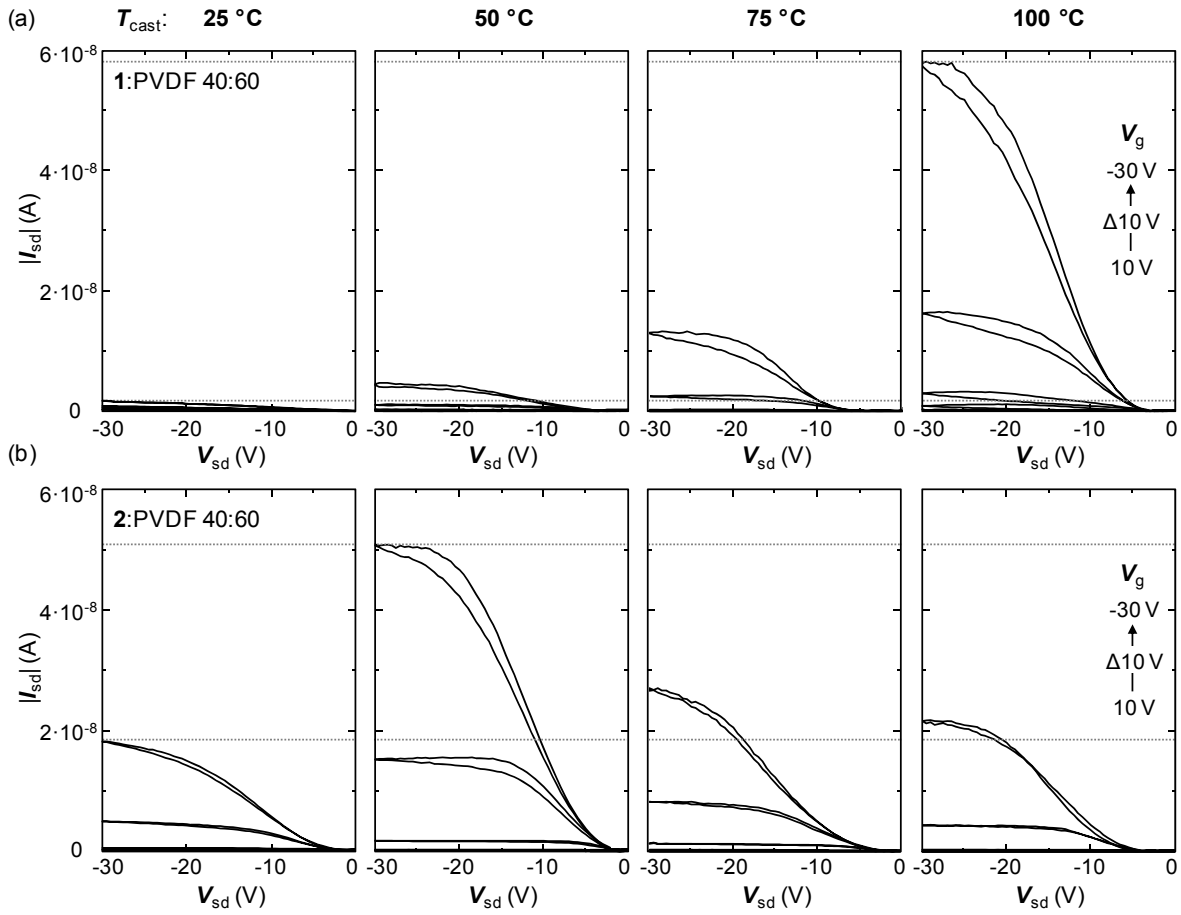

Figure 3. (a) Output characteristics of bottom-gate bottom-contact FETs (L = 10 μm; W = 10 mm) of **1**:PVDF and (b) **2**:PVDF 40:60 blend films fabricated at 25, 50, 75 and 100 °C. In all graphs, forward and backward scans are shown. Gray dotted lines indicate $I_{sd,\ max}$ of FETs comprising **1**:PVDF blend films produced via solvent evaporation at 100 and 25 °C, respectively and **2**:PVDF binaries fabricated at 50 and 25 °C, respectively.

From the above it is clear that very similar device characteristics (charge-carrier mobility μ_{FET} ~5 x 10^{-4} cm^2/Vs; ON-OFF ratio ~10^3) can be obtained for both arylacetylenes, provided that a finely phase-separated blend structure is induced. Importantly, the melting-temperature-reducing and solubilizing hexyloxy side-chains in compound **2** did not negatively affect charge transport. Furthermore, the results presented in this chapter show that a key for providing meaningful comparisons between different semiconducting species – even simple derivatives – is to select processing conditions that are adjusted to the phase behavior of the respective system to yield comparable structures of their solid state. Simple binary crystallization temperature/composition diagrams of the individual component in the solvent selected can be useful to identify a suitable processing window for this purpose, both with respect of processing temperatures and solution concentrations.

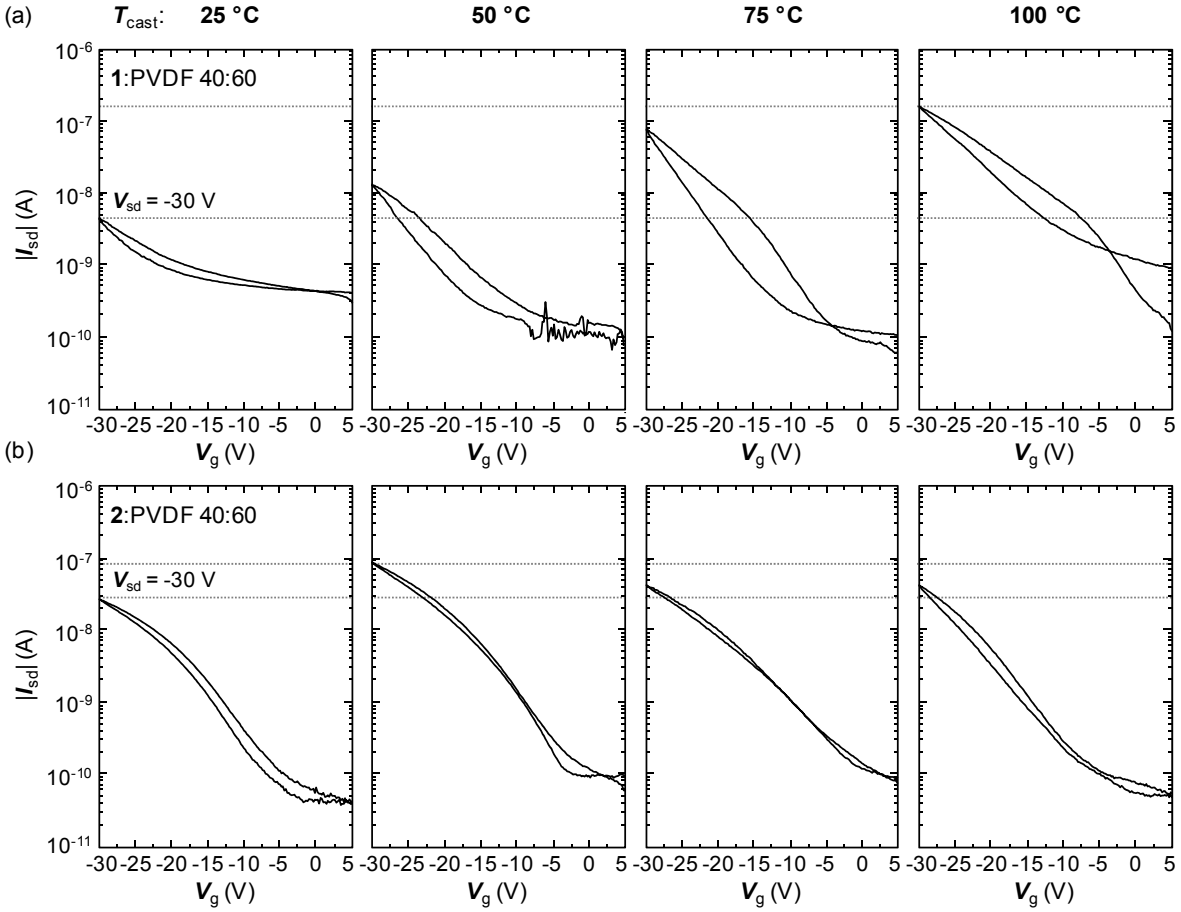

Figure 4. (a) Transfer characteristics of bottom-gate bottom-contact FETs (L = 10 μm; W = 10 mm) of **1**:PVDF and (b) **2**:PVDF 40:60 blend films fabricated at 25, 50, 75 and 100 °C. In all graphs, forward and backward scans are shown. Gray dotted lines indicate $I_{sd,\ max}$ of FETs comprising **1**:PVDF blend films produced via solvent evaporation at 100 and 25 °C, respectively and **2**:PVDF binaries fabricated at 50 and 25 °C, respectively.

Percolation

After having established optimum processing conditions of typical blends of PVDF with both semiconducting compounds **1** and **2**, it was proceeded to explore the maximum content of the insulating polymer that could be added without dramatically deteriorating the electronic properties of such blends. For this purpose the focus was on **2**:PVDF binaries as they allow for a significantly broader processing window both with respect of deposition temperature and composition when compared to the **1**:PVDF system. Thus, FETs were fabricated with active layers of a range of compositions *via* solvent evaporation at 50 °C.

Remarkably, the electronic performance of the devices was found to *increase* by more than one order of magnitude when certain amounts of the insulating PVDF were added to the semiconductor, as indicated by the significantly increased source-drain currents and

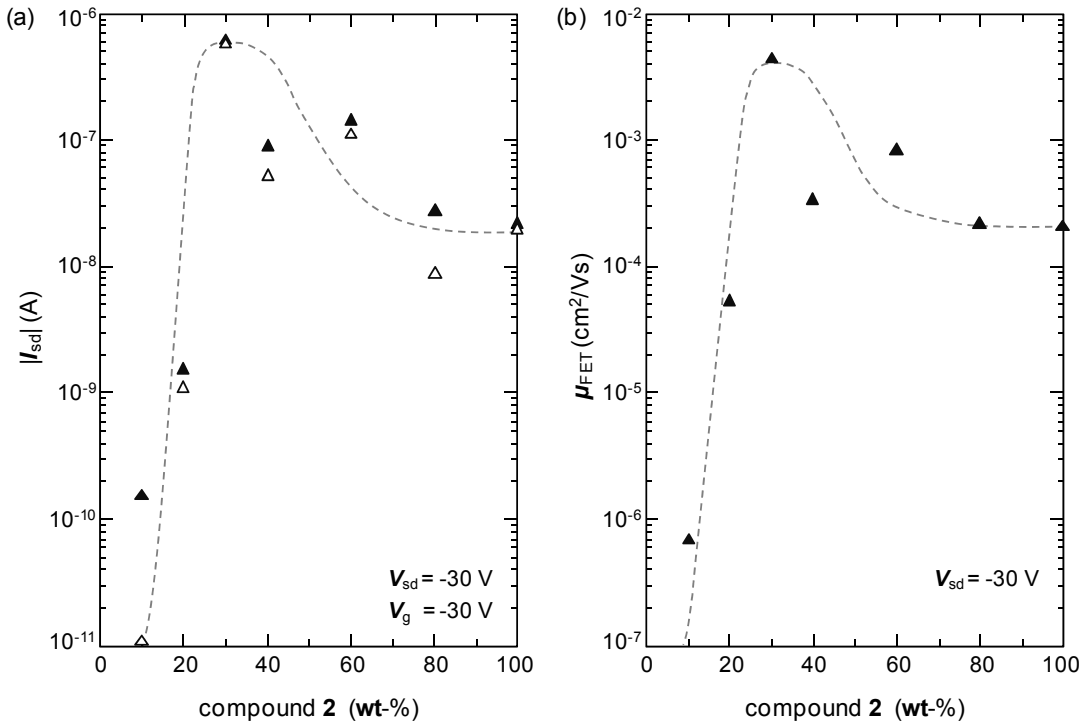

Figure 5. (a) Source-drain currents, I_{sd}, of **2**:PVDF binaries of different compositions solidified at 50 °C at $V_{sd} = V_g = -30$ V, deduced from FET transfer (filled symbols) and output characteristics (open symbols). (b) Corresponding field-effect mobilities deduced from the saturated regime in FET transfer characteristics (dashed lines are a guide to the eye only).

field-effect mobilities (Figure 5). Maximum device performance was reached for a blend comprising only ~30 wt-% of the semiconductor **2**. The latter featured ON-currents of ~5 x 10^{-7} A, field-effect mobilities in the saturation regime of ~4 x 10^{-3} cm^2/Vs and ON-OFF ratios of 10^3 compared to corresponding values of, resp. ~2 x 10^{-8} A, ~2 x 10^{-4} cm^2/Vs and 10^2 for the neat compound **2**. Evidently, adding the insulating polymer PVDF to the small-molecular semiconductor enhanced the electronic performance of the latter species. This beneficial phenomenon is attributed to improved film-forming properties of such blends. At high small molecule content (≥80 wt-%), film formation is dominated by that species and the amount of polymeric material appears to be insufficient to provide for the generation of continuous and homogenous active layers. As a consequence, the resulting brittle and discontinuous films featured negatively affected charge transport. On the other hand, blends comprising >70 wt-% of the insulating polymer appeared to feature a solid-state structure in which the organic semiconducting compound increasingly failed to form a percolating network required for electronic transport.

CONCLUSIONS

In summary, blends of two small-molecular arylacetylene derivatives with the semi-crystalline, insulating polymer PVDF were presented that exhibit FET characteristics comparable to those of the neat semiconductors. The chemical design of the two semiconducting compounds was selected in such a way that it allows facile synthesis protocols with readily accessible up-scaling options and permits control of their thermal properties. Beneficially, selection of processing controls was found to be more critical in obtaining optimum device performance than molecular design, which indicates that electronic characteristics can be tailored from the outset while processing parameters can be adjusted according to the phase behavior of the active compound.

EXPERIMENTAL

Materials. 9,10-Bis(phenylethynyl)anthracene (**1**) was purchased from Alfa Aesar GmbH & Co KG, Karlsruhe, Germany, and used as received.
9,10-Bis[3,4-bis(hexyloxy)phenylethynyl]anthracene (**2**) was synthesized according to a previously reported procedure.[39] Poly(vinylidene fluoride) (PVDF) (M_w = 534 kg/mol) was acquired from Aldrich, Steinheim, Germany. Cyclohexanone was purchased from Acros, Geel, Belgium, and used as received.

Sample preparation. Blends for thermal analysis and optical microscopy were prepared by co-dissolving the semiconducting species and PVDF in cyclohexanone (~2 wt-% total solids content) at 100 °C, followed by solvent evaporation at ambient conditions or at ~100 °C. Blends for FETs were prepared by co-dissolving the different materials in cyclohexanone (~6 wt-% solids content) at 100 °C, followed by subsequent adjustment of the solution temperatures to the respective processing temperatures of 25, 50, 75 or 100 °C. To allow film fabrication under isothermal conditions, solutions, metal substrate holders and substrates (doped silicon-silicon oxide (Si-SiO_2)) were equilibrated for ca. 10 min at the designated temperature before spin-drop-casting active layers with a Laurell WS-400B-6NPP/LITE spin-coater at 500 rpm.

Thermal analysis. Differential scanning calorimetry (DSC) was conducted under N_2 atmosphere at a scan rate of 10 °C/min with a Mettler Toledo DSC 822^e instrument. For DSC analysis of **1**, **2** and PVDF in cyclohexanone, medium pressure 120 μl Mettler stainless steel crucibles sealed with Viton O-rings were utilized. The total sample weight varied between 20 and 40 mg. For characterization of the dried blend films, amounts of ~5 mg were sealed in Al standard 40 μl crucibles.

Optical microscopy. Room temperature optical microscopy was carried out with a Leica DM4000M polarizing microscope. Variable-temperature polarized optical microscopy was performed with a Leica DMRX microscope equipped with a Mettler Toledo FP82HT hot stage. For construction of temperature/composition diagrams of binaries of low semiconductor contents, blend films were heated at 10 °C/min in the hot stage under N_2 atmosphere; in these cases transition temperatures were deduced from the disappearance of birefringence of the respective crystalline phases. At higher arylacetylene contents, peak endo- and exotherm temperatures recorded by DSC were employed.

Field-effect transistors (FETs). Bottom-gate bottom-contact field-effect transistors were fabricated on highly doped Si-wafers with a thermally grown ~250 nm SiO_2 layer. The two layers served as the gate electrode and gate insulator, respectively. Au source and drain electrodes (30 nm thick) were defined by standard photolithography (channel length, $L = 10$ μm; channel width, $W = 10$ mm). Prior to use, the Si-SiO_2 substrates were cleaned in an ultrasonic bath with acetone and isopropyl alcohol, followed by drying with a nitrogen flow. Electronic characterization of the FETs was carried out in a N_2 atmosphere with a Keithley 4200 semiconductor parameter analyzer.

References

(1) C. K. Chiang, C. R. Fincher, Y. W. Park, A. J. Heeger, H. Shirakawa, E. J. Louis, S. C. Gau, A. G. MacDiarmid, *Phys. Rev. Lett.* **1977**, *39*, 1098.

(2) Y. Cao, P. Smith, A. J. Heeger, *Synth. Met.* **1992**, *48*, 91.

(3) J. H. Burroughes, D. D. C. Bradley, A. R. Brown, R. N. Marks, K. Mackay, R. H. Friend, P. L. Burns, A. B. Holmes, *Nature* **1990**, *347*, 539.

(4) J. J. M. Halls, C. A. Walsh, N. C. Greenham, E. A. Marseglia, R. H. Friend, S. C. Moratti, A. B. Holmes, *Nature* **1995**, *376*, 498.

(5) G. Yu, J. Gao, J. C. Hummelen, F. Wudl, A. J. Heeger, *Science* **1995**, *270*, 1789.

(6) M. Mushrush, A. Facchetti, M. Lefenfeld, H. E. Katz, T. J. Marks, *J. Am. Chem. Soc.* **2003**, *125*, 9414.

(7) C. R. Newman, C. D. Frisbie, D. A. da Silva Filho, J.-L. Brédas, P. C. Ewbank, K. R. Mann, *Chem. Mater.* **2004**, *16*, 4436.

(8) J. E. Anthony, *Angew. Chem. Int. Ed.* **2008**, *47*, 452.

(9) H. E. Katz, Z. Bao, S. L. Gilat, *Acc. Chem. Res.* **2001**, *34*, 359.

(10) K. M. Coakley, M. D. McGehee, *Chem. Mater.* **2004**, *16*. 4533.

(11) S. Allard, M. Forster, B. Souharce, H. Thiem, U. Scherf, *Angew. Chem. Int. Ed.* **2008**, *47*, 4070.

(12) I. McCulloch, M. Heeney, C. Bailey, K. Genevicius, I. MacDonald, M. Shkunov, D. Sparrowe, S. Tierney, R. Wagner, W. Zhang, M. L. Chabinyc, R. J. Kline, M. D. McGehee, M. F. Toney, *Nature Mater.* **2006**, *5*, 328.

(13) A. R. Murphy, J. M. J. Fréchet, *Chem. Rev.* **2007**, *107*, 1066.

(14) D. M. de Leeuw, M. M. J. Simenon, A. R. Brown, R. E. F. Einerhand, *Synth. Met.* **1997**, *87*, 53.

(15) K. Kawano, R. Pacios, D. Poplavskyy, J. Nelson, D. D. C. Bradley, J. R. Durrant, *Sol. Energy Mater. Sol. Cells* **2006**, *90*, 3520.

(16) M. Jorgensen, K. Norrman, F. C. Krebs, *Sol. Energy Mater. Sol. Cells* **2008**, *92*, 686.

(17) T. D. Anthopoulos, G. C. Anyfantis, G. C. Papavassiliou, D. M. de Leeuw, *Appl. Phys. Lett.* **2007**, *90*, 122105.

(18) D. J. Gundlach, Y. Y. Lin, T. N. Jackson, S. F. Nelson, D. G. Schlom, *IEEE Electron Device Lett.* **1997**, *18*, 87.

(19) C. D. Dimitrakopoulos, D. J. Mascaro, *IBM J. Res. Dev.* **2001**, *45*, 11.

(20) D. Knipp, R. A. Street, A. Volkel, J. Ho, *J. Appl. Phys.* **2003**, *93*, 347.

(21) R. Ruiz, D. Choudhary, B. Nickel, T. Toccoli, K.-C. Chang, A. C. Mayer, P. Clancy, J. M. Blakely, R. L. Headrick, S. Iannotta, G. G. Malliaras, *Chem. Mater.* **2004**, *16*, 4497.

(22) G. Dennler, C. Lungenschmied, H. Neugebauer, N. S. Sariciftci, A. Labouret, *J. Mater. Res.* **2005**, *20*, 3224.

(23) F. C. Krebs, H. Spanggard, T. Kjaer, M. Biancardo, J. Alstrup, *Mater. Sci. Eng., B* **2007**, *138*, 106.

(24) A. Facchetti, T. J. Marks, *Transparent Electronics, From Synthesis to Applications*; Wiley: Chichester, United Kingdom, **2010**.

(25) J. E. Anthony, D. L. Eaton, S. R. Parkin, *Org. Lett.* **2002**, *4*, 15.

(26) B. A. Jones, M. J. Ahrens, M.-H. Yoon, A. Facchetti, T. J. Marks, M. R. Wasielewski, *Angew. Chem. Int. Ed.* **2004**, *43*, 6363.

(27) K. Takimiya, Y. Kunugi, T. Otsubo, *Chem. Lett.* **2007**, *36*, 578.

(28) H. Yan, Z. Chen, Y. Zheng, C. Newman, J. R. Quinn, F. Dötz, M. Kastler, A. Facchetti, *Nature* **2009**, *457*, 679.

(29) J. Smith, A. Bashir, G. Adamopoulos, J. E. Anthony, D. D. C. Bradley, R. Hamilton, M. Heeney, I. McCulloch, T. A. Anthopoulos, *Adv. Mater.* **2010**, *22*, 3598.

(30) X. Guo, R. P. Oritz, Y. Zheng, Y. Hu, Y.-Y. Noh, K.-J. Baeg, A. Facchetti, T. J. Marks, *J. Am. Chem. Soc.* **2011**, *133*, 1405.

(31) S. Goffri, C. Müller, N. Stingelin-Stutzmann, D. W. Breiby, C. P. Radano, J. W. Andreasen, R. Thompson, R. A. J. Janssen, M. M. Nielsen, P. Smith, H. Sirringhaus, *Nature Mater.* **2006**, *5*, 950.

(32) D. Sparrowe, M. Baklar, N. Stingelin, *Org. Electron.* **2010**, *11*, 1296.

(33) J. Smith, R. Hamilton, I. McCulloch, N. Stingelin-Stutzmann, M. Heeney, D. D. C. Bradley, T. D. Anthopoulos, *J. Mater. Chem.* **2010**, *20*, 2562.

(34) R. E. Martin, F. Diederich, *Angew. Chem. Int. Ed.* **1999**, *38*, 1350.

(35) J. M. Tour, *Acc. Chem. Res.* **2000**, *33*, 791.

(36) J. Cornil, Y. Karzazi, J. L. Brédas, *J. Am. Chem. Soc.* **2002**, *124*, 3516.

(37) V. A. L. Roy, Y.-G. Zhi, Z.-X. Xu, S.-C. Yu, P. W. H. Chan, C.-M. Che, *Adv. Mater.* **2005**, *17*, 1258.

(38) T. Yasuda, K. Kashiwagi, Y. Morizawa, T. Tsutsui, *J. Phys. D: Appl. Phys.* **2007**, *40*, 4471.

(39) L. Valentini, D. Bagnis, A. Marrocchi, M. Seri, A. Taticchi, J. M. Kenny, *Chem. Mater.* **2008**, *20*, 32.

(40) Q. Meng, J. Gao, R. Li, L. Jiang, C. Wang, H. Zhao, C. Liu, H. Li, W. Hu, *J. Mater. Chem.* **2009**, *19*, 1477.

(41) A. Marrocchi, F. Silvestri, M. Seri, A. Facchetti, A. Taticchi, T. J. Marks, *Chem. Commun.* **2009**, 1380.

(42) A. Marrocchi, M. Seri, C. Kim, A. Facchetti, A. Taticchi, T. J. Marks, *Chem. Mater.* **2009**, *21*, 2592.

(43) M. Kivala, F. Diederich, *Acc. Chem. Res.* **2009**, *42*, 235.

(44) F. Silvestri, A. Marrocchi, *Int. J. Mol. Sci.* **2010**, *11*, 1471.

(45) F. Silvestri, A. Marrocchi, M. Seri, C. Kim, T. J. Marks, A. Facchetti, A. Taticchi, *J. Am. Chem. Soc.* **2010**, *132*, 6108.

(46) R. R. Schrock, *Polyhedron* **1995**, *14*, 3177.

(47) K. Weiss, A. Michel, E.-M. Auth, E. H. F. Bunz, T. Mangel, K. Mullen, *Angew. Chem. Int. Ed.* **1997**, *36*, 506.

(48) K. Sonogashira, *Metal Catalyzed Cross-Coupling Reactions*; A. de Meijere, F. Diederich, Ed., Wiley-VCH: Weinheim, Germany, **1998**.

(49) P. Siemsen, R. C. Livingston, F. Diederich, *Angew. Chem. Int. Ed.* **2000**, *39*, 2632.

(50) W. Zhang, S. Kraft, J. S. Moore, *J. Am. Chem. Soc.* **2004**, *126*, 329.

(51) B. Liang, M. Dai, J. Chen, Z. Yang, *J. Org. Chem.* **2005**, *70*, 391.

(52) F. Monnier, F. Turtaut, L. Duroure, M. Taillefer, Org. Lett. **2008**, *10*, 3203.

(53) Y. Y. Kuang, F. E. Chen, *Helv. Chim. Acta* **2009**, *92*, 897.

(54) D. A. Fulmer, W. C. Shearouse, S. T. Mendonza, J. Mack, *Green Chem.* **2009**, *11*, 1821.

(55) H. Meng, F. Sun, M. B. Goldfinger, G. D. Jaycox, Z. Li, W. J. Marshall, G. S. Blackman, *J. Am. Chem. Soc.* **2005**, *127*, 2408.

(56) J. E. Anthony, *Chem. Rev.* **2006**, *106*, 5028.

(57) C. Müller, S. Goffri, J. W. Andreasen, D. W. Breiby, H. D. Chanzy, R. A. J. Janssen, M. M. Nielsen, C. P. Radano, H. Sirringhaus, P. Smith, N. Stingelin-Stutzmann, *Adv. Funct. Mater.* **2007**, *17*, 2674.

Chapter VII

Conclusions and Outlook

CONCLUSIONS

In the work presented in this thesis, a comprehensive picture of structure-property interrelations is provided on the basis of selected functional small-molecular organic species. The effect of modifications of their chemical structure and processing conditions on certain macroscopic characteristics is monitored by means of different optic and electronic properties including, *e.g.* refractive-index modulation and semiconductivity.

In the first part, a series of molecular trisazobenzene derivatives is employed that feature optical active units in their side-groups. This functionality allows optically addressing of the species explored and, hence, reveals potential correlations between molecular structure, their phase behavior and optical performance. It is found that only compounds exhibiting decoupling flexible spacers between the benzene core and the azobenzene units, as well as additional dipolar end-groups feature a latent liquid-crystalline (LC) phase at elevated temperatures and, concomitantly, allow formation of stable holographic volume gratings in thin films of the trisazobenzene species investigated. Intriguingly, those same compounds display a remarkable "post-development", *i.e.*, an increase of the amplitude of refractive-index modulation in holographic experiments after writing of optical gratings is arrested. That latter characteristic can be controlled by applying particular post-processing annealing protocols, permitting tailoring of order in photo-aligned domains with light *and* temperature.

In a subsequent study, trisazobenzene based alignment layers are employed for orientation of common LC compounds, such as cyanobiphenyls. Surface analysis of the neat trisazobenzene films and optical characterization of LC cells fabricated with such layers reveal an inter-molecular attraction between the azobenzene containing alignment layer and the deposited liquid-crystalline species, resulting in the formation of ordered macroscopic domains that can readily be patterned.

After having unveiled order related effects on selected *optical* characteristics, the interrelation of structure and *electronic* functionalities, *i.e.* the influence of molecular architecture tailoring and processing routes on charge transport properties, is studied based on blends of semiconducting small molecules and insulating polymers. It is demonstrated that under judiciously chosen processing conditions, *i.e.* at elevated temperatures, α-quaterthiophene:polyethylene binaries can be fabricated with insulator contents as high as 80 to 90 wt-% without sacrificing the electronic performance when compared to the neat semiconducting species. For many manufacturing techniques, however, preparation of

Scheme 1. Illustration of the interdependence of structural features of the different length scales addressed in this work, highlighting the demand for bridging all structural regimes involved for efficiently tailoring specific functionalities of materials systems.

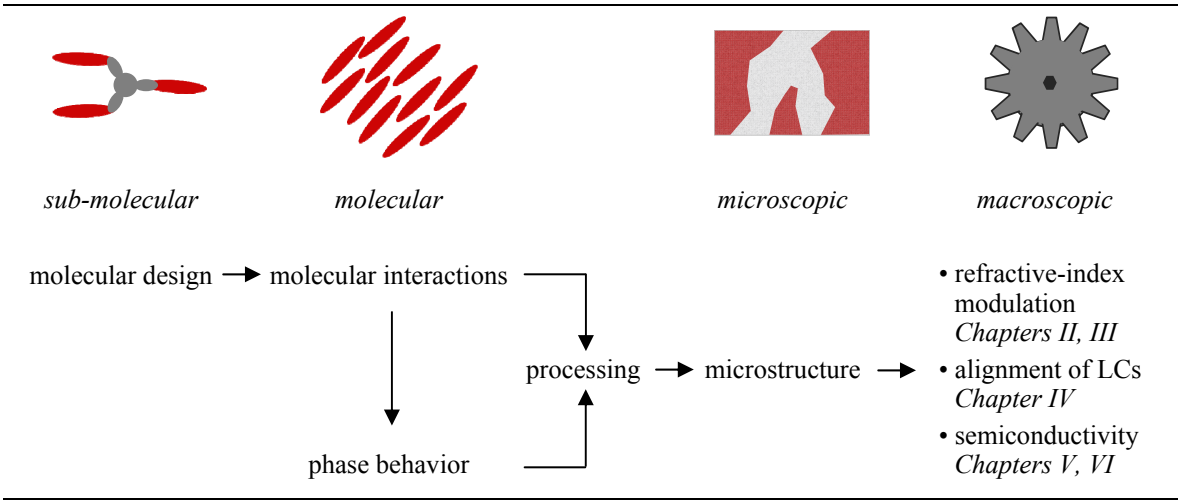

active layers at ambient conditions is preferable. Hence, selective modification of the molecular architecture of an arylacetylene derivative by attaching solubilizing side-chains is employed to manipulate the phase behavior resulting in a decrease of the semiconductor's melting temperature and, hence, increasing its solubility in common solvents. Most intriguingly, fine and homogeneous microstructures were obtained when room temperature processing blends of this derivative with poly(vinylidene fluoride) from homogeneous solutions; Semiconducting characteristics of field-effect transistors of blends thus produced are found to be comparable to those of devices comprising the non-substituted arylacetylene prepared at elevated temperatures.

Accordingly, results obtained with the organic systems discussed in this work illustrate the major effects of manipulations on the sub-molecular and molecular level on the microstructure and, therewith, on the macroscopic characteristics induced. This work once more underlines that control of structures on all length scales is pivotal for developing a fundamental understanding of structure-property interrelationships and, hence, for successfully tailoring materials functionalities or for imparting entirely new properties to a particular system (*cf.* Scheme 1).

OUTLOOK

On the basis of selected materials systems, it will be proposed in the following, how the structure-property concepts addressed in this thesis can be expanded toward other functionalities and fields of applications.

Blends with trisazobenzene derivatives for angle multiplexing

One major disadvantage of the trisazobenzene systems presented in this thesis is their poor mechanical characteristics, making fabrication of free-standing films with neat compounds cumbersome if not impossible. Accordingly, trisazobenzene thin films need to be supported by a substrate, *e.g.* glass. In order to realize small-molecule based self-supporting optically active layers, blends of azobenzene containing species and transparent (non light scattering) polymers are promising candidates. Whereas the optical activity is imparted by the small molecule, the polymer provides mechanical robustness, environmental stability as well as flexibility with processing options of the blends. If fabrication of millimeter-thick films is realizable, holographic writing and reading processes can be expanded, using the entire volume of the blend instead of its surface only, by inscribing several data layers at the same lateral position. This approach, enabled, for instance, by the so-called angle multiplexing technique, allows efficient data storage with high density.[1-4] However, to allow writing even in deeper layers of such storage media, the optical density of the films has to be adjusted by reducing the azobenzene content to levels as low as about 0.2 to 0.4 wt-%, depending on the film thickness and the chemical structure of the azobenzene species.[4] It has been demonstrated for a series of azobenzene containing co-polymers, though, that the stability of holographic information inscribed is strongly depending on cooperative effects in the optical active moiety[4-6] and, hence, the microstructure of blends fabricated has to be carefully controlled. Ideally, the azobenzene containing species are arranged in phase-separated domains that are distributed homogeneously within the polymeric matrix. Besides the chemical compatibility between the azobenzene species and the matrix material and the processing parameters applied, addition of compatibilizers or surfactants can be utilized as a potential instrument for tailoring the microstructure to be induced. Diblock co-polymers exhibiting an optical inactive block with chemical affinity for the matrix polymer and an azobenzene containing optical active block are interesting candidates for that purpose,[7-10] providing additional means to manipulate the interface and, hence, the degree of phase separation, between

azobenzene domains and matrix polymer. Accordingly, resulting ternary systems may provide a variety of tools for fine tuning the holographic performance of active layers.

Membranes

Another emerging field where structural characteristics over a wide range of length scales play an important role, is related to the regulation of the transport of substances through membranes, analogical to many processes found in nature.[11] The working principle of these selective barriers is based on a difference in chemical potential such as gradients in concentration, pressure or electric field, working as a driving force for transport across the membrane.[12] This allows separating different substances, including gases, liquids or particles in suspensions, etc., according to their size, shape or chemical nature.[13] Whereas the microstructure and the molecular arrangement, *i.e.* the size of the pores or the interconnected free volume of a species, respectively, is responsible for the size and/or shape exclusion properties of such separation layers, the chemical interaction of the membrane with the permeand can increase the selectivity drastically. Accordingly, separation of, for instance, polar/non-polar or aromatic/aliphatic, organic mixtures is possible when carefully adjusting the chemical characteristics of the membrane material.[14] Blends of different organic species or organic/inorganic hybrid materials are promising candidates for further increasing the selectivity of membranes. However, being of multi-component composition and, hence, of higher complexity than simple membranes based on neat compounds, they require comprehensive understanding of the interplay of chemical structure, phase behavior, operating conditions, microstructure and the regulation characteristics of the barrier layers. Intriguingly, recent research interests are also directed toward membrane materials that can be controlled with external stimuli, imparted, *e.g.* by photo-responsive species, related to the azobenzene compounds discussed in *Chapters II - IV*.[15-17] In these membranes, azobenzene modified pores are employed that are able to change their size when stimulated with light or heat. Thus, the option of actively manipulating the separation process with well-controllable parameters allows combining *adaptable* size exclusion with chemical selectivity in multi-functional barrier layers.

Blends with an active matrix

In the semiconductor:insulator blends discussed in this work, the polymeric matrix was selected to provide improved processing conditions, as well as mechanical robustness and environmental stability to the binary systems explored. However, when broadening the

range of polymeric matrices, the semiconducting properties can be combined with the introduction of other functionalities such as, *e.g.* ferroelectricity and piezoelectricity. For instance, when utilizing the ferroelectric co-polymer poly(vinylidene fluoride-co-trifluor-ethylene) (PVDF-TrFE)[18] – instead of the homopolymer PVDF – charge injection of an electrode into the semiconductor can be modified, depending on the polarization of the co-polymer, as recently has been demonstrated for binary systems of P3HT and PVDF-TrFE.[19-21] This highly interesting phenomenon, which allows for a matrix-induced switching between a high- and low-resistance state in organic resistive diodes, is achieved by means of an appropriate electrical pulse. Furthermore, phase-separated blends of the two components enable fabrication of non-volatile memories, where the two polarization states are used as binary levels. Thus, tailoring of the phase behavior and the microstructure of such blends and control of associated macroscopic properties can be employed as a source toward truly multi-functional device architectures.

Molecular organic ferromagnetism

Finally, magnetism represents one material property that was not addressed in the present study. In organic materials, this field of research is often referred as "molecular organic ferromagnetism", aiming at – as one of the main objectives – designing light-weight magnets.[22-26] In addition, these compounds, in principle, allow fabrication of transparent magnets and a potential to crystallize in non-centrosymmetric space groups is providing second-order nonlinear optical effects, offering new magneto-optic applications.[26-28] Ferromagnetism, however, is a cooperative phenomenon of magnetic spins in a compound, requiring detailed control of the solid-state structure induced during processing. Only when featuring coupling between spins, ordering of these spins and, hence, ferromagnetic behavior below a critical temperature, is possible. Encouragingly, the organic nature of molecular magnets allows tailoring of the molecular interaction and the microstructure induced through chemical modifications, as well as control of processing parameters – as shown in this work for selected optical and semiconducting systems. In analogy, the magnetic response can be manipulated by molecular design, as, *e.g.* by particular substituents, and their influence on the microstructural arrangement and, ultimately, the materials' magnetic characteristics.

References

(1) F. H. Mok, *Opt. Lett.* **1993**, *18*, 915.

(2) A. Saishoji, D. Sato, A. Shishido, T. Ikeda, *Langmuir* **2007**, *23*, 320.

(3) M. Häckel, L. Kador, D. Kropp, H.-W. Schmidt, *Adv. Mater.* **2007**, *19*, 227.

(4) H. Audorff, K. Kreger, R. Walker, D. Haarer, L. Kador, H.-W. Schmidt, *Adv. Polym. Sci.* **2010**, *228*, 59.

(5) A. Natansohn, P. Rochon, *Chem. Rev.* **2002**, *102*, 4139.

(6) P. Forcen, L. Oriol, C. Sanchez, R. Alcala, K. Jankova, S. Hvilsted, *J. Appl. Phys.* **2008**, *103*, 123111-1.

(7) G. Mao, J. Wang, S. R. Clingman, C. K. Ober, J. T. Chen, E. L. Thomas, *Macromolecules* **1997**, *30*, 2556.

(8) K. Moriya, T. Seki, M. Nakagawa, G. Mao, C. K. Ober, *Macromol. Rapid Commun.* **2000**, *21*, 1309.

(9) C. Frenz, A. Fuchs, H.-W. Schmidt, U. Theissen, D. Haarer, *Macromol. Chem. Phys.* **2004**, *205*, 1246.

(10) T. Breiner, K. Kreger, R. Hagen, M. Häckel, L. Kador, A. H. E. Müller, E. J. Kramer, H.-W. Schmidt, *Macromolecules* **2007**, *40*, 2100.

(11) H. Bader, K. Dorn, B. Hupfer, H. Ringsdorf, *Adv. Polym. Sci.* **1985**, *64*, 1.

(12) M. Mulder, *Basic Principles of Membrane Technology, Second Edition*; Kluwer Academic Publishers: Dordrecht, The Netherlands, **1996**.

(13) M. Ulbricht, *Polymer* **2006**, *47*, 2217.

(14) B. Smitha, D. Suhanya, S. Sridhar, M. Ramakrishna, *J. Membr. Sci.* **2004**, *241*, 1.

(15) T. Kunitake, N. Nakashima, M. Shimomura, Y. Okahata, K. Kano, T. Ogawa, *J. Am. Chem. Soc.* **1980**, *102*, 6644.

(16) J.-I. Anzai, T. Osa, *Tetrahedron* **1994**, *50*, 4039.

(17) N. Liu, D. R. Dunphy, P. Atanassov, S. D. Bunge, Z. Chen, G. P. Lopez, T. J. Boyle, C. J. Brinker, *Nano Lett.* **2004**, *4*, 551.

(18) Y. Higashihata, J. Sako, T. Yagi, *Ferroelectrics* **1981**, *32*, 85.

(19) K. Asadi, D. M. de Leeuw, B. de Boer, P. W. M. Blom, *Nature Mater.* **2008**, *7*, 547.

(20) K. Asadi, T. G. de Boer, P. W. M. Blom, D. M. de Leeuw, *Adv. Funct. Mater.* **2009**, *19*, 3173.

(21) R. C. G. Naber, K. Asadi, P. W. M. Blom, D. M. de Leeuw, B. de Boer, *Adv. Mater.* **2010**, *22*, 933.

(22) P. M. Allemand, K. C. Khemani, A. Koch, F. Wudl, K. Holczer, S. Donovan, G. Grüner, J. D. Thompson, *Science* **1991**, *259*, 303.

(23) M. Tamura, Y. Nakazawa, D. Shiomi, K. Nozawa, Y. Hosokoshi, M. Ishikawa, M. Takahashi, M. Kinoshita, *Chem. Phys. Lett.* **1991**, *186*, 401.

(24) R. Chiarelli, M. A. Novak, A. Rassat, J. L. Tholence, *Nature* **1993**, *363*, 147.

(25) O. Kahn, *Molecular Magnetism*; VCH: Weinheim, Germany, **1993**.

(26) D. Gatteschi, *Adv. Mater.* **1994**, *6*, 635.

(27) C.-T. Chen, K. S. Suslick, *Coord. Chem. Rev.* **1993**, *128*, 293.

(28) C. Janiak, *Dalton Trans.* **2003**, 2781.

Appendix

Synthesis and Characterization of Trisazobenzene Derivatives

GENERAL SYNTHETIC CONCEPT

Typically, three-arm star-shaped molecules were either created by an amidation or esterification reaction, both representing largely uncomplicated reaction types and, hence, conveniently allowing introduction of different polar groups or hydrogen bonding moieties.

In detail, the molecules based on trisamide derivatives were synthesized by a threefold amidation of acid chlorides containing side-groups together with 1,3,5-benzene trisamide. Molecules based on trisester derivatives were obtained in a similar manner, however, utilizing 1,3,5-trishydroxybenzene (*cf.* Scheme 1). When the molecules were based on 1,3,5-trimesic acid, *i.e.* when the direction of the amide or ester linkage was reversed, the photoactive side-groups comprised amino-groups or hydroxyl-function, respectively.

In a typical procedure, the photoactive chromophores were formed by a common azo-coupling reaction. The aliphatic spacers with terminal ethyl esters were introduced by etherification and subsequent saponification to the corresponding acids. Azobenzene compounds with carbonic acids were, finally, converted to reactive acid chloride species. In addition, side-groups with amino- or hydroxyl-function in the spacer moieties were utilized if the core was based on trimesic acid derivatives. An amino-function was obtained by introducing a t-Boc protected aminopropyl-spacer with subsequent cleavage of the protecting group, whereas in the case of hydroxyl-functionalized spacer moieties bromopropanol was used as reagent for the etherification. Mono- and bi-substituted products, as well as residual photochromic side-groups were analyzed by thin-layer chromatography (TLC) and oligomeric size-exclusion chromatography (SEC). Subsequently, they were removed by common techniques, *e.g.* flash-chromatography and recrystallization. In addition, all compounds were fully characterized by ^{1}H-nuclear magnetic resonance (NMR), ^{13}C-NMR, infrared (IR) spectroscopy, as well as elemental analysis (EA).

Scheme 1. Overview of the synthesis routes to trisazobenzene-trisamide and -trisester derivatives **1**-**10**.

Synthesis routes to trisazobenzene-trisamides:

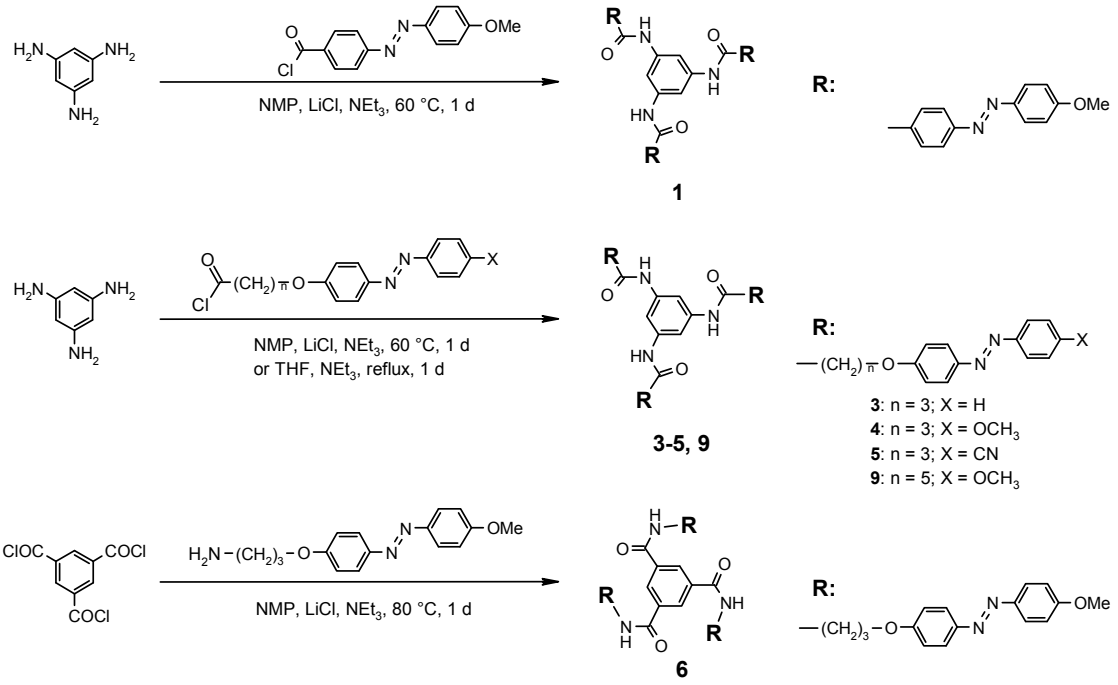

Synthesis routes to trisazobenzene-trisesters:

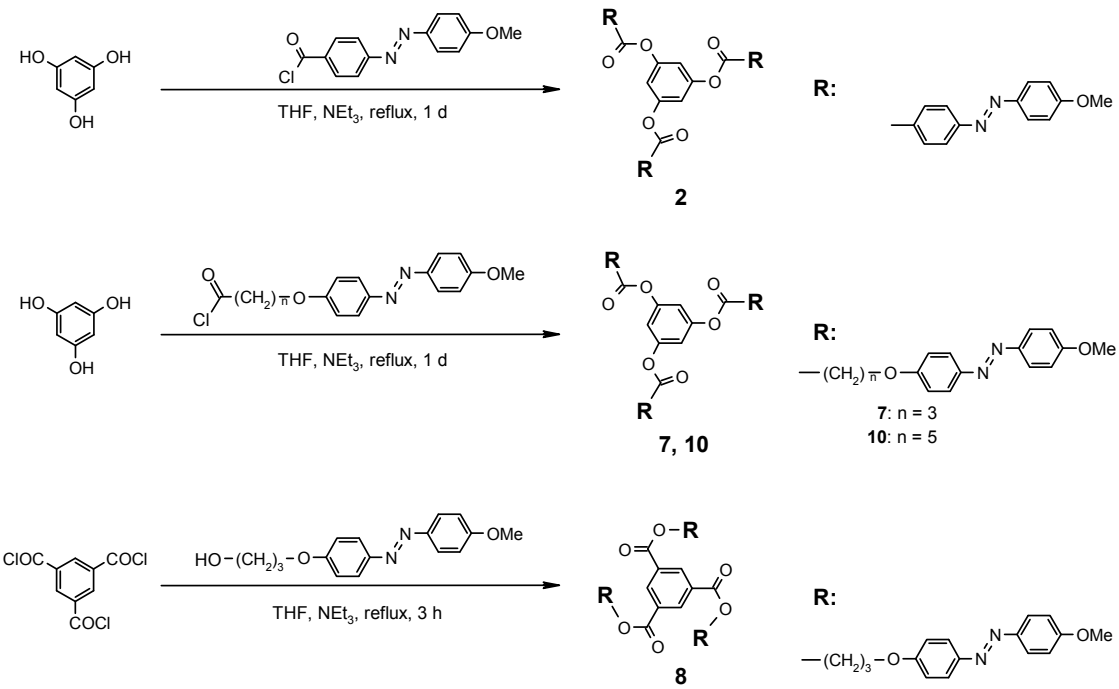

CHARACTERIZATION METHODS

^{1}H-nuclear magnetic resonance (NMR) and ^{13}C-NMR. NMR-spectra were recorded with a Bruker AC 300 spectrometer (300 MHz and 75 MHz, respectively).

Fourier transform infrared (FTIR). FTIR-spectra were recorded with a BIO-RAD Digilab FTS-40 (FTIR).

Oligomeric size-exclusion chromatography (Oligo-SEC). Oligo-SEC-measurements were performed utilizing a Waters 515-HPLC pump with stabilized THF as eluent at a flow rate of 0.5 ml/min. 20 μl of a solution with a concentration of approx. 1 mg/ml were injected into a column setup, which consists of a guard column (Varian; 5 x 0.8 cm; mesopore gel; particle size 3 μm) and two separation columns (Varian; 30 x 0.8 cm; mesopore gel; particle size 3 μm). The compounds were monitored with a Waters 486 tuneable UV detector at 254 nm and a Waters 410 differential RI detector.

Elemental analysis (EA). EA were performed with a HEKAtech elemental analyzer EA 3000 (Euro Vector CHNS) charged with tungsten oxide and copper. Detection was performed utilizing a GC-setup equipped with a thermal conductivity detector.

SYNTHETIC PROCEDURES

General preparation method 1

In a flame-dried flask 1.4 mmol of 1,3,5-trisaminobenzene, 0.1 g LiCl and 1 ml triethylamine were dissolved in 20 ml dry NMP. Then the solution was cooled to 0 °C and 4 equivalents (5.5 mmol) of azobenzene based acid chloride were added. The reaction mixture was allowed to warm to room temperature and subsequently stirred for 12 h at 60 °C. The solution was cooled to room temperature and poured into ice-water. The solid was filtered off and washed several times with water.

Trisamides based on trimesic acid were prepared in a similar manner.

General preparation method 2

In a flame-dried flask 1.4 mmol of phloroglucine and 1 ml triethylamine were dissolved in 30 ml dry THF. Then the solution was cooled to 0 °C and 4 equivalents (5.5 mmol) of 4-azobenzene based acid chloride were added. The reaction mixture was allowed to warm to room temperature and refluxed for 12 h at 60 °C. The formed suspension was cooled to room temperature, the triethylammonium-salt was filtered off and washed several times with THF. Subsequently, the solvent was evaporated off.

Trisesters based on trimesic acid were prepared in a similar manner.

1,3,5-Benzenetrisamide based on 1,3,5-triamonobenzene

The synthesis of 1,3,5-tris-{4-[(4-methoxyphenyl)azo]benzoylamino}benzene (**1**) was carried out according to *General preparation method 1*.

The crude product was recrystallized from THF/EtOH yielding an orange solid (39%).

^{1}H-NMR (DMSO-d_6): δ = 3.88 (s, 9H), 7.16 (d, 6H), 7.96 (dd, 12H), 8.13 (s, 3H), 8.20 (d, 6H), 10.5 (s, 3H) ppm.

^{13}C-NMR (DMSO-d_6): δ = 56.6, 109.9, 115.6, 122.9, 125.8, 130.0, 137.2, 140.1, 147.1, 154.5, 163.2, 165.7 ppm.

IR (KBr): 3308, 2838, 1654, 1600, 1540, 1503, 1418, 1258, 1139, 1052, 855, 836 cm^{-1}.

El.Vol. (Oligo-GPC): 16.05 ml.

Elemental analysis (N,C,H): calc.: 15.04%, 68.81%, 4.69%; found: 14.44%, 67.82%, 4.76%.

The synthesis of 1,3,5-tris-{4-[4-(phenylazo)phenoxy]butyrylamino}benzene (**3**) was carried out according to *General preparation method 1*.

After flash-chromatography in ethyl acetate/cyclohexane (2/3) a yellow solid (yield: 24%) was obtained.

^{1}H-NMR (DMSO-d_6): δ = 2.04 (quintet, 6H), ~2.5 (6H), 4.10 (t, 6H), 7.10 (d, 6H), 7.5 (m, 9H), 7.66 (s, 3H), 7.83 (m, 12H), 9.97 (s, 3H) ppm.

^{13}C-NMR (DMSO-d_6): δ = 24.6, 32.7, 67.4, 115.0, 122.2 (2C), 124.6, 129.3, 130.8, 139.5, 146.1, 152.0, 161.4, 170.6 ppm.

IR (KBr): 3312, 3219, 3040, 2942, 2868, 1651, 1603, 1555, 1500, 1452, 1325, 1252, 1142, 1053, 839 cm^{-1}.

El.Vol. (Oligo-GPC): 15.90 ml.

Elemental analysis (N,C,H): calc.: 13.67%, 70.34%, 5.58%; found: 13.19%, 70.56%, 5.69%.

The synthesis of 1,3,5-tris-{4-[4-[(4-methoxyphenyl)azo]phenoxy]butyrylamino}benzene (**4**) was carried out according to *General preparation method 1*.

After recrystallization from THF/MeOH a yellow solid (yield: 32%) was obtained.

^{1}H-NMR (DMSO-d_6): δ = 2.05 (quintet, 6H), ~2.5 (6H), 3.83 (s, 9H), 4.11 (t, 6H), 7.09 (d, 12H), 7.67 (s, 3H), 7.82 (m, 12H), 9.97 (s, 3H) ppm.

^{13}C-NMR (DMSO-d_6): δ = 25.0, 33.0, 55.9, 67.8, 114.8, 115.3, 124.4 (2C), 139.8, 146.4, 146.5, 158.5, 161.1, 161.8, 171.0 ppm.

IR (KBr): 3289, 3071, 1667, 1599, 1501, 1455, 1318, 1250, 1148, 1028, 941, 841 cm^{-1}.

El.Vol. (Oligo-GPC): 15.73 ml.

Elemental analysis (N,C,H): calc.: 12.45%, 67.64%, 5.68%; found: 12.09%, 67.13%, 5.76%.

The synthesis of 1,3,5-tris-{4-[4-[(4-cyanophenyl)azo]phenoxy]butyrylamino}benzene (**5**) was carried out according to *General preparation method 1*.

After flash-chromatography in THF/hexane (3/1) a yellow solid (yield: 23%) was obtained.

^{1}H-NMR (DMF-d_7): δ = 2.19 (quintet, 6H), 2.65 (t, 6H), 4.26 (t, 6H), 7.23 (d, 6H), 7.87 (s, 3H), 7.9-8.1 (m, 24H), 10.06 (s, 3H) ppm.

^{13}C-NMR (DMF-d_7): δ = 25.2, 33.1, 68.3, 113.4, 115.6, 118.9, 123.4 (2C), 125.8, 134.2, 140.5, 147.0, 155.0, 163.2, 171.6 ppm.

IR (KBr): 3341, 3090, 2844, 2226, 1698, 1599, 1501, 1418, 1254, 1138, 1043, 847 cm^{-1}.

El.Vol. (Oligo-GPC): 15.48 ml.

Elemental analysis (N,C,H): calc.: 16.86%, 68.66%, 4.85%; found: 16.23%, 68.53%, 4.96%.

The synthesis of 1,3,5-tris-{6-[4-[(4-methoxyphenyl)azo]phenoxy]hexanoylamino}benzene (**9**) was carried out according to *General preparation method 2*, but performed at room temperature.

Recrystallization from THF/EtOH yielded a yellow powder (87%).

^{1}H-NMR (DMSO-d_6): δ = 1.45 (m, 6H), 1.62 (m, 6H), 1.74 (m, 6H), 2.30 (t, 6H), 3.82 (s, 9H), 4.04 (t, 6H), 7.06 (m, 12H), 7.64 (s, 3H), 7.80 (m, 12H), 9.86 (s, 3H) ppm.

^{13}C-NMR (DMSO-d_6): δ = 25.0, 25.1, 28.3, 36.3, 55.5, 67.8, 114.5, 114.9, 124.0, 124.1 (2C), 139.5, 146.0, 146.1, 160.9, 161.4, 171.2 ppm.

IR (KBr): 3282, 3050, 2942, 1667, 1599, 1501, 1441, 1318, 1248, 1148, 1105, 1028, 841cm^{-1}.

El.Vol. (Oligo-GPC): 15.54 ml.

Elemental analysis (N,C,H): calc.: 11.50%, 69.02%, 6.34%; found: 11.00%, 68.59%, 6.49%.

1,3,5-Benzenetrisamide based on 1,3,5-trimesic acid

The synthesis of benzene-1,3,5-tricaboxylic acid-tris-{4-[4-[(4-methoxyphenyl)azo]phenoxy]butyl}amide (**6**) was carried out according to *General preparation method 1.*

After flash-chromatography in THF/hexane (3/1) a yellow solid was obtained (yield: 13%).

^{1}H-NMR (DMSO-d_6): δ = 2.03 (quintet, 6H), 3.48 (m, 6H), 3.83 (s, 9H), 4.15 (t, 6H), 7.09 (m, 12H), 7.81 (m, 12H), 8.43 (s, 3H), 8.84 (m, 3H) ppm.

^{13}C-NMR (DMSO-d_6): δ = 28.7, 36.5, 55.6, 66.7, 114.6, 115.0, 124.2 (2C), 128.6, 135.1, 146.1, 146.2, 160.9, 161.5, 165.7 ppm.

IR (KBr): 3428, 3071, 2932, 2837, 1651, 1599, 1501, 1468, 1246, 1147, 1030, 841 cm^{-1}.

El.Vol. (Oligo-GPC): 15.81 ml.

Elemental analysis (N,C,H): calc.: 12.45%, 67.64%, 5.68%; found: 11.48%, 67.26%, 5.99%.

1,3,5-Benzenetrisester based on 1,3,5-trihydroxybenzene

The synthesis of 1,3,5-tris-{4-[(4-methoxyphenyl)azo]benzoyloxy}benzene (**2**) was carried out according to *General preparation method 2.*

The crude product was recrystallized from THF/EtOH yielding an orange solid (50%).

^{1}H-NMR ($CDCl_3$): δ = 3.90 (s, 9H), 7.03 (d, 6H), 7.24 (s, 3H), 7.97 (dd, 12H), 8.32 (d, 6H) ppm.

^{13}C-NMR ($CDCl_3$): δ = 56.0, 114.7, 123.0, 125.7, 130.2, 131.7, 147.4, 151.9, 156.3, 163.2, 164.4, 166.5 ppm.

IR (KBr): 3027, 2844, 1741, 1600, 1501, 1453, 1252, 1130, 1064, 835 cm^{-1}.

El.Vol. (Oligo-GPC): 16.14 ml.

Elemental analysis (N,C,H): calc.: 9.99%, 68.57%, 4.32%; found: 9.83%, 68.79%, 4.40%.

The synthesis of 1,3,5-tris-{4-[4-[(4-methoxyphenyl)azo]phenoxy]butyryloxy}benzene (**7**) was carried out analog to *General preparation method 2,* but performed at room temperature.

After flash-chromatography in CH_2Cl_2/THF (40/1) a yellow solid (yield: 40%) was obtained.

^{1}H-NMR ($CDCl_3$): δ = 2.26 (quintet, 6H), 2.79 (t, 6H), 3.89 (s, 9H), 4.14 (t, 6H), 6.86 (s, 3H), 6.99 (m, 12H), 7.89 (m, 12H) ppm.
^{13}C-NMR ($CDCl_3$): δ = 24.4, 30.9, 55.5, 66.7, 112.8, 114.1, 114.7, 124.3 (2C), 147.0, 147.1, 151.0, 160.7, 161.6, 170.8 ppm.
IR (KBr): 3071, 2942, 2837, 1761, 1601, 1500, 1454, 1369, 1317, 1248, 1147, 1030, 943, 843 cm^{-1}.
El.Vol. (Oligo-GPC): 15.78 ml.
Elemental analysis (N,C,H): calc.: 8.28%, 67.45%, 5.36%; found: 8.22%, 67.37%, 5.41%.

The synthesis of 1,3,5-tris-{6-[4-[(4-methoxyphenyl)azo]phenoxy]hexanoyloxy}benzene (**10**) was carried out according to *General preparation method 2.*
Recrystallization from THF/EtOH yielded a yellow powder (86%).
^{1}H-NMR ($CDCl_3$): δ = 1.62 (m, 6H), 1.84 (m, 12H), 2.58 (t, 6H), 3.87 (s, 9H), 4.04 (t, 6H), 6.84 (s, 3H), 6.98 (dd, 12H), 7.87 (dd, 12H) ppm.
^{13}C-NMR ($CDCl_3$): δ = 24.9, 26.0, 29.2, 34.6, 55.9, 68.2, 113.1, 114.5, 115.0, 124.7, 124.7, 147.3, 147.4, 151.5, 161.4, 161.9, 171.6 ppm.
IR (KBr): 3050, 2942, 2870, 1765, 1599, 1501, 1462, 1422, 1318, 1250, 1127, 1024, 918, 843 cm^{-1}.
El.Vol. (Oligo-GPC): 15.55 ml.
Elemental analysis (N,C,H): calc.: 7.65%, 68.84%, 6.05%; found: 7.61%, 69.33%, 6.23%.

1,3,5-Benzenetrisester based on 1,3,5-trimesic acid

The synthesis of benzene-1,3,5-tricaboxylic acid-tris-{4-[4-[(4-methoxyphenyl)azo]phenoxy]butyl}ester (**8**) was carried out according to *General preparation method 2.*
After flash-chromatography in toluene/THF a yellow solid was obtained (yield: 63%).
^{1}H-NMR ($CDCl_3$): δ = 2.32 (quintet, 6H), 3.88 (s, 9H), 4.20 (t, 6H), 4.62 (t, 6H), 7.00 (m, 12H), 7.88 (m, 12H), 8.87 (s, 3H) ppm.
^{13}C-NMR ($CDCl_3$): δ = 28.6, 29.7, 55.1, 62.9, 64.6, 114.1, 114.6, 124.3 (2C), 131.3, 134.6, 147.0, 147.1, 160.6, 161.6, 164.8 ppm.
IR (KBr): 3073, 2965, 2880, 1730, 1599, 1500, 1421, 1319, 1236, 1147, 1028, 985, 839 cm^{-1}.
El.Vol. (Oligo-GPC): 15.91 ml.
Elemental analysis (N,C,H): calc.: 8.28%, 67.45%, 5.36%; found: 8.01%, 67.08%, 5.47%.

ACKNOWLEDGMENTS

One essential fact I realized very early when entering the scientific world: most often people surrounding you are more important than a mere striving for scientific results. Hence, as a multitude of individuals have contributed to this project, I would like to express my deepest gratitude to all who made this time an unforgettable "phase" of my life.

First and foremost, I would like to thank my truly unique advisor Paul Smith for giving me the possibility to spend my Ph.D. time in his Polymer Technology "clique". The stimulating spirit he created in his group is without comparison and inspired me a lot – both scientifically, as well as personally. Furthermore, I'm especially indebted to my co-supervisor Natalie Stingelin (Imperial College London, United Kingdom) – not only for her invaluable support and advice during the last years, but also for opening many doors for me and connecting me to her impressive academic network. I thank both, Paul and Natalie, for advancing my skills, working with me on my weak spots and, most importantly, for always believing in me.

Hans-Werner Schmidt (University of Bayreuth, Germany) is gratefully acknowledged for being co-examiner of the work presented in this thesis, for his synthetic expertise making the realization of Chapters II - IV possible, and for the hospitality I received during my numerous stays in Bayreuth.

I'm also extremely thankful to Assunta Marrocchi (University of Perugia, Italy) for the synthesis of arylacetylene derivative presented in Chapter VI, for being a fantastic host in Italy and for co-examining my thesis.

Dick Broer (Technical University of Eindhoven, The Netherlands) is gratefully acknowledged for being co-examiner of this work, for his advice with alignment layers addressed in Chapter IV, and for his hospitality during my visit in Eindhoven.

In addition, different people have contributed experimentally to make this thesis possible, for which I am tremendously grateful. I'm particularly indebted to Klaus Kreger (University of Bayreuth, Germany) for planning and conducting the synthesis of trisazobenzene compounds discussed in Chapters II - IV and to Sandra Ganzleben, Doris Hanft and Christina Löffler (University of Bayreuth, Germany) for their invaluable assistance in material synthesis. Hubert Audorff and Lothar Kador (University of Bayreuth, Germany) are thankfully acknowledged for their invaluable support, making the holographic characterization presented in Chapters II and III possible. Furthermore, Cees Bastiaansen and Ivelina Sishmanova (Technical University of Eindhoven, The Netherlands) are gratefully acknowledged for their help with LC cell fabrication and characterization introduced in

Chapter IV, as well as for their hospitality at TU/e. I would like to thank Luigi Vaccaro (University of Perugia, Italy) and Maria Laura Santarelli (University of Rome Sapienza, Italy) for supporting the synthesis of arylacetylene compound discussed in Chapter VI and for their great hospitality in Italy. Moreover, I'm highly thankful to Mohammed Baklar, Liyang Yu and Thomas Anthopoulos (Imperial College London, United Kingdom) for invaluable expert assistance with the characterization of field-effect transistors presented in Chapters V and VI.

Martin Heeney, Iain McCulloch, Maxim Shkunov and David Sparrowe (then Merck Chemicals, United Kingdom) are gratefully acknowledged for their hospitality during my stays in Southampton. Thanks also to Dimitri Kokkinis and Prabath Lewdeni (ETH Zurich, Switzerland) for their experimental contributions.

An enormous "THANKS" goes to all the members and associates of the Polymer Technology Group for making my time here something really special; scientifically in the lab as well as socially whenever we had the possibility to spend some time together. Especially Walter Caseri, Fabien Choffat and Christian Müller are acknowledged for stimulating my scientific interests with their enthusiasm during my Semester and Diploma projects in the Polymer Technology Group. I would like to thank Kirill Feldman for invaluable support with AFM, numerous stimulating discussions and, of course, for treating us with his home-smoked fish. Karin Bernland is thankfully acknowledged for expert assistance with SEM and I thank Werner Schmidheiny for manufacturing more than only essential equipment. Furthermore, I would in particular like to express my thanks to Markus Trummer, Felix Koch, Irene Bräunlich, Jan Giesbrecht, Jérôme Lefèvre, Matthias Gössi, Raphael Schaller, Andreas Brunner, Marc Simonet, Kurt Pernstich, Susanne Köppl, Sara Fornera, Joanna Wong, Stephan Busato, Vappu Hämmerli, Harald Lehmann, Thomas Schweizer, Theo Tervoort, Ueli Suter and Wolfgang Kaiser – it was you guys who made the difference!

Many thanks also to Geordies' for being the platform of numerous fruitful discussions, memorable group events and the nucleus of many brilliant ideas.

In addition, the Materials Research Center (MRC) of ETH Zurich is gratefully acknowledged for initiating this project with seed funding.

Finally, I would like to thank Janine, my family and my friends for their patience, support, encouragement and, most importantly, simply for always being there for me.